THESIS

APPLYING TWO BINNED METHODS TO THE SIMPLE BIOSPHERE MODEL (SIB) FOR IMPROVING THE REPRESENTATION OF SPATIALLY VARYING PRECIPITATION AND SOIL WETNESS

Submitted by

Isaac D. Medina

Department of Atmospheric Science

In partial fulfillment of the requirements

For the Degree of Master of Science

Colorado State University

Fort Collins, Colorado

Fall 2011

Master's Committee:

Advisor: A. Scott Denning

David A. Randal
Jorge A. Ramirez

ABSTRACT

APPLYING TWO BINNED METHODS TO THE SIMPLE BIOSPHERE MODEL (SIB) FOR IMPROVING THE REPRESENTATION OF SPATIALLY VARYING PRECIPITATION AND SOIL WETNESS

Representing subgrid-scale variability is a continuing challenge for modelers, but is crucial for accurately calculating the exchanges of energy, moisture, and momentum between the land surface and atmospheric boundary layer. Soil wetness is highly spatially variable and difficult to resolve at grid length scales (~100 km) used in General Circulation Models (GCMs). Currently, GCMs use an area average precipitation rate that results in a single soil wetness value for the entire grid area, and due to the highly nonlinear relationship between soil wetness and evapotranspiration, significant inaccuracies arise in the calculation of the grid area latent heat flux. Using a finer GCM resolution will not solve this problem completely and other methods of modeling need to be considered.

For this study, the binned and alternative binned method of Sellers et al. (2007) are applied to the Simple Biosphere Model (SiB) for improving the representation of spatially varying precipitation, soil wetness and surface-atmosphere fluxes. The methods are tested in a dry, semi-arid, and wet biome for two off-line precipitation distribution experiments, and results are compared to an explicit method, which is ideal for resolving subgrid-scale variability, and the bulk method (area averaged), which is currently in use with GCMs. Results indicate that the alternative binned method better captures the spatial variability in soil wetness and grid area flux calculations produced by the explicit method, and deals realistically with spatially varying precipitation at little additional computational cost to the bulk method.

ACKNOWLEDGEMENTS

I would like to acknowledge and greatly thank the following people who have made the completion of my thesis possible:

I thank my advisor, Dr. A. Scott Denning, for the opportunity to work with the best scientists in our field at CMMAP. I also thank my committee members, Dr. David A. Randal and Dr. Jorge A. Ramirez, for their interest in my research.

I also express my gratitude to Dr. Ian T. Baker for all of his scientific insight and mentoring, and the Biocycle Group for all of their support and encouragement.

Finally, I am grateful for the support and understanding from my family and friends.

TABLE OF CONTENTS

CHAPTER 1

Introduction

1.1 Soil Moisture Heterogeneity and Earth's Climate System

Interactions between the land surface and atmosphere are important for modeling earth's climate system. The lower boundary of the atmosphere is the oceanic or continental surface, where a number of biological, chemical and physical processes take place. The land surface is defined by non homogenous variables that are difficult to resolve at length scales (~100 x 100 km) used for general circulation model (GCM) grid areas. This is especially true when it comes to the representation of soil moisture heterogeneity. Soil moisture varies at very fine length scales and using a finer GCM resolution may never completely close the scaling gap, so other modeling methods need to be used. Representing soil moisture heterogeneity improves the representation of land surface processes in hydrological and climate models (Ryu and Famiglietti, 2006), and is the prerequisite for properly representing the seasonal hydrological cycle within large scale atmospheric models (Ronda et al. 2002). Representing sub-grid scale variability is a continuing challenge for modelers, but is crucial for accurately calculating the exchanges of energy, moisture, and momentum between the land surface and atmospheric boundary layer, since the land surface is responsible for much of the spatial and temporal variability in the climate system.

The only significant source of energy for the circulation of the atmosphere is solar radiation. It is difficult to explain the long-term behavior of the atmosphere without an adequate understanding of the mechanisms that convert absorbed solar radiation at the surface into local

heat storage, infrared cooling, and latent heat (LH) and sensible heat (SH) releases (Avissar and Verstraete, 1990). Fluxes of LH and SH from the land surface have significant effects on weather and climate. SH increases the temperature of the overlying air column and warms the planetary boundary layer (PBL), and LH is the energy equivalent to water that is evaporated and transpired (through vegetation) from the land surface (Sellers et al., 1997). Therefore, it is important to adequately characterize the land surface since LH fluxes are directly associated with the transfer of water from the land surface though evapotranspiration (Avissar and Verstraete, 1990). Evapotranspiration is largely controlled by the availability of water at the surface, gradient of humidity between the surface and atmosphere, and the wind profile. Convection often moves LH into the atmosphere where heat is released through condensation forming clouds and eventually precipitation. The atmospheric radiation budget is strongly affected by clouds, so relative to SH, LH has a nonlocal impact on the atmosphere (figure 1.1a).

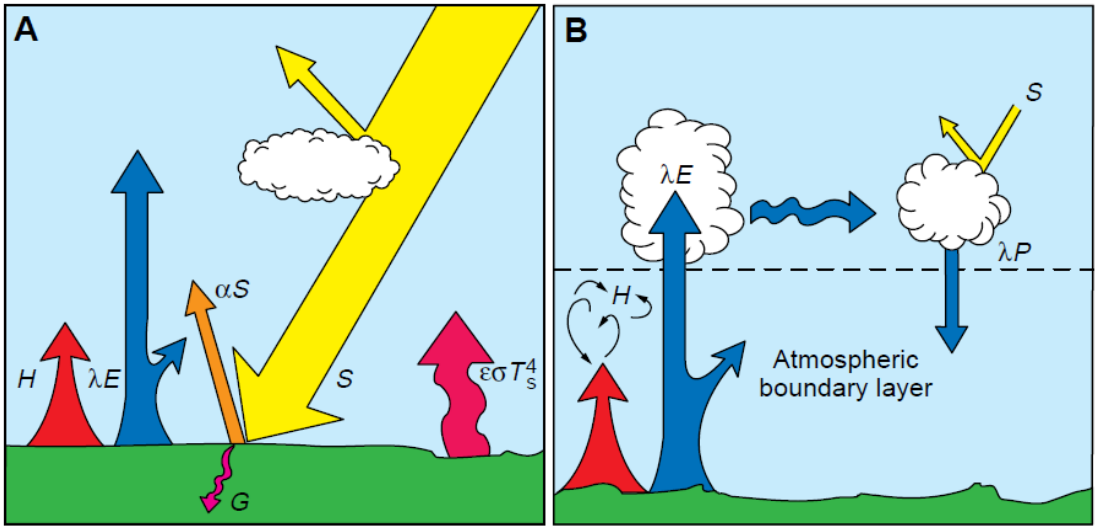

Figure 1.1a. (A) The surface radiation budget as a result of the interactions between the land surface and the atmosphere, where S is the insolation (function of latitude, longitude, and time of day), αS is reflected insolation, G is the ground heat flux, H is the SH flux, E is the evapotranspiration rate, λ is the latent heat of vaporization, and $\varepsilon\sigma T^4$ is long wave radiation emitted from the surface. (B) Heat fluxes and their affect on the atmosphere, where P is the precipitation (Sellers et al., 1997).

1.2 Soil Moisture Control on Thermal Conductivity, Albedo and Bowen Ratios

Soil moisture has a pronounced non local affect on the atmosphere by controlling the surface parameters such as thermal conductivity and albedo, which influence the exchange of heat and moisture between the surface and the atmosphere. This interaction between the land surface and the atmosphere dictates the circulation of the atmosphere and the climate system.

For a given heat flux temperature profile at the surface, the thermal conductivity and heat capacity are the determining factors. The rate heat is exchanged by conduction between the surface and underlying soil is equal to the temperature gradient times the thermal conductivity, and this is known as the soil heat flux (Bonan 2008:132-133). The thermal conductivity of soils is greatly dependent on soil water content (volumetric water content). When the soil is dry, the surface contact between particles is very small, but when the soil is wet, a film of water forms around each particle and heat can be transferred through the water when the films merge (Avissar and Verstraete, 1990). Over time, the change in soil temperature is proportional to the thermal conductivity and inversely proportional to the heat capacity, so thermal conductivity dictates the rate of heat transfer and heat capacity determines the change in temperature as a result of the heat transfer (Bonan 2008:132-133). Since the soil water content is a great determining factor here, improving the representation of this variable will improve the representation of thermal conductivity and the heat fluxes between the surface and underlying soil.

The influence of soil moisture on albedo is another reason for representing subgrid scale heterogeneity. Precipitation, soil type, and soil processes such as infiltration, runoff and the rate of evapotranspiration together define the soil moisture content and albedo. The soil albedo decreases with coarser particle sizes and with increasing soil wetness since radiation is trapped through multiple reflections between the particles and trapped by internal reflection in wet soils

(Bonan, 2008:200). In the absence of vegetation, surface conditions can be described by an emissivity, albedo, roughness parameter, soil conductivity, and soil moisture content, where these parameters greatly influence exchanges of heat and moisture between the atmosphere and ground by controlling the absorption of solar radiation, emission of thermal radiation, and the transfer of momentum (Avissar and Verstraete, 1990). Since the exchanges of moisture and heat greatly affect the atmospheric circulation, the non-local effect of soil moisture is evident as well as the importance of representing its spatial variability.

The availability of moisture at the soil surface dictates the Bowen ratio, so a good representation of the land surface hydrological features needs to be described (Avissar and Verstraete, 1990). The Bowen ratio is the ratio of SH to LH (SH/LH). When the ratio is less than one (greater than one), a greater portion of available energy is transferred to the atmosphere as LH (SH). Relative to dry soils, wet soils have a lower Bowen ratio, resulting in a moister and shallower PBL. Cooler surface temperatures from wetter soils, leads to smaller emissions of longwave (LW) radiation at the surface, and the higher moisture content in the PBL produces greater downwelling atmospheric LW radiation which is absorbed at the surface as the albedo decreases (Bonan 2008:218). In general, wetter soils will increase net radiation at the surface and increase the available energy that can be exchanged with the PBL, creating conditions favorable for convection and precipitation.

1.3 Soil Moisture Heterogeneity, Climate Change and the World

The increased frequency and severity of droughts due to climate change is a great concern for many regions of the world. Modeling the predictability of changes to water

resources is highly dependent on the representation of soil moisture. Aside from the oceans, soil moisture is another slowly varying component, which can influence weather through its impact on evaporation and other surface energy fluxes (Koster et al. 2004). A number of AGCM studies have shown that in continental mid-latitude summers, oceanic impacts on precipitation are minute relative to soil moisture impacts (Koster et al. 2000). The multi-model study by Koster et al. (2004), highlights regions where soil moisture has a strong coupling to precipitation. Results were based on an average of the ratio of ensemble variances for a dozen AGCM groups participating in two experiments conducted by the Global Land Atmosphere Coupling Experiment (GLACE) (figure 1.3a).

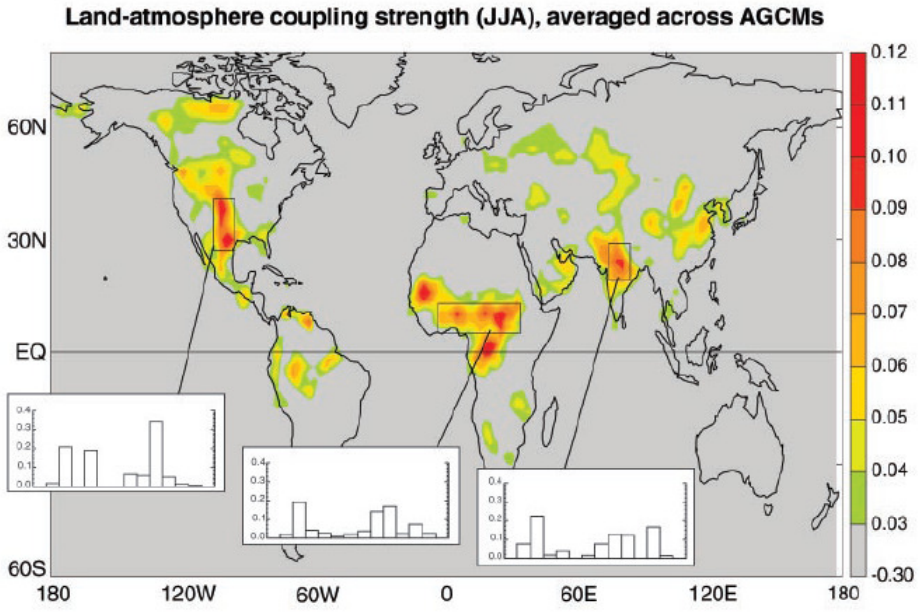

Figure 1.3a. Land-atmosphere coupling strength diagnostic for boreal summer showing "hotspot" regions (averaged across twelve models), where the impact of soil moisture on precipitation is the greatest. (insets) Areally averaged coupling strengths for the 12 individual models over the outlined, representative hotspot regions (Koster et al., 2004).

The "hotspots" highlighted in the figure 1.3a, are typically regions outside of the tropics or regions where evaporation is mostly controlled by net radiative energy. Unfortunately, many of these "hotspot" regions are located in densely populated areas, such as India and in regions

highly dependent on agriculture like the Great Plains of North America. Even though many regions of the world are not within the "hotspot" zones, water impacts will be felt in those locations through the scarcity of food or the sharing of water resources. Waterborne diseases as a result of changing water resources is another great concern, as changes in water flow impact interactions with sewage and other contaminants at the surface and below ground. Therefore, it is important to improve the representation of soil moisture heterogeneity in models to improve the predictability of possible societal impacts due to changes in water resources as a result of climate change.

1.4 The Nonlinear Relationship Between Soil Wetness and Evapotranspiration

There are many factors contributing to surface heterogeneity and these include vegetation, terrain, soil characteristics, and spatially varying climatology. Improving the representation of land surface heterogeneity is a continuing challenge and numerous studies have been done in this area. In the case of soil moisture and evapotranspiration, the highly nonlinear stress function relating the two parameters increases the difficulty in modeling, and using simple area averaging (bulk method) is not adequate. This can be expressed with equation 1.4a, where f is the nonlinear function of the heterogeneous variable x and an overbar is a grid area average.

$$\overline{f(x)} \neq f(\bar{x}) \qquad (1.4a)$$

Equation 1.4a states, the grid average of the effects of the heterogeneous variable x on the nonlinear function f is not equivalent to the grid average of the heterogeneous variable x applied to the nonlinear function f. Therefore, it is important to address the problems associated with current modeling of subgrid scale variability since numerical weather prediction models using a

grid spacing of 100 km or greater expect a subgrid-scale variability of soil moisture as large as the total amount of water potentially available in the soil (Wetzel and Chang, 1988), and additionally, estimations have shown that a forcing of approximately 10 W/m^2 (~10 mm per month in water flux) can produce significant climatic effects at the regional scale (Dickinson, 1992).

Currently, GCM's use the bulk approach for calculating evapotranspiration using a single soil moisture value for the entire grid area. At a given time, the value of the stress function relating the area averaged soil moisture value to evapotranspiration, such as the one used in the study by Sellers et al. (2007) (figure 1.4a), may be confined to one region of the curve as little or no precipitation is observed.

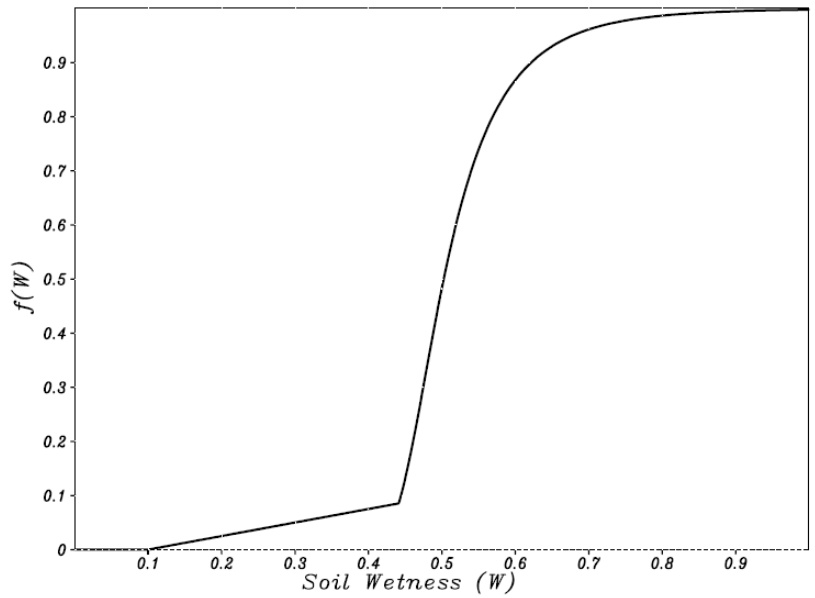

Figure 1.4a. Soil moisture stress function based on data from Colello et al. (1998), (Sellers et al., 2007).

When significant precipitation occurs (convective storm), the area averaged soil moisture value increases and the value of the stress function may change drastically as it is highly nonlinear, and causes inaccuracies in the calculation of evapotranspiration.

Studies have indicated a significant difference in evapotranspiration using spatially varying soil moisture over the bulk approach. Wetzel and Chang (1987, 1988) studied these impacts and found that with the bulk approach, evapotranspiration was (overestimated) and underestimated in (wet) and dry conditions when compared to an approach that used normally distributed soil moisture. In the study, during the spring and early summer, wet soils produced smaller evapotranspiration fluxes with spatially varying soil moisture leaving more water available for evapotranspiration during the dry summer. In a similar study, the macro scale hydrologic model used by Ronda et al. (2002), produced estimates of LH fluxes that were larger in dry conditions and lower in wet conditions (figure 1.4b).

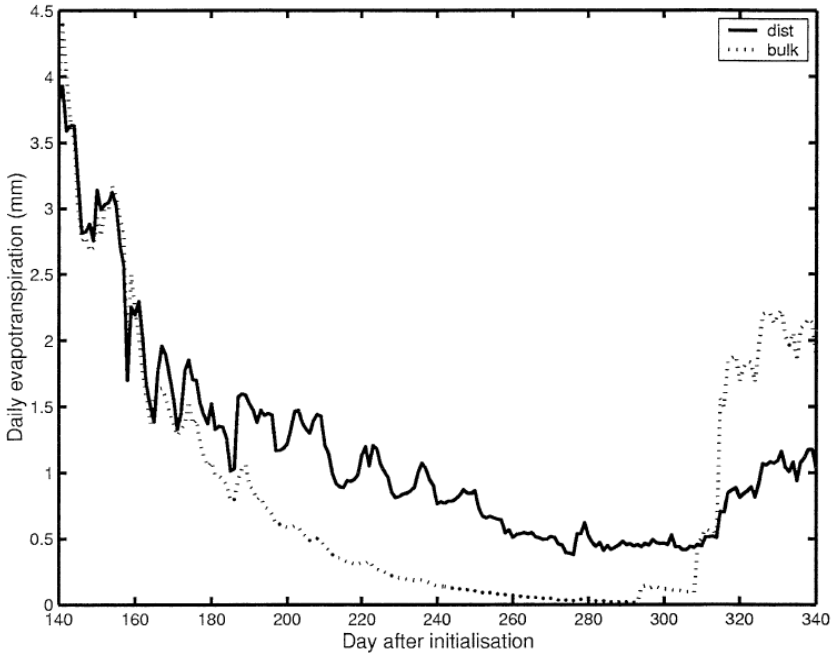

Figure 1.4b. Daily averaged evapotranspiration for the dry season and beginning of the wet season using atmospheric forcings obtained in Niger during the Sahelian Energy Balance Experiment (SEBEX) (Ronda et al., 2002).

With the incorporation of horizontally varying relative saturation over the grid cell using a quasi-distributed approach, the LH flux estimates from the bulk method approached zero at the end of the dry season, while the estimates from the quasi-distributed approach gradually decreased, and

with the onset of the wet season, bulk estimates were greater than those of the quasi-distributed approach.

A number of studies have focused on the role of soil moisture in controlling LH and SH fluxes. Most cases have shown a reduction in precipitation rates in continental interiors when surface evaporation rates were reduced (Sellers et al., 1997). Other studies have shown that runoff is very sensitive to soil moisture heterogeneity. Gedney and Cox (2003) demonstrated that runoff was underestimated when soil moisture was not allowed to vary spatially, and with the use of TOPMODEL, the topographically driven soil moisture heterogeneity increased runoff calculations.

1.5 Current Modeling Methods in the Literature

Clearly, the dynamics of soil moisture, runoff, surface LH and SH fluxes are especially affected by subgrid scale aggregation due to highly nonlinear relationships as discussed in the previous section. Current methods in the literature include tiling (patches) and representing the subgrid scale heterogeneity through integration of processes over analytical or empirical probability density functions (PDFs). Tiling methods assume that discrete homogeneous subregions can be identified to cover the grid area and surface calculations are done separately for each tile and aggregated through an average of the different tiles weighted by the fraction of area they cover, while PDF methods involve integration along intervals of the PDFs used to represent the surface heterogeneity (Giorigi and Avissar, 1997).

The binning approach for representing soil moisture heterogeneity (which is a variation of the tiling method) of Sellers et al. (2007), found that underestimations in grid area flux

calculations with simple area averaging decreased, since binning improved the sampling along the highly nonlinear function relating evapotranspiration and soil moisture (figure 1.5a).

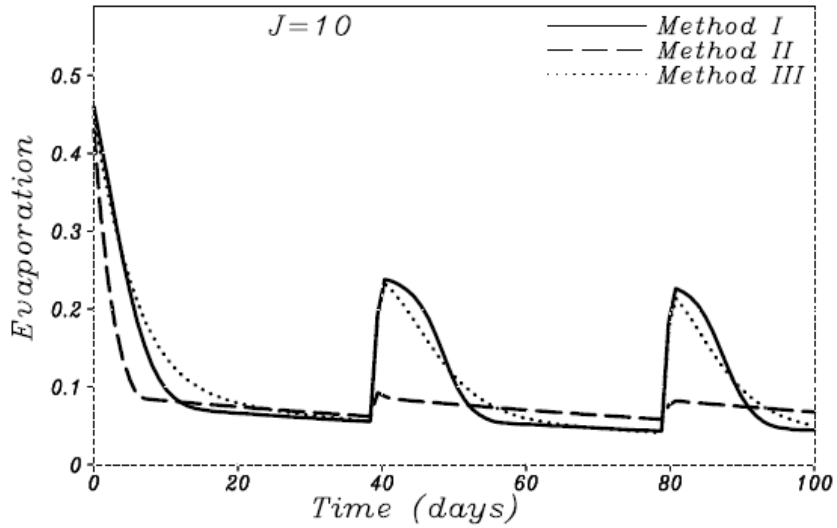

Figure 1.5a. Time series of grid area evapotranspiration, as calculated by method I (explicit method where 10^6 individual models define the grid area and fluxes are area averaged to give a single grid value), method II (Bulk Method), and method III (Binned, J=10 or ten individual models define the grid area and fluxes are area averaged to give a single grid value) initialized with a Gaussian soil moisture distribution and rainfall events on days 40 and 80 (Sellers et al., 2007).

In the study, the distribution of soil moisture was represented by binning and fractional areas were assigned to each bin. As the soil moisture distribution changed over time, that change was represented by a change in the fractional areas as bin values were unchanging in the study. Grid area fluxes were calculated by summing the bin flux values multiplied by their fractional areas. Ten bins was adequate for representing subgrid scale variability and with increasing bin size, results converged to those of the explicit method (method I). Other studies have used a variation of the tiled approach where different surface types are strongly coupled horizontally to produce a homogeneous interface. This approach is not always ideal since specific surface conditions can influence one another (e.g. a large cool and wet area can be influenced by the instability from a small hot and dry area) and cause errors in flux estimations (Giorigi and Avissar, 1997). Essery et al. (2002) studied the impacts of this tiling approach or aggregate method (different surface type resistances were added in parallel and used in single surface energy and moisture budgets

for each grid cell) and compared the results to a tiling approach where each tile was treated separately, and found that the tiling approach reduced evaporation and when coupling to a GCM, produced larger differences in surface fluxes when compared to the aggregate approach due to atmospheric feedbacks. In figure 1.5b, decreased LH fluxes in the tiled method resulted in a warmer and drier lower atmosphere, less cloud cover, an increased amount of downward short wave radiation and a reduction in longwave radiation.

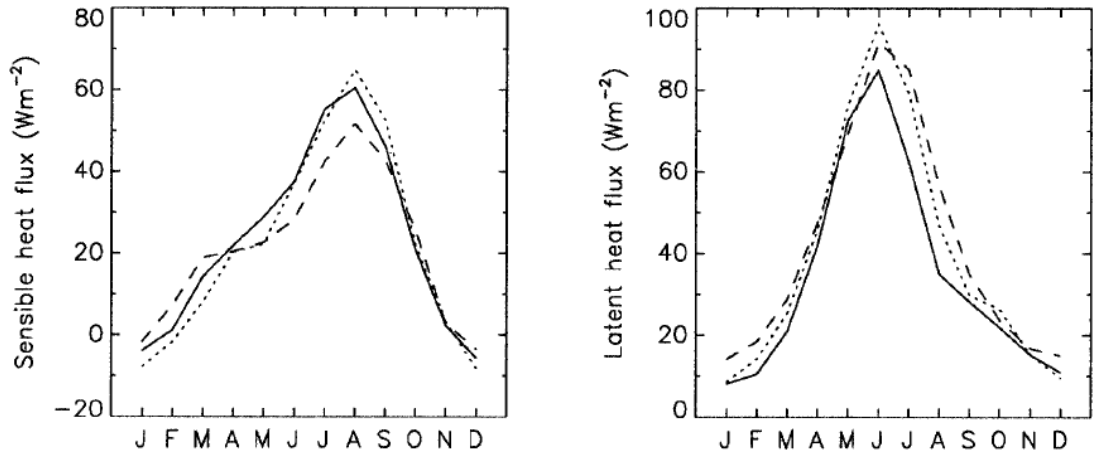

Figure 1.5b. HadAM3 GCM and MOSES 2 simulated surface energy fluxes for the tiled method (solid line), coupled aggregate model (dashed line) and off-line aggregate model (dotted line) for a grid box in Colorado (Essery et al., 2003).

Regardless of the method used for improving the representation of surface heterogeneity, an important factor missing from most studies is the lack of spatially varying meteorology. Using a spatially varying surface with area averaged meteorology does not completely describe the spatial variability. In the case of soil moisture heterogeneity, representing the distribution of spatially varying precipitation is very important, but ignored in GCMs.

Currently in GCMs, large scale (frontal or stratiform type) and small scale (convective type) precipitation is predicted as a grid area average or a single grid area precipitation value for every time step. The even distribution of large scale precipitation is adequate since precipitation rates are typically evenly distributed in those situations. However, evenly distributing small

scale precipitation is problematic and decreases the physical realism of thunderstorm events that only cover fractions of the grid area. When precipitation from a thunderstorm that covers say 15% of the grid area is evenly distributed over the entire grid, the rainfall rates are very light and mostly intercepted by the vegetation canopy, when in reality, 15% of the grid should be experiencing heavy precipitation that falls through the vegetation canopy and runs off or infiltrates the soil surface.

A study by Eltahir and Bras (1993) indicated that vegetation increased the surface roughness and the eddy transport of heat and water vapor near the surface, and as a result, evaporation of intercepted precipitation occurred at rates higher than potential evaporation. Additionally, in the study, the work of Dickinson and Henderson-Sellers (1988), which used BATS to evaluate the climatic impacts of the deforestation of the Amazon Basin was introduced, where simulated interception loss for the entire basin when compared to interception loss measured at a single basin site showed overestimations of about 150% (figure 1.5c). Dickinson (1989) explained that the overestimation of surface net radiation and a large canopy storage capacity were the sources for the high interception loss. However, in another study Shuttleworth and Dickinson (1989) suggested that a much more serious source of error was the neglect of spatial variability in rainfall. Other studies have shown that improving the areal distribution of precipitation alone alters the balance between evapotranspiration and runoff. Pitman et al. (1990) studied the impacts of precipitation distributions over tropical forest ecosystems. In the study, two experiments were conducted, one with grid area averaged precipitation and the second with only a fraction of the grid area receiving precipitation. Results showed that with improved precipitation distributions, the surface

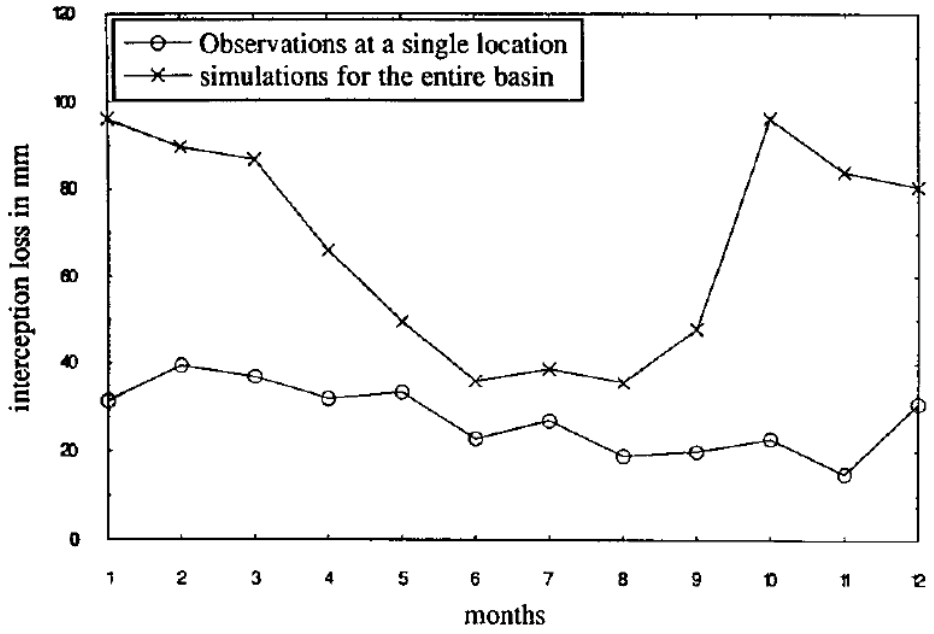

Figure 1.5c. Interception storage loss from simulations of Dickinson and Henderson-Sellers (1988) with the observations of Shuttleworth (1988a) (Eltahir and Bras, 1993).

climatology transitioned from an evaporative dominated regime to a runoff dominated regime. Even though the results from this study were also dependent on the hydrologic structure of the model, clearly there was a sensitive relationship between surface hydrology and precipitation distribution.

Some land surface models, such as, the Simple Biosphere Model (SiB), have implemented schemes to address precipitation dispersal. SiB has incorporated two precipitation distributions to differentiate between large scale and convective precipitation (figure 1.5d) Sato et al. (1989b). When convective precipitation occurs, the rate determines the fraction of the grid area that receives precipitation. This distribution performs better than simple area averaged and evenly distributed precipitation. Unfortunately, the precipitation that does reach the surface is then evenly distributed within the column, and does not completely capture the hydrological effects of

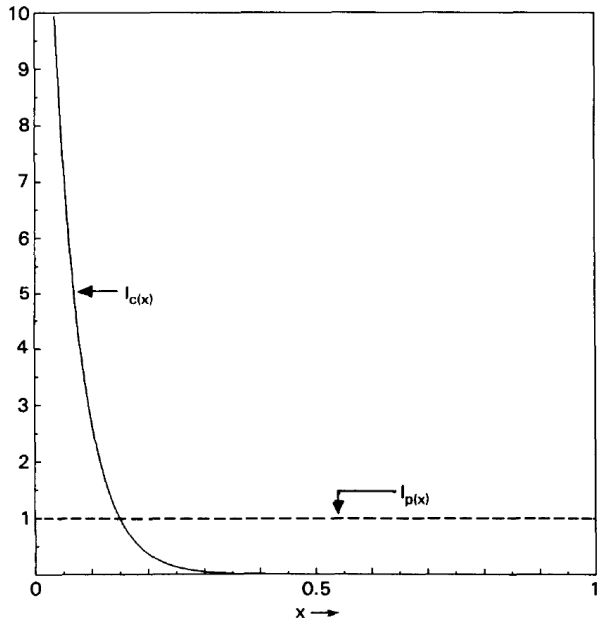

Figure 1.5d. Precipitation area-amount relationship used in SiB. The variable x refers to the fraction of the grid area; the variable I(x) refers to the relative amount of precipitation. Note that the large scale precipitation I_p(x) is almost invariant over the grid area while convective precipitation, I_c(x), is non-uniformly distributed (Sato et al., 1989b).

non-uniform precipitation. This is a problem that will be addressed in this study and is a problem with all GCM's. The distributions of precipitation over grid areas greatly affect the interception, runoff, surface and subsurface hydrology and the transport of LH into the atmosphere.

1.6 Focus for this Study

To mitigate the current sub-grid scale variability problem, the methods of Sellers et al. (2007) will be used with SiB to improve the representation of soil moisture heterogeneity and spatially varying precipitation. Sellers et al. (2007) introduced two binned methods for calculating grid area evapotranspiration fluxes and soil wetness. Binning was used to describe the soil wetness distribution and a spatially integrated stress term for the entire grid area was calculated by numerically integrating the stress function over the binned distribution, and used

for calculating single grid area fluxes (Sellers et al., 2007). Results were compared to the bulk method (currently in use with GCM's) and an explicit method, which was taken as the ideal method for representing sub-grid scale variability. For this study, all four methods will be applied to total plant available water (PawTot), which is a variable representative of the entire soil column containing roots. Binning will be used to describe the distribution of PawTot along the highly non linear stress curve (figure 1.6a), where each bin will represent an individual SiB model.

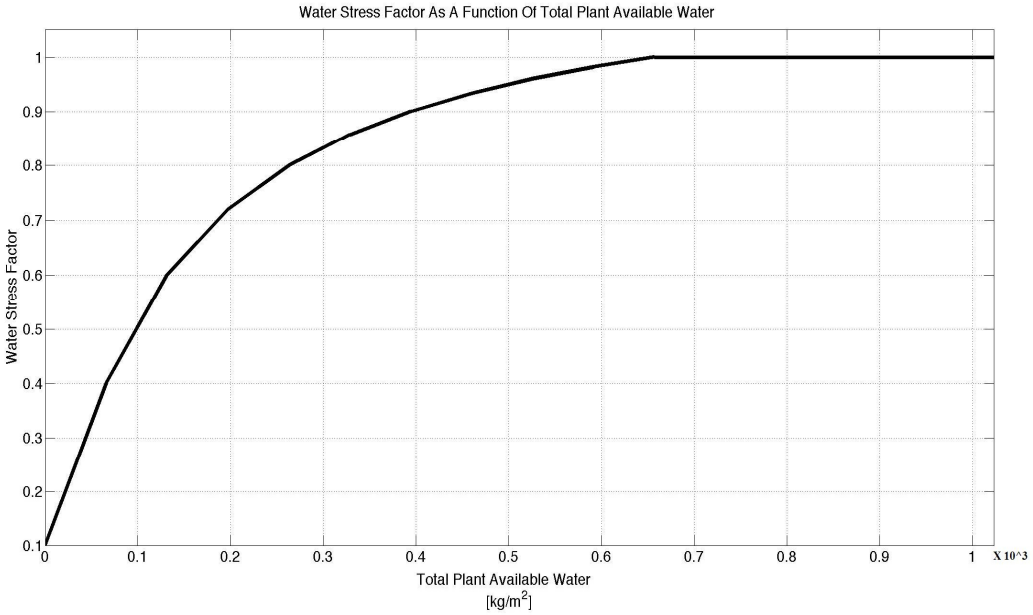

Figure 1.6a. Water stress factor as a function of PawTot for Oklahoma City, OK (SiB, biome 6).

Numerical integrations over the binned distribution will give single grid area fluxes. Spatially varying meteorology from observations and stochastically generated from the WGEN program (Richardson et al., 1984) will be randomly applied to the grid area, and all methods will be compared.

In this study, we hope to improve the representation of soil moisture heterogeneity and spatially varying precipitation at little additional computational cost to the bulk method. Chapter 2 gives a brief description of the models used in this study, methods are described in

chapter 3, results are discussed in chapter 4, and chapter 5 has concluding remarks as well as future work related to this research.

CHAPTER 2

Description of Models

Models used for this research will now be described. Section 2.1 is a brief overview of the Simple Biosphere Model (SiB), section 2.2 is a short presentation of the hydrology in SiB, and section 2.3 discusses the stochastic weather generating model, WGEN.

2.1 The Simple Biosphere Model (SiB)

The point by point (pbp) Simple Biosphere Model (SiB) version 3.0 is a third generation land surface model (LSM) that directly addresses the effect of vegetation on the interaction between the land surface and the atmosphere, by modeling the physiological and biophysical processes influencing radiation, momentum, mass and heat transfer (Sellers et al., 1997). SiB is comprised of ten soil layers, a single vegetation layer (vegetation phenology can be described with satellite data) with twelve different vegetation types available and an iterative photosynthesis-conductance model incorporated into the vegetation layer. All vegetation types have morphological, optical, and physiological time-invariant vegetation and ground parameters. An in depth model description can be found in Sellers et al., 1986, Sellers et al., 1996 a and b and Randall et al., 1996.

2.2 SiB Hydrology

To account for the hydrological effects of convective and large scale precipitation, two precipitation distributions are used in SiB. It is assumed that rainfall is distributed according to equation 2.2a and figure 2.2a, where $I_{c,p(X)}$ is the relative amount of convective (c) or large scale (p) precipitation as a function of the fractional area and the convective or large scale constants a_c, b_c, c_c, a_p, b_p, c_p (Sato et al. 1989b).

$$I_{c,p(X)} = a_{c,p} e^{-b_{c,p} X} + c_{c,p} \tag{2.2a}$$

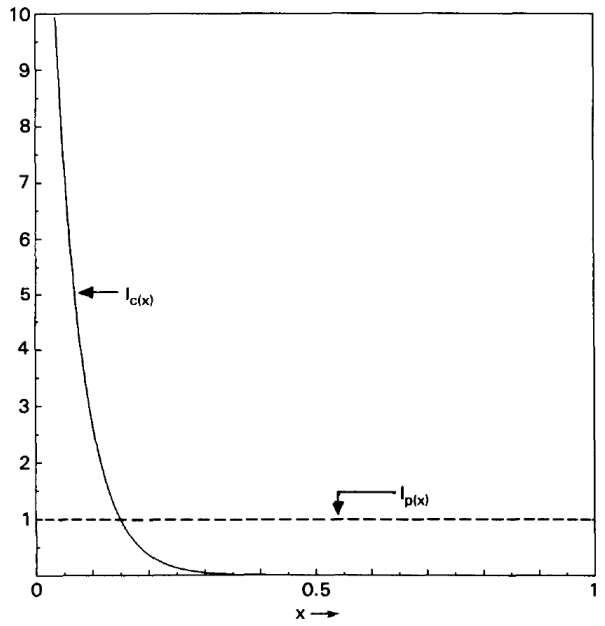

Figure 2.2a. Precipitation area-amount relationship used in SiB. $I_{(X)}$ is the relative amount of precipitation and X is the fraction of the grid area (Sato et al., 1989b).

Since both types of precipitation can occur together, the total amount of precipitation is given in equation 2.2b, where P is the total precipitation during a time step and P_c and P_p are convective and large scale precipitation rates (mm).

$$PI_{(X)} = (P_c a_c + P_p a_p) e^{-bX} + (P_c c_c + P_p c_p) \tag{2.2b}$$

The dynamics of precipitation intercepted by the vegetation canopy is described in figure 2.2b and equation 2.2c, where M_c is the amount of canopy interception, $PI_{(x)}$ is the precipitation, D_c is the water drainage rate, and the last term on the right hand side corresponds to an assumed

distribution of the precipitation for more realistic runoff (Sato et al., 1989b, Sellers et al., 1996 a, b, and c).

$$\frac{\partial M_c}{\partial t} = PI_{(x)} - D_c - \frac{E_{wc}}{P_w} \tag{2.2c}$$

Equation 2.2d describes the evaporation (λE_{ci}) rate from the wet portion of the vegetation canopy, where $e^*(T_c)$ is the saturation vapor pressure at the canopy temperature, *ea* is the

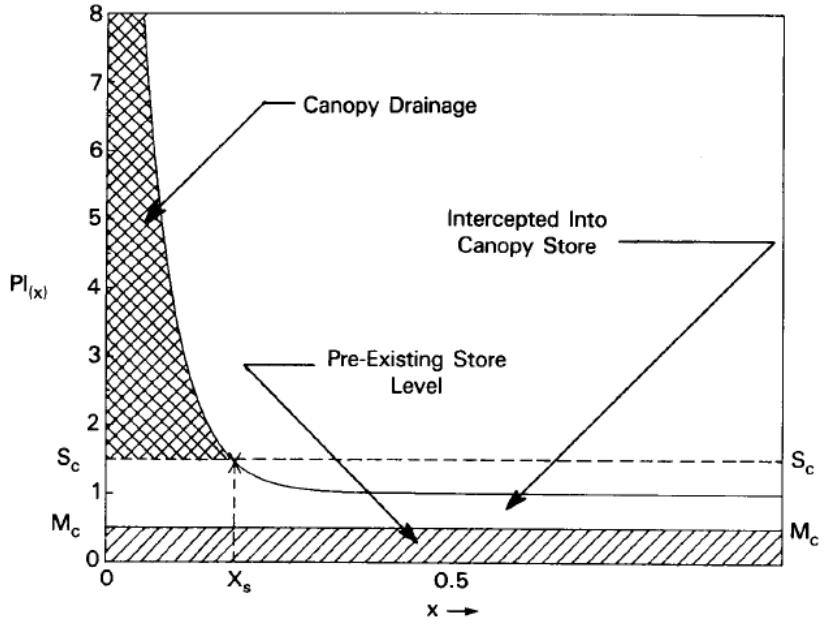

Figure 2.2b. Dynamics of precipitation intercepted by the vegetation canopy in SiB. Mc is water already stored on the canopy before precipitation interception and is uniformly distributed over the grid (hatched region). The integral of the water amount above Mc is the total amount of water intercepted by the canopy. Xs is the fraction of the grid area where intercepted rainfall added to the preexisting water storage (Mc) exceeds the canopy storage limit Sc. All water above Sc drains off the canopy and everything below Sc is added to the canopy interception store (Sato et al., 1989b).

canopy air space (CAS) vapor pressure, *rb* is the bulk canopy boundary layer resistance, ρ is the density of water, c_p is the specific heat of air and γ is the psychrometric constant.

$$\lambda E_{ci} = \frac{(e^*(T_c) - ea)}{rb} \frac{\rho c_p}{\gamma} \tag{2.2d}$$

The surface interception storage is calculated as the sum of the inputs (D_c) and the outputs (runoff, infiltration, evaporation). Evaporation from surface interception (λE_{gi}) is

calculated using equation 2.2e, where T_g is the ground temperature, r_d is the aerodynamic resistance between the ground and CAS, and w_g is the ground wetness fraction.

$$\lambda E_{gi} = \frac{e^*(T_g) - e_a}{r_d} \frac{\rho c_p}{\gamma} w_g \tag{2.2e}$$

Overland flow is generated for the fraction of the grid where the residual rainfall rate exceeds the local soil hydraulic conductivity.

Soil liquid will now be addressed (Dai et al., 2005). Infiltration, runoff, gradient diffusion, gravity and soil water extraction from roots for transpiration dictate the vertical soil moisture transport. Equation 2.2f is used to govern the evolution of soil water.

$$\frac{\partial w_{liq}}{\partial t} = -\frac{\partial q}{\partial z} - f_{root} \lambda E_{ct} + M_{i1} \tag{2.2f}$$

Here w_{liq} is the soil water mass (kg/m^2), f_{root} is the root fraction, M_{i1}, is the mass rate of melting (+) or freezing (-) of soil ice, and q is the water flow. Transpiration (λE_{ct}) is calculated using equation 2.2g, where g_c is the canopy conductance and w_c is the canopy wet fraction.

$$\lambda E_{ct} = \frac{e^*(T_c) - e_a}{(1/g_c) + 2r_b} \frac{\rho c_p}{\gamma} (1 - w_c) \tag{2.2g}$$

Darcy's law expresses the vertical flow within soil layers (equation 2.2h).

$$q = -K\left[\frac{\partial \psi}{\partial z} - 1\right] \tag{2.2h}$$

K is the hydraulic conductivity, ψ is the soil negative potential, and the +1 term accounts for gravitational drainage. The drainage of water out of the bottom of the soil column to create base flow is simply the hydraulic conductivity of layer ten (equation 2.2i), and any excess water from saturated soil layers is also added to base flow.

$$q_{10} = K_{10} \tag{2.2i}$$

Evaporation from the top soil layer (λE_{gs}) is calculated using equation 2.2j, where h_{soil} is the relative humidity of the soil pore space and r_{soil} is the soil surface resistance.

$$\lambda E_{gs} = \frac{h_{soil} e^{*}(T_g) - e_a}{r_{soil} + r_d} \frac{\rho c_p}{\gamma} (1 - w_g) \tag{2.2j}$$

There is no horizontal exchange of hydrological parameters between grid cells in SiB, and once a grid cell soil column has saturated, it is assumed that runoff flows directly into the ocean.

Soil moisture is predicted from an unevenly spaced layers model. A tridiagonal system of equations results when Darcy's law is integrated over the layer thicknesses (the temporal variability in water mass needs to equal the net flow across the bounding interfaces plus the rate of internal source or sink) and water flow terms across layer interfaces are linearly expanded with first order Taylor expansion. Surface and subsurface runoff is calculated separately over saturated and unsaturated areas. The saturated fraction is dependent on a non-dimensional water table depth and a constant topographic feature that governs the soil moisture state. Saturation excess runoff (Dunne runoff) and runoff that is proportional to the soil moisture state at the surface in the unsaturated part make up surface runoff. Finally, subsurface or base flow is comprised of bottom drainage and saturation excess runoff. Water balance is maintained in SiB using equation 2.2k, where P is precipitation, Ev is evapotranspiration, R is surface and subsurface runoff, $dqsoil$ is the change in soil water, $dqsnow$ is the change in snow, and $dqstor$ is the change in canopy and surface interception storage.

$$water\_balance = P - (Ev + R) - (dqsoil + dqsnow + dqstor) \tag{2.2k}$$

2.3 WGEN

The WGEN program generates daily values of precipitation (inches), maximum temperature (°F), minimum temperature (°F), and daily averaged short wave radiation (ly) with two user options (Richardson and Wright, 1984). With the first option, daily values of the four variables are produced for a specified number of years with program supplied statistical data, and with option two, the program reads user supplied values of precipitation and the three other variables are calculated based on the user and program supplied data. Using option one for this study, the model first generates precipitation as an independent variable, while the other three variables are calculated based on the wet or dry status of the day. Generated variable values will be close to monthly means obtained from actual data, however, due to temporal and spatial smoothing from the model or topography and other factors, a correction procedure is offered for temperature and precipitation output.

The wet or dry status of each day is determined using a first-order Markov chain model and the precipitation amount on a wet day is generated using a two-parameter gamma distribution. The Markov chain model only depends on the precipitation status of the previous day (wet or dry), where a wet day is defined as a day with a rainfall measurement greater than or equal to 0.01 inches (Haan, 1977). Finally, the procedure for generating daily values of short wave radiation, maximum and minimum temperatures is based on the weakly stationary generating process (Matalas, 1967).

CHAPTER 3

Methods

To mitigate the current sub-grid scale variability problem, the methods of Sellers et al. (2007) will be used with SiB to improve the representation of soil moisture heterogeneity and spatially varying precipitation. Section 3.1 is a brief overview of the methods of Sellers et al. (2007), Section 3.2 discusses the meteorological drivers developed for this study, and section 3.3 applies the methods to SiB.

3.1 The Methods of Sellers et al. (2007)

In the study by Sellers et al. (2007), evapotranspiration (E) was only a function of a constant potential evapotranspiration (Ep) and a stress function that only depended on soil wetness ($f(W)$) (equation 3.1a).

$$E = Epf(W) \tag{3.1a}$$

The stress function that related evapotranspiration to soil wetness is presented in figure 3.1a.

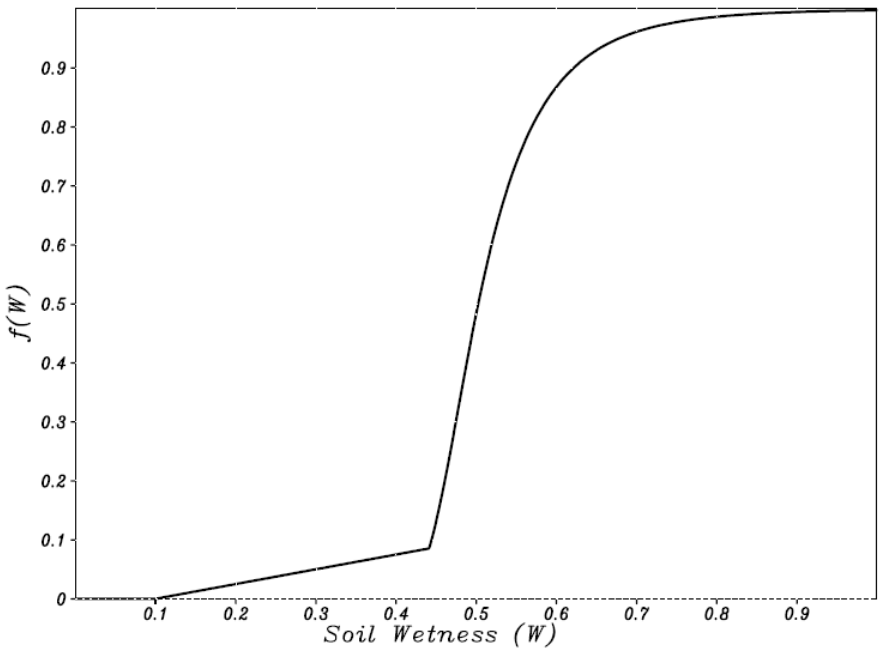

Figure 3.1a. Soil moisture stress function based on data from Colello et al. (1998) (Sellers et al., 2007).

Four methods were used to calculate grid area evaportranspiration rates and soil wetness for an arbitrary grid area normalized to an area of unity. The methods included the explicit method, bulk method, binned method, and an alternative binned method. The idea was to improve the sampling along the highly nonlinear curve of the stress function when calculating grid area evapotranspiration rates and soil wetness at little additional computational cost to the bulk method.

The explicit method is the best way to represent soil wetness heterogeneity and accurately calculate grid area evapotranspiration rates. With this method, the grid area was divided into 10^6 cells each represented by a soil wetness value from the initial Gaussian distribution and a highly simplified model introduced in equation 3.1a. For every time step, 10^6 calculations were performed and area integrated to give a single grid area value (equation 3.1b).

$$E = Ep\int_A f(W)da \tag{3.1b}$$

Obviously this method is computationally expensive and is not practical for global GCM simulations.

The bulk method, which is currently used in GCM's, poorly samples the highly nonlinear curve as only a single soil wetness value $<W>$ is used to represent the grid area distribution. The single soil wetness value may settle the stress function value onto the most nonlinear part of the curve, and when precipitation events occur, the new area averaged soil wetness value moves the initial stress function value to another part of the curve, causing inaccuracies in grid area calculations (equations 3.1c and d).

$$E = Epf(<W>) \tag{3.1c}$$

$$<W> = \int_A W da \tag{3.1d}$$

In the study, only a single grid area calculation was needed for every time step, making it computationally cheap. Unfortunately, this method did not resolve the subgrid-scale variability and caused inaccuracies in the calculation of grid area fluxes.

A binned method is now introduced, which avoids the computational inaccuracies represented in the bulk method, and the high computational cost of the explicit method. With this method, the initial soil wetness distribution was binned into J bins of equal range (1.0/J) (where 1.0 means completely saturated), and an additional bin was used for a soil wetness value of zero. When J was equal to ten, the soil wetness bin intervals were 0-0.1, 0.1-0.2, 0.2-0.3, …0.9-1.0 and an additional bin for 0. The average soil wetness value for the jth bin (W_j) was represented by the midpoint value of the jth bin interval, so the soil wetness value for j=1 was 0.05, j=2 was 0.15, etc. Binning the initial soil wetness distribution assigned fractional areas (a_j) to the bins, and as the soil wetness distribution changed over time, that change was reflected in

the fractional area as bin values were unchanging. Grid area fluxes were calculated using equation 3.1e.

$$E = Ep\sum_{j=1}^{J} f(W_j)a_j \tag{3.1e}$$

The conservation of relative area (equation 3.1f) and the conservation of water (ignoring runoff) (equation 3.1g) were two laws maintained in the study.

$$\sum_{j=1}^{J} a_j = 1.0 \tag{3.1f}$$

$$\frac{d}{dt}\left[\sum_{j=1}^{J} W_j a_j\right] = P - E \tag{3.1g}$$

For every time step, new fractional areas were calculated as the soil wetness distribution changed. Assuming uniform precipitation and evapotranspiration, the change in the soil wetness midpoint value was calculated using equation 3.1h.

$$\delta W_j = (-Epf(W_j) + P)\Delta t \tag{3.1h}$$

To incorporate the change into the soil wetness distribution at (t + Δt), the soil wetness bin values that bracketed the new soil wetness value for the jth bin were determined with equation 3.1i.

$$W_k < W_j + \delta W_j < W_{k+1} \tag{3.1i}$$

In equation 3.1i, the subscript *k* represents the bin number that now brackets the new interim soil wetness value for the jth bin. New fractional areas corresponding to (t + Δt) were calculated in a separate array b_k, where $k = 1,J$ and b_k values initialized to zero at the beginning of each time step. The new fractional areas for each bin were calculated using equations 3.1j, 3.1k and 3.1l.

$$b_k = b_k + (1 - H)a_j \tag{3.1j}$$

$$b_{k+1} = b_{k+1} + Ha_j \tag{3.1k}$$

$$H = \frac{((W_j + \delta W_j) - W_k)}{(W_{k+1} - W_k)} \tag{3.1l}$$

For every time step, equations 3.1h, 3.1i, 3.1j, 3.1k, and 3.1l were completed for all bins (j=1,J).

A modified version of the explicit method is introduced as the alternative binned method. In the binned method, changes to the soil wetness distribution were reflected in changes to the fractional areas representing the bins. With the alternative binned method, fractional areas remained unchanged and the soil wetness distribution for each fractional area was allowed to change over time. With ten bins, the original soil wetness distribution (10^6 values) was sorted and beginning with the wettest values down to the driest values, every 10^5 values were averaged (this gave 10 soil wetness values). The grid area was divided into ten equal fractional areas and each fractional area was assigned an averaged soil wetness value and defined by the highly simplified model presented in equation 3.1a. As in the binned method, grid area fluxes were calculated using equation 3.1e, but over time soil wetness values changed and fractional areas remained unchanged.

3.2 Atmospheric Forcing Adjustments

In the current study, SiB models were forced with meteorology from observations and the WGEN program (Richardson and Wright, 1984). SiB meteorological drivers contain thirty minute observations giving a total of 48 observations per day and 1488 observations for a 31 day month. Atmospheric boundary conditions in SiB drivers include air temperature (K), vapor pressure (Pa), atmospheric surface pressure (Pa), wind speed (m/s), short wave radiation (W/m^2), long wave radiation (W/m^2) and convective and large-scale precipitation (mm/s). To facilitate two meteorological experiments for three biomes used in this study, 100 SiB meteorological

drivers were created for each biome. The WGEN program was used to produce 100 instances of July meteorology for each biome, and twelve years of ARM site observations for the month of July were then adjusted to WGEN variable outputs to create the meteorological drivers.

WGEN daily values of precipitation (inches), maximum temperature (°F), minimum temperature (°F), and daily averaged short wave radiation (ly) were converted to the appropriate units before adjusting the driver observations. The observed minimum and maximum daily temperatures were adjusted to WGEN output, and the remainder of the temperatures for that day, were adjusted to fit between the new minimum and maximum temperatures without any unrealistic jumps. Short wave radiation was adjusted by multiplying the observed short wave radiation values by the ratio of the WGEN daily averaged short wave radiation to the observed daily averaged short wave radiation. Precipitation had a total of three possible adjustments, the first was for the case of observed precipitation and precipitation generated by WGEN, the second was for the case of observed precipitation and no precipitation generated by WGEN, and the third was for the case of no observed precipitation and precipitation generated by WGEN. For the first case, adjustments were made by multiplying the observed precipitation values by the ratio of daily WGEN precipitation to the daily sum of observed precipitation, case two required setting the values of observed precipitation to zero and the third case divided daily WGEN precipitation by four, creating a two hour precipitation event that occurred at a randomly chosen time of the day. Despite the different precipitation rates and times of occurrence, all drivers received the same amount of monthly precipitation.

The set of 100 newly created drivers was used for a highly spatially varying meteorological experiment. For the second experiment, six drivers out of the 100 newly created drivers were randomly chosen to create a second set of drivers where each of the six drivers

represented a random fraction of the second set of 100 drivers (fractions of the drivers are the same driver). With the second set of drivers, fractions of the grid area received the same meteorology. To avoid sub-grid scale variability within sub-grid scale variability, only the large scale precipitation distribution option in SiB was used in this study.

3.3 Applying the Methods to SiB

In this section, the applicability of the methods of Sellers et al. (2007) with SiB is presented. Section 3.31 is a brief discussion on the diagnostic variable that was used to apply the methods, and sections 3.32, 3.33, 3.34, and 3.35 describe the explicit, bulk, binned, and alternative binned method respectively.

3.31 Diagnostic Variable for Method Applicability

Model complexity is the reason for the difficulty of applying the methods discussed in section 3.1 to a land surface model. The simple toy model presented in section 3.1 only had a single soil layer and no vegetation. SiB, on the other hand, is a model with ten soil layers that interact with the vegetation canopy. Total plant available water (PawTot, kg/m^2) is a SiB variable that is dependent on the saturation of the soil column and is used to diagnose the water stress for the vegetation canopy, and as the soil column saturation evolves over time, this is reflected in PawTot. Therefore, PawTot was the diagnostic variable used for applying the methods.

For the calculation of PawTot in SiB, plant available water (Paw, volumetric) is first calculated for soil layers ($i=1,I$) containing roots using equation 3.31a.

$$Paw_i = \left[\frac{W_i}{(dz_i)(\rho_{H_2O})} \right] - wp \tag{3.31a}$$

In equation 3.31a, wp is the wilting point (volumetric), ρH_2O is the density of water (1000 kg/m^3), W_i is the soil water mass per unit area (kg/m^2) for the *ith* soil layer, and dz_i is the depth of the *ith* soil layer (m). PawTot is then calculated using equation 3.31b.

$$PawTot = \sum_{i=1}^{I} (Paw_i)(dz_i)(\rho H_2O) \tag{3.31b}$$

The fraction of PawTot (PawFrac, unit less) that is available to plants is calculated as the ratio of PawTot to the maximum amount of PawTot (PawMax, kg/m^2) using equations 3.31c and d, where fc is the field capacity (volumetric).

$$PawFrac = \frac{PawTot}{PawMax} \tag{3.31c}$$

$$PawMax = \sum_{i=1}^{I} (fc - wp) dz_i \tag{3.31d}$$

Finally, the function relating PawTot to stress is calculated using equation 3.31e where S is the shape parameter having a value of 0.2.

$$Stress = \frac{(1+S)(PawFrac)}{(S + PawFrac)} \tag{3.31e}$$

For a completely dry soil column up the wilting point (WP), the stress function has a value of 0.1, and from field capacity (FC) to a completely saturated soil column, the value is 1.0. Water stress is maximized when the value approaches 0.1 and there is no stress at and beyond FC.

The methods of Sellers et al. (2007) were used to improve the sampling along the highly nonlinear curve relating soil wetness to stress (figure 3.1a), but for the current study, the methods

were used to improve the sampling along the highly nonlinear curve relating water stress to PawTot, such as the curve for SiB- biome 6 in figure 3.31a.

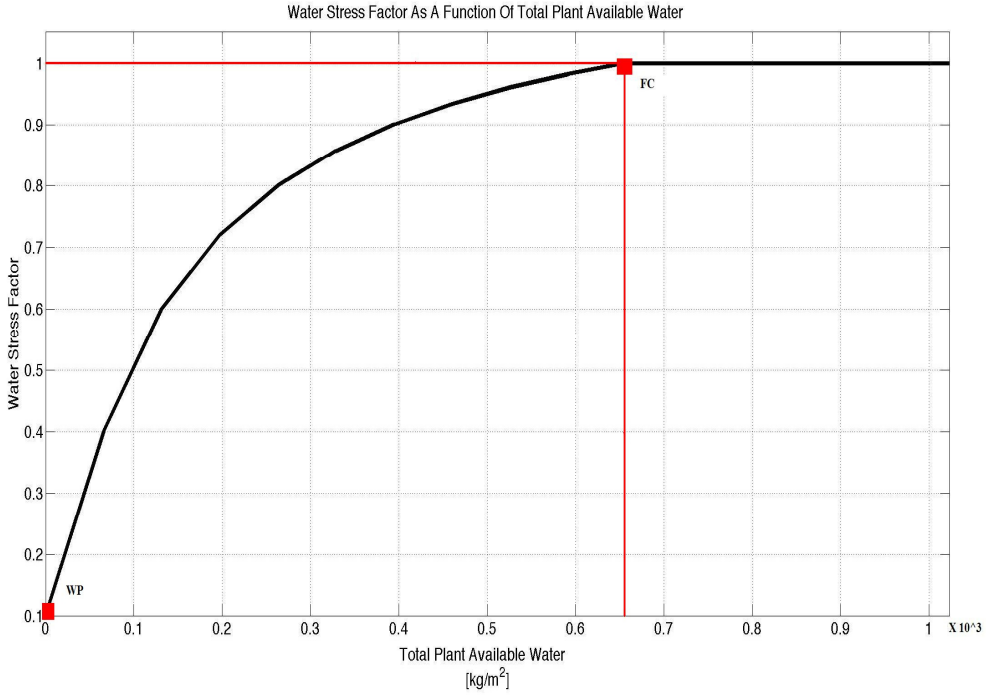

Figure 3.31a. Water stress factor as a function of PawTot for SiB-biome 6 (Oklahoma City, OK).

Using PawTot as the diagnostic variable, the methods described in section 3.1 were used to improve the representation of spatially varying PawTot and grid area fluxes as two meteorological experiments were conducted.

Methods were applied to three SiB Biomes to test the applicability in a dry (biome 9), semi-arid (biome 6) and wet biome (biome 3). Biome 9 is a broadleaf shrub and bare soil biome forced with meteorology from Phoenix, AZ with a total of 50.8 mm of precipitation for the duration of the study, biome 6 is a short vegetation/C4 grassland forced with meteorology from Oklahoma City, OK with a total of 152.4 mm of precipitation for the duration of the study, and biome 3 is a broadleaf and need leaf tree biome forced with meteorology from Baton Rouge, La with a total of 302.77 mm of precipitation for the duration of the study. In the following four

sections, the methods are described in biome 6 and the other two biomes have identical experimental set ups.

3.32 Explicit Method

An arbitrary grid area normalized to an area of unity (1.0) was divided into 100 cells of equal area and randomly initialized with a Gaussian PawTot distribution (figure 3.32a). In the initial distribution, all stress values were on the most nonlinear part of the curve bounded by water stress values of 0.5895 and 0.6031 (figure 3.31a). Each cell in the grid was represented by a SiB model with a soil column saturation representative of the PawTot value for that cell. Two meteorological experiments were conducted over the

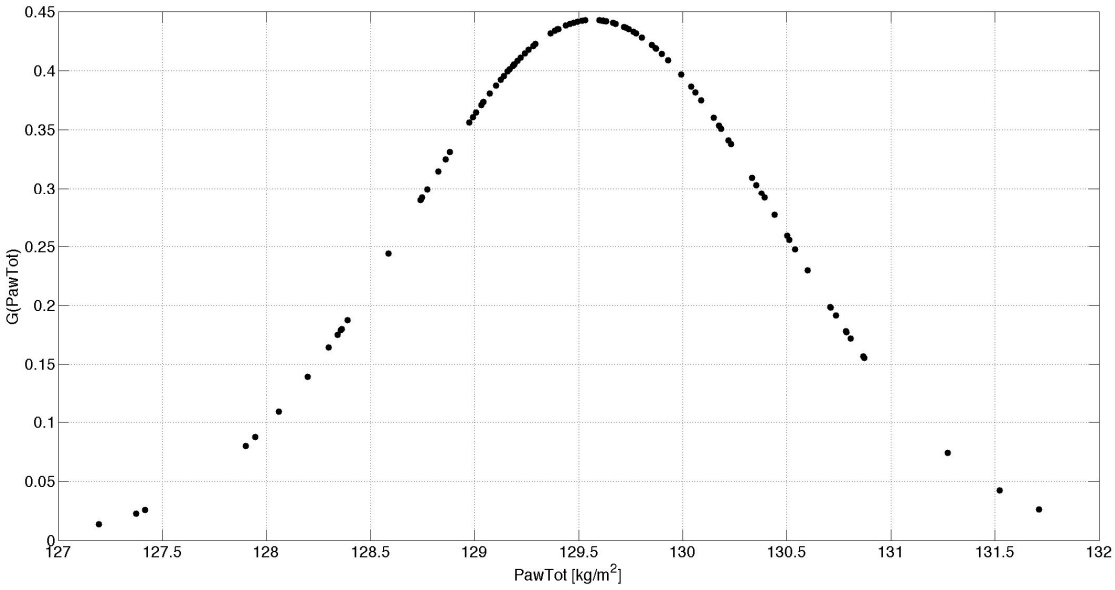

Figure 3.32a. Initial Gaussian distribution of PawTot centered on a mean value of 129.5693 kg/m^2 for SiB-biome 6 (Oklahoma City, OK).

grid area and the results from these experiments were taken as the explicit representation of sub-grid scale variability and used as the standard for judging the other methods.

For the first meteorological experiment, fractions of the cells received the same meteorology representative of convective storm events covering fractions of the grid area (fractional area distribution), and in the second experiment every cell received different meteorology, creating high spatial variability (highly spatially varying distribution). The two sets of drivers used for these experiments are described in section 3.2. For every single driver in both experiments, daily precipitation events were forced to occur on randomly selected SiB models rather than the distribution used in Sellers et al. (2007), which distributed precipitation events over a fraction of each bin. This distribution of precipitation was chosen because of its resemblance to the stochastic nature of precipitation events, which are not limited to specific regions of the grid area. Other forcings associated with the precipitation events also forced the randomly chosen SiB models. The same set of drivers in both experiments were used for the two month (62 day) duration of the study (July drivers were also used to force August) and for every time step (ten minute time step with hourly output) 100 individual model runs took place and grid area calculations were performed using equation 3.32a.

$$Grid\_Area\_Fluxes = \int_A (SiB\_Output)da \tag{3.32a}$$

Fractional areas remained constant for the experiment and the state of each cell was allowed to evolve over time. Individual cell fluxes and runoff did not interact with neighboring cells and were assumed to go directly into the atmosphere and ocean respectively.

3.33 Bulk Method

The initial PawTot distribution used in the explicit method was area averaged to give a single PawTot value for the entire grid area (equation 3.33a).

$$< PawTot >= \int_A (PawTot) da \tag{3.33a}$$

The grid area was defined by a single SiB model with a soil column saturation representative of the area averaged PawTot value, and was forced with area averaged meteorology (100 drivers averaged) for both meteorological experiments. This method only required a single model run for every time step and grid area calculations are expressed in equation 3.33b.

$$Grid\_Area\_Fluxes = SiB\_Output \tag{3.33b}$$

This method is currently used in GCM's and is very cheap computationally when compared to the explicit method.

3.34 Binned Method

The binned method is introduced to improve the sampling along the highly nonlinear stress curve (figure 3.31a) at a cheaper computational cost than the explicit method. The idea is to always have two bins represent the endpoints, that is a bin for the WP and the saturated end, two bins to always represent the interval between the FC and saturated end, and a varying number of bins to represent the highly nonlinear interval between the WP and FC. The number of bins that represent the interval between the WP and FC will depend on the number of bins the modeler chooses to use. Therefore, if the modeler chooses to use ten bins (total of 12 bins) the number of bins between the WP and FC will equal eight and if twenty bins are used (total of 22 bins) there will be 18 bins between the WP and FC. When using ten bins (total of 12 bins), the interval between the WP and FC is divided into eight intervals and the interval between the FC and saturated end is divided into two intervals. Bin values are represented by the midpoint

values for those bin intervals. Finally, the two endpoints have bin values of 0.0 for the WP, and the saturated PawTot value (varies for different biomes) for the saturated bin.

For the binned method, the initial PawTot distribution was binned into J number of bins and fractional areas (a_j) were assigned to each bin. The grid area was represented by J SiB models each with a soil column saturation representative of their midpoint PawTot value, and for every time step grid area calculations were made using equation 3.34a.

$$Grid\_Area\_Fluxes = \sum_{j=1}^{J} (SiB\_Output)_j a_j \tag{3.34a}$$

As the PawTot distribution changed over time, the change was reflected in the fractional area as the bin values were unchanging in this method. Over a time step, the conservation of relative area (equation 3.34b) and the conservation of water (equation 3.34c) were two laws that were maintained.

$$\sum_{j=1}^{J} a_j = 1.0 \tag{3.34b}$$

$$\Delta\left[\sum_{j=1}^{J} PawTot_j a_j\right] = \Delta\left[PawTot(P - Ev - R)_{(Grid\_Area)}\right] \tag{3.34c}$$

Rearranging equation 3.34c into equation 3.34d tells us that over a time step, the change in the grid area PawTot as a result of the change in the grid area water balance (right hand side (RHS)) is equal to the change in the grid area PawTot value (left hand side (LHS)), where on the LHS, that change is reflected in the fractional areas as PawTot bin values are unchanging.

$$\begin{aligned}&\left[\sum_{j=1}^{J} PawTot_j a_{j(old)}\right] - \left[\sum_{j=1}^{J} PawTot_j a_{j(new)}\right] = \\ &\left[PawTot(P - Ev - R)_{(Grid\_Area)}\right]_{(old)} - \left[Pawtot(P - Ev - R)_{(Grid\_Areas)}\right]_{(new)}\end{aligned} \tag{3.34d}$$

For the two month (62 day) duration of this study, fractional areas were updated only at the end of every day (hour 24), and new fractional areas were used for grid area calculations on the

following day. To incorporate changes to the midpoint bin values for the next day, the bin values bracketing the new bin value were determined using equation 3.34e.

$$PawTot_k < PawTot_j + \delta PawTot_j < PawTot_{k+1} \tag{3.34e}$$

In equation 3.34e, the subscript k represents the bin number that now brackets the new interim PawTot value for the jth bin. New fractional areas corresponding to (t + Δt) were calculated in a separate array b_k, where $k = 1, J$ and b_k values were initialized to zero at the beginning of each time step. The new fractional areas for each bin were calculated using equations 3.34f, 3.34g and 3.34h.

$$b_k = b_k + (1 - H)a_j \tag{3.34f}$$

$$b_{k+1} = b_{k+1} + Ha_j \tag{3.34g}$$

$$H = \frac{((PawTot_j + \delta PawTot_j) - PawTot_k)}{(PawTot_{k+1} - PawTot_k)} \tag{3.34h}$$

After calculating the new fractional areas, the soil column saturation distribution at hour 24 for each bin was adjusted to reproduce the PawTot bin values for initializing the next day (PawTot bin values are unchanging in this method). For the adjustments, the soil water profile remained the same (shape), but was multiplied by a factor, which increased or decreased the saturation based on the PawTot bin value needed for that bin. At hour 24 for each day, equations 3.34e, 3.34f, 3.34g, and 3.34h and the soil column saturation adjustment were completed for all bins ($j=1,J$).

For both precipitation experiments, daily meteorology was distributed based on the percentage of SiB models that received precipitation in the explicit method, where that percentage was multiplied by the number of bins being used, and that value rounded to the nearest integer equaled the number of SiB models that were randomly chosen to receive

precipitation. For example, if twenty SiB models out of 100 receive precipitation in the explicit method and ten bins are being used (total of 12 bins), then 2 bins (nearest integer to 2.4) receive precipitation. The precipitation rates for every time step were based on the total fractional area occupied by the bins and the area average precipitation, and the other meteorological forcings were an average of the wet forcings from the explicit method. The remaining bins received meteorology that was an average of the dry forcings used for the dry SiB models in the explicit method.

3.35 Alternative Binned Method

The alternative binned method is a modified version of the explicit method, where the PawTot distribution is allowed to change over time and that change is not reflected in the fractional areas as they are unchanging in this method. The initial PawTot distribution is sorted and averaged based on the number of bins the modeler chooses to use. Using ten bins, every ten values of the sorted PawTot values were averaged giving ten PawTot values representative of the driest bin up to the wettest bin. The grid area was then divided into ten equal fractional areas and each fractional area was represented by a SiB model having a soil column saturation representative of its assigned averaged PawTot value. As in the binned method, grid area fluxes were calculated using equation 3.34a, but fractional areas remained unchanged over time.

For both precipitation experiments, daily meteorology was distributed as it was in the binned method, based on the percentage of SiB models that received precipitation in the explicit method, where that percentage was multiplied by the number of bins being used, and that value rounded to the nearest integer equaled the number of SiB models that were randomly chosen to

receive precipitation. Precipitation rates for every time step were based on the total fractional area occupied by the bins and the area average precipitation, and the other meteorological forcings were an average of the wet forcings from the explicit method. The remaining bins received meteorology that was an average of the dry forcings used for the dry SiB models in the explicit method.

CHAPTER 4

Results

Results from the binned, alternative binned, and bulk method will be compared to the explicit method for the two precipitation experiments. Section 4.1 discusses results from the fractional area precipitation distribution, section 4.2 focuses on the highly spatially varying precipitation distribution, and figures from this chapter are in section 4.3.

4.1 Fractional Area Precipitation Distribution

4.11 Total Plant Available Water (PawTot) and Stress

Figures 4.11a, b and c (figures are at the end of the chapter) are time series of grid averaged rainfall and PawTot for all methods in biomes 9, 6 and 3 respectively. In panels A2, B2 and C2 PawTot for the bulk, alternative binned and explicit method were initialized at the same averaged value. However, initialization for the binned method varied and depended on the bin size. When the initial PawTot distribution was binned, bin midpoint values were used rather than the average of the initial distribution in order to apply the scheme from section 3.34. Unfortunately, the average of the initial distribution was either higher or lower than the average of the bin midpoint values representing the distribution. This resulted in drier and wetter grid

averaged PawTot time series relative to the explicit method, where some of the drier time series were drier than the bulk method.

In addition to the initialization issue, time series of grid averaged PawTot in the binned method indicated periods of no precipitation when precipitation did occur (e.g. panel A2 hour 800 for binned 10) and periods that seemed like more precipitation than what actually occurred (e.g. panel B2 hour 1400 for binned 50) relative to the explicit method, all as a result of the precipitation distribution. As mentioned in section 3.34, daily precipitation events occurred on randomly chosen bins where rainfall rates were determined based on the fractional area occupied by the bins and the grid averaged rainfall rate. Since fractional areas in the binned method varied over time, the total fractional area occupied by the randomly chosen bins to receive precipitation was either greater or smaller than the fractional area that received precipitation in the explicit method. When the total fractional area that received precipitation in the binned method was larger (but not as large as the total grid area as in the bulk method) than the area that received precipitation in the explicit method, rainfall rates were lighter than in the explicit method, but heavier than in the bulk method. This increased canopy interception and rainfall that reached the surface infiltrated a larger area relative to the explicit method, which resulted in a higher grid averaged PawTot value as the wet fractional area in the binned method had a greater contribution to the grid average than the wet fractional area in the explicit method. When the total fractional area occupied by the wet bins was much smaller than the fractional area in the explicit method, rainfall rates were very heavy, water was mostly lost to runoff, and water that did infiltrate the surface contributed very little to the grid average since the fractional area was very small. The precipitation distribution could have been changed to select bins that had fractional areas that

occupied the same area occupied by the bins in the explicit method, but this would have decreased the physical realism of the stochastic nature of precipitation events.

The alternative binned method performed the best in all biomes, where absolute errors (defined here as the absolute value of the difference between an explicit method grid value and the equivalent grid value from the other methods) for PawTot did not exceed 3 (kg/m^2). As expected, with an increased bin size, time series converged to the explicit method. The precipitation distribution in this method was not problematic, since precipitation that fell on the total fractional area occupied by the wet bins was much closer to the total fractional area occupied by the wet bins in the explicit method (fractional areas remained constant with this method). In all biomes, the bulk method showed a drier time series relative to the explicit method as a result of area averaged meteorology. Even though water was evenly distributed over the grid area in this method (the other methods were comprised of multiple columns), very light rainfall rates and very high canopy interception rates dominated and resulted in a drier time series. Figure 4.11d shows the grid averaged column integrated soil water mass for all methods and biomes. The spatial heterogeneity in soil water was well captured in the alternative binned method, but varied in the binned method due to the reasons mentioned above, and was not well captured in the bulk method.

Time series for the grid averaged water stress factor for all methods and biomes is shown in figure 4.11e. When figure 4.11e is compared to panels A2, B2, and C2 in figures 4.11a, b, and c, all methods except the bulk method generally follow their PawTot time series. In the bulk method, the single PawTot value calculated for the grid area at every time step caused erratic behavior in the calculation of stress as changing PawTot values moved up and down the highly nonlinear stress curve in figure 3.31a. For the other methods, increased sampling along the

nonlinear curve with multiple SiB models eliminated that behavior, and from further analysis it was concluded that the stressed bins contributed more to the grid average stress than the wet bins.

4.12 LH Flux

The bulk method LH flux was always the highest relative to all methods, with the greatest contributions coming from the canopy intercepted LH flux as more precipitation was intercepted with this method, and the ground LH flux, where water that did reach the surface contributed more to the total LH flux as water was evenly distributed over the entire grid rather than in a fraction of the grid as in the other methods.

In the binned method the grid averaged LH flux only exceeded the explicit method for all bin sizes when the total fractional area occupied by the wet bins was larger than the area occupied by the wet bins in the explicit method. The greatest contributions to the LH flux at those times came from the canopy intercepted LH flux as well as the ground LH flux. When the total fractional area occupied by the bins that received precipitation was much smaller than the area occupied in the explicit method, the grid averaged LH flux was much smaller since the LH flux in that small area contributed very little to the grid average.

The grid averaged LH flux for the alternative binned method was very close to the explicit method for all bin sizes, and absolute errors were very small relative to the other methods and never exceeded 20 (W/m^2). This was not surprising because during precipitation events the total area that received precipitation was very close to the explicit method. The ground

intercepted LH flux contributed very little to the total LH flux and will not be discussed in the evaluation.

Absolute errors for the bulk and binned method for the grid averaged LH flux for all biomes are presented in figure 4.12a, and diurnal composites for all methods and biomes are presented in figures 4.12b, c, and d. In biome 9, the time integrated LH flux was over estimated by 15% in the bulk method, underestimated by 36%, 30%, and 10% in the binned method for 10, 20 and 50 bins respectively, and estimation errors in the alternative binned method were less than 1%. For biome 6, the time integrated LH flux was over estimated by 12% in the bulk method, underestimated by 8%, 3%, and 4% in the binned method for 10, 20 and 50 bins, and underestimated by 3%, 1%, and less than 1% in the alternative binned method for 10, 20 and 50 bins. In biome 3, the time integrated LH flux was overestimated by 28% in the bulk method, underestimated by 11%, 4%, and 2 % in the binned method for 10, 20 and 50 bins, and estimation errors in the alternative binned method were less than 1%.

Figure 4.12e shows the absolute errors for the grid averaged canopy intercepted LH flux in all biomes for the bulk and binned method. For biome 9, the time integrated canopy intercepted LH flux was overestimated by 179% in the bulk method, underestimated by 37%, 49%, and 8% in the binned method for 10, 20 and 50 bins respectively, and overestimated by 9%, 2%, and 3 % in the alternative binned method for 10, 20 and 50 bins. In biome 6, the time integrated canopy intercepted LH flux was overestimated by 215% in the bulk method, overestimated by 13%, 56%, and 70% in the binned method for 10, 20 and 50 bins, and estimation errors in the alternative binned method were less than 1%. For biome 3, the time integrated canopy intercepted LH flux was overestimated by 273% in the bulk method, overestimated by 20%, 19%, and 24% in the binned method for 10, 20 and 50 bins, and

overestimated by 5%, underestimated by 6% and overestimated by 5% in the alternative binned method for 10, 20 and 50 bins.

Absolute errors for all biomes for the grid averaged ground LH flux are presented in figure 4.12f for the bulk and binned method. In biome 9, the time integrated ground LH flux was overestimated by 6% in the bulk method, underestimated by 44%, 38%, and 14% in the binned method for 10, 20 and 50 bins respectively, and estimation errors were less than 1% in the alternative binned method. For biome 6, the time integrated ground LH flux was overestimated by 45% in the bulk method, underestimated by 10%, 15%, and 37% in the binned method for 10, 20 and 50 bins, and underestimated by 3% in the alternative binned method for 10 bins and estimation errors for 20 and 50 bins were less than 1%. In biome 3, the time integrated ground LH flux was overestimated by 4% in the bulk method, underestimated by 16%, 9%, and 7% in the binned method for 10, 20, and 50 bins, and underestimated by 4%, and overestimated by 1% in the alternative binned method for 10, and 20 bins with a less than 1% estimation error for 50 bins.

Figure 4.12g shows absolute errors for the grid averaged canopy transpiration in all biomes for the bulk and binned method. For biome 9, the time integrated canopy transpiration was overestimated by 2% in the bulk method, underestimated by 10%, 5%, and 1% in the binned method for 10, 20 and 50 bins respectively, and estimation errors were less than 1% in the alternative binned method. In biome 6, the time integrated canopy transpiration was underestimated by 8% in the bulk method, underestimated by 11%, and overestimated by 12%, and 11% in the binned method for 10, 20 and 50 bins, and underestimated by 3% and 2% in the alternative binned method for 10 and 20 bins with estimation errors at less than 1% for 50 bins. For biome 3, the time integrated canopy transpiration was underestimated by 7% in the bulk

method, underestimated by 15%, 7%, and 3% in the binned method for 10, 20 and 50 bins, and estimation errors were less than 1% in the alternative binned method.

4.13 SH Flux

The bulk method SH flux was always the lowest relative to all methods, and in the binned method the grid averaged SH flux exceeded the explicit method for all bin sizes when the total fractional area occupied by the wet bins was smaller than the area occupied in the explicit method. When this occurred, a larger fraction of the grid area remained dry and had a greater contribution to the grid averaged SH flux. The grid averaged SH flux for the alternative binned method was very close to the explicit method for all bin sizes, and absolute errors were very small relative to the other methods and never exceeded 20 (W/m^2). Figure 4.13a shows absolute errors in all biomes for the grid averaged SH flux for the bulk and binned method, and figures 4.13b, c, and d are diurnal composites for all methods and biomes.

In biome 9, the time integrated SH flux was underestimated by 2% in the bulk method, overestimated by 6%, 5%, and 2% in the binned method for 10, 20, and 50 bins respectively, and estimation errors were less than 1% in the alternative binned method. For biome 6, the time integrated SH flux was underestimated by 15% in the bulk method, overestimated by 10%, 4%, and 4% in the binned method for 10, 20, and 50 bins, and overestimated by 4% and 2% in the binned method for 10 and 20 bins and estimation errors were less than 1% with 50 bins. In biome 3, the time integrated SH flux was underestimated by 23% in the bulk method, overestimated by 8%, and 2% in the binned method for 10 and 20 bins and estimation errors

were less than 1% for 50 bins, and in the alternative binned method estimation errors were less than 1%.

4.14 Total Runoff

The time integrated grid averaged total runoff (surface and subsurface) in biome 9 was $3.3x10^{-3}$ (kg/m^2) for the bulk, alternative binned, and explicit method, while total runoff was 3.45, 1.75, and 0.65 (kg/m^2) in the binned method for 10, 20, and 50 bins respectively. For biome 6, the time integrated grid averaged total runoff was 0.011 (kg/m^2) in the bulk method, 2.13 (kg/m^2) in the explicit method, 6.47, 2.56, and 2.19 (kg/m^2) in the binned method for 10, 20 and 50 bins, and 2.62, 2.22, and 2.01 (kg/m^2) in the alternative binned method for 10, 20, and 50 bins. In biome 3, the time integrated grid averaged total runoff was 0.007 (kg/m^2) in the bulk method, 0.45 (kg/m^2) in the explicit method, 13.44, 9.81, and 2.52 (kg/m^2) in the binned method for 10, 20, and 50 bins, and 0.56, 0.70, and 0.29 (kg/m^2) in the alternative binned method for 10, 20, and 50 bins.

Clearly, the binned method was dominated by runoff (relative to the other methods) as a result of the precipitation distribution and changing fractional areas. As discussed in section 4.11, when the fractional area occupied by the wet bins was much smaller than the area occupied in the explicit method, rainfall rates were very heavy and water was mostly lost to runoff. The time integrated total runoff in the alternative binned method was very close to the explicit method since the occupied area by the wet bins was usually close to occupied area in the explicit method, and resulted in similar rainfall rates. In the bulk method, time integrated total runoff was lower than the explicit method with the exception of biome 9 where runoff was the same for

the bulk, explicit, and alternative binned method (methods with constant fractional areas) due to very light rainfall in the experiment, which resulted in very little total runoff.

4.15 CAS Temperature and Relative Humidity (RH)

Figures 4.15a, b, and c are diurnal plots for the grid averaged CAS temperature for all methods and biomes, and are analogous to the plots in figures 4.13b, c, and d. Absolute errors were as high as 6°C in the bulk and binned method, and never exceeded 1°C in the alternative binned method. For all biomes, the CAS temperature was the lowest with the bulk method, the binned method showed some difference when compared to the explicit method, but was small relative to the bulk method, and in the alternative binned method the CAS temperature converged to the explicit method. Diurnal plots for the grid averaged CAS relative humidity are shown in figures 4.15d, e, and f for all methods and biomes. Absolute errors were as high as 45% in the bulk method, 20% in the binned method, and never exceeded 4% in the alternative binned method. When compared to the explicit method in all biomes, the grid area in the bulk method had a higher CAS relative humidity, the binned method had a lower CAS relative humidity, and the CAS relative humidity in the alternative binned method converged to the explicit method.

Relative to the other methods, the bulk method had the lowest CAS temperature as well as the highest CAS relative humidity as a result of having the largest LH flux. During precipitation events, in the bulk method all components that contributed to the grid area total LH flux came from the entire grid area rather than a fraction of the grid as in the other methods, where the total LH flux was a grid average of the wet and dry fractions. Additionally, in the

binned and alternative binned method the CAS temperature and CAS relative humidity were not too different when compared to the explicit method, as a result of the meteorological distribution. Recall, that in the experiment fractions of the grid area received the same meteorological events, and in section 4.2 the highly spatially varying meteorological experiment should produce different results.

4.16 Total Plant Available Water Distribution Plots

In the binned method, the evolution of the distribution of PawTot over time was represented by changes to the bin fractional areas. For comparison with the binned method, the distribution of PawTot for the explicit and alternative binned method was binned at hour 24 for selected days to produce PawTot distribution plots. Hour 24 was selected since fractional areas in the binned method were updated at that time. Distribution plots for days 2 (hours 25-48), 3 (hours 49-72) and 9 (hours 193-216) in biome 6 (see figure 4.11a) are shown in figures 4.16a, b and c for the binned method for 10, 20, and 50 bins respectively and in figures 4.16d, e and f for the alternative binned method for 10, 20, and 50 bins (bin wetness increases to the right). Days 2 and 9 were dry and day 3 had a precipitation event. On day 3, for the binned and alternative binned method, a bin size of 10 indicated a distribution that moved to the right (to the wetter bins) while wet peaks appeared for bin sizes of 20, and 50. As the distribution dried down (day 9), the entire distribution moved to the left for a bin size of 10 and for bin sizes of 20 and 50, wet peaks moved to the left and began to merge with the drier peaks since the wetter bins dried faster than the drier bins. Figures 4.16g, h, i, j, k, and l are similar plots in biome 6 (see figure 4.11a)

for days 46 (hours 1081-1104), 47 (hours 1105-1128) and 49 (hours 1153-1176) where days 46 and 49 were dry and day 47 had a precipitation event.

From the PawTot distribution plots, the alternative binned method better captured the spatial heterogeneity for the distribution of PawTot produced by the explicit method. The binned method performed poorly because of the initialization issue and precipitation distribution (see section 4.11). These findings were concluded for all biomes.

4.2 Highly Spatially Varying Precipitation Distribution

4.21 Total Plant Available Water (PawTot) and Stress

Figures 4.21a, b and c are time series of grid averaged rainfall and PawTot for all methods in biomes 9, 6 and 3 respectively. The initialization issue was still a problem in the binned method (as discussed in section 4.11) since bin midpoint value averages were used to represent the initial PawTot distribution rather than the actual distribution average. This resulted in drier and wetter grid averaged PawTot time series relative to the explicit method, where some of the drier time series were drier than the bulk method.

The precipitation distribution was more problematic in this experiment than in section 4.1. Focusing on the explicit method, in this experiment precipitation occurred at different times and at different rates (100 different drivers); while in section 4.1 fractions of the grid area received the same meteorology. Since the precipitation rate and distribution in the binned method was based on the number of SiB models that received precipitation in the explicit method and the grid averaged rainfall, it became problematic when very few SiB models received precipitation in the explicit method. For example, say 8% of the grid area receives

precipitation in the explicit method, then one bin (nearest integer to 0.92 if we are using 12 bins) in the binned method receives precipitation, but fractional areas vary in this method and if the randomly chosen bin has a very large fractional area, the rainfall rate is very light (results approach those of the bulk method) and if the fractional area is very small, the rainfall rate is very heavy and water is mostly lost to runoff. This behavior is quite apparent in the PawTot time series in figures 4.21a, b, and c where at times some of the time series dry down very quickly or suddenly increase in wetness.

The alternative binned method performed the best in all biomes, where absolute errors for PawTot did not exceed 12 (kg/m^2). The precipitation distribution in this method was not problematic, since precipitation that fell on the total fractional area occupied by the wet bins was much closer to the total fractional area occupied by the wet bins in the explicit method (fractional areas remained constant in this method). In all biomes, the bulk method showed a drier time series relative to the explicit method as a result of area averaged meteorology. Even though water was evenly distributed over the grid area in this method (the other methods are comprised of multiple columns), very light rainfall rates and very high canopy interception rates dominated and resulted in a drier time series. Figure 4.21d shows the grid averaged column integrated soil water mass for all biomes. The spatial heterogeneity in soil water was well captured in the alternative binned method, but varied in the binned method due to the reasons mentioned above, and was not well captured in the bulk method.

Time series for the grid averaged water stress factor for all methods and biomes is shown in figure 4.21e. When figure 4.21e is compared to panels A2, B2, and C2 in figures 4.21a, b, and c, all methods except the bulk method generally follow their PawTot time series. In the bulk method, the single PawTot value calculated for the grid area at every time step caused erratic

behavior in the calculation of stress as changing PawTot values moved up and down the highly nonlinear stress curve in figure 3.31a. For the other methods, increased sampling along the nonlinear curve with multiple SiB models eliminated that behavior, and from further analysis it was concluded that the stressed bins contributed more to the grid average stress than the wet bins.

4.22 LH Flux

With the exception of the binned method in biome 9 for 10 bins, the bulk method LH flux was always the highest, with the greatest contributions coming from the canopy intercepted LH flux as more precipitation was intercepted with this method, and the ground LH flux, where water that did reach the surface contributed more to the total LH flux as water was evenly distributed over the entire grid rather than in a fraction of the grid as in the other methods. For the duration of the experiment in biome 9, a bin size of 10 produced results that were similar to those found with the bulk method as a result of precipitation events that occurred over the same bins that had a total fractional area that was slightly smaller than the bulk method and much larger than the wet areas in the explicit method. With heavier rainfall rates relative to the bulk method, the canopy intercepted LH flux and the ground LH flux were about 1% greater, and the total LH flux was about 8% greater than in the bulk method.

For all other bin sizes and biomes, the binned method grid averaged LH flux only exceeded the explicit method when the total fractional area occupied by the wet bins was larger than the area occupied by the wet bins in the explicit method. The greatest contributions to the LH flux at those times came from the canopy intercepted LH flux as well as the ground LH flux.

When the total fractional area occupied by the bins that received precipitation was much smaller than the area occupied in the explicit method, the LH flux was much smaller since the LH flux in that small area contributed very little to the grid average.

The grid averaged LH flux for the alternative binned method was very close to the explicit method for all bin sizes, and absolute errors were very small relative to the other methods and never exceeded 45 (W/m^2). The ground intercepted LH flux contributed very little to total LH flux for all methods and will not be discussed.

Absolute errors for the bulk and binned method for the grid averaged LH flux for all biomes are presented in figure 4.22a, and diurnal composites for all methods and biomes are presented in figures 4.22b, c, and d. In biome 9, the time integrated LH flux was over estimated by 54% in the bulk method, overestimated by 62%, and underestimated by 30%, and 36% in the binned method for 10, 20 and 50 bins respectively, and overestimated by 23%, 13%, and 2% in the alternative binned method for 10, 20, and 50 bins. For biome 6, the time integrated LH flux was over estimated by 45% in the bulk method, underestimated by 2%, 19%, and 12% in the binned method for 10, 20 and 50 bin, and underestimated by 5%, 2%, and overestimated by 3% in the alternative binned method for 10, 20 and 50 bins. In biome 3, the time integrated LH flux was overestimated by 85% in the bulk method, underestimated by 26%, 22%, and 7% in the binned method for 10, 20 and 50 bins, and overestimated by 7%, 1%, and 3% in the alternative binned method for 10, 20, and 50 bins.

Figure 4.22e shows absolute errors for the grid averaged canopy intercepted LH flux in all biomes for the bulk and binned method. For biome 9, the time integrated canopy intercepted LH flux was overestimated by 420% in the bulk method, overestimated by 421%, 48%, and 1% in the binned method for 10, 20 and 50 bins, and overestimated by 238%, 123%, and 27% in the

alternative binned method for 10, 20 and 50 bins. In biome 6, the time integrated canopy intercepted LH flux was overestimated by 581% in the bulk method, overestimated by 175%, underestimated by 32%, and overestimated by 14% in the binned method for 10, 20 and 50 bins, and overestimated by 141%, 46%, and 16% in the alternative binned method for 10, 20, and 50 bins. For biome 3, the time integrated canopy intercepted LH flux was overestimated by 496% in the bulk method, underestimated by 14%, 34%, and overestimated by 6% in the binned method for 10, 20 and 50 bins, and overestimated by 71%, 12% and 9% in the alternative binned method for 10, 20 and 50 bins.

Absolute errors for all biomes for the grid averaged ground LH flux are presented in figure 4.22f for the bulk and binned method. In biome 9, the time integrated ground LH flux was overestimated by 27% in the bulk method, overestimated by 28%, underestimated by 47%, and 54% in the binned method for 10, 20 and 50 bins respectively, and overestimated by 19%, 13%, and 2% in the alternative binned method for 10, 20, and 50 bins. For biome 6, the time integrated ground LH flux was overestimated by 59% in the bulk method, underestimated by 4%, 31%, and 35% in the binned method for 10, 20 and 50 bins, and underestimated by 23% , 12%, and overestimated by 6% in the alternative binned method for 10, 20, and 50 bins. In biome 3, the time integrated ground LH flux was overestimated by 17% in the bulk method, underestimated by 40%, 32%, and 12% in the binned method for 10, 20, and 50 bins, and overestimated by 5%, 1%, and 5% in the alternative binned method for 10, 20, and 50 bins.

Figure 4.22g shows absolute errors for the grid averaged canopy transpiration in all biomes for the bulk and binned method. For biome 9, the time integrated canopy transpiration was underestimated by 3% in the bulk method, underestimated by 1%, 7%, and 2% in the binned method for 10, 20 and 50 bins respectively, and estimation errors were less than 1% in the

alternative binned method. In biome 6, the time integrated canopy transpiration was underestimated by 25% in the bulk method, underestimated by 22%, 16%, and 5% in the binned method for 10, 20 and 50 bins, and underestimated by 7%, 1%, and overestimated by 2% in the alternative binned method for 10, 20, and 50 bins. For biome 3, the time integrated canopy transpiration was underestimated by 7% in the bulk method, underestimated by 25%, 17%, and 8% in the binned method for 10, 20 and 50 bins, and underestimated by 3%, 1%, and overestimated by 1% in the alternative binned method for 10, 20, and 50 bins.

4.23 SH Flux

With the exception of the binned method in biome 9 with 10 bins, the bulk method SH flux was always the lowest relative to all methods in all biomes. As discussed in the previous section, the binned method in biome 9 with 10 bins produced a larger grid averaged LH flux that resulted in a smaller grid averaged SH flux when compared to the bulk method. For all other bin sizes and biomes, the binned method grid averaged SH flux exceeded the explicit method when the total fractional area occupied by the wet bins was smaller than the area occupied by the wet bins in the explicit method. When this occurred, a larger fraction of the grid area remained dry and had a greater contribution to the grid averaged SH flux. The grid averaged SH flux for the alternative binned method was very close to the explicit method for all bin sizes, and absolute errors were very small relative to the other methods and never exceeded 30 (W/m^2). Figure 4.23a shows absolute errors in all biomes for the grid averaged SH flux for the bulk and binned method, and figures 4.23b, c, and d are diurnal composites for all methods and biomes.

In biome 9, the time integrated grid averaged SH flux was underestimated by 10% in the bulk method, underestimated by 13%, overestimated by 4%, and 5% in the binned method for 10, 20, and 50 bins respectively, and underestimated by 4%, 2%, and less than 1% in the alternative binned method for 10, 20, and 50 bins. For biome 6, the time integrated grid averaged SH flux was underestimated by 37% in the bulk method, underestimated by 10%, overestimated by 15%, and 9% in the binned method for 10, 20, and 50 bins, and overestimated by 2%, 1%, and underestimated by 3% in the alternative binned method for 10, 20, and 50 bins. In biome 3, the time integrated grid averaged SH flux was underestimated by 66% in the bulk method, overestimated by 17%, 15%, and 5% in the binned method for 10, 20, and 50 bins, and underestimated by 7%, 1%, and 2% in the alternative binned method for 10, 20, and 50 bins.

4.24 Total Runoff

The time integrated grid averaged total runoff (surface and subsurface) in biome 9 was 3.3×10^{-3} (kg/m^2) for the bulk, alternative binned, and explicit method, while total runoff was 2.1×10^{-3}, 5.66, and 5.84 (kg/m^2) in the binned method for 10, 20, and 50 bins respectively. For biome 6, the time integrated grid averaged total runoff was 0.011 (kg/m^2) in the bulk method, 0.087 (kg/m^2) in the explicit method, 12.65, 143.83, and 23.21 (kg/m^2) in the binned method for 10, 20 and 50 bins, and 0.011 (kg/m^2) for all bin sizes in the alternative binned method. In biome 3, the time integrated grid averaged total runoff was 0.007 (kg/m^2) in the bulk method, 0.055 (kg/m^2) in the explicit method, 33.69, 28.69, and 12.85 (kg/m^2) in the binned method for 10, 20, and 50 bins, and 0.007, 0.007, and 0.008 (kg/m^2) in the alternative binned method for 10, 20, and 50 bins.

As in section 4.1, with the exception of 10 bins in biome 9, the binned method was dominated by runoff (relative to the other methods) as a result of the precipitation distribution and changing fractional areas. Recall that in biome 9 with the binned method for 10 bins, results were very similar to those found with bulk method, which included runoff. High runoff rates with the other bin sizes and biomes were a consequence of distributing precipitation over a much smaller fractional area relative to the explicit method. Since the precipitation distribution was not problematic in the alternative binned method, where fractional areas were constant and the occupied area by the wet bins was usually close to the occupied area by the wet bins in the explicit method, excessive runoff did not occur. In the bulk method, time integrated total runoff was lower than the explicit method with the exception of biome 9 where runoff was the same for the bulk, explicit, and alternative binned method (methods with constant fractional areas) due to very light rainfall for the duration of the experiment, which resulted in very little total runoff. This was also the reason for similar total runoff rates between the bulk and alternative binned method in biomes 6 and 3, where rainfall rates were not heavy enough to produce significant runoff.

4.25 CAS Temperature and Relative Humidity (RH)

Figures 4.25a, b, and c are diurnal plots for the grid averaged CAS temperature for all methods and biomes, and are analogous to the plots in figures 4.23b, c, and d. Absolute errors were as high as 10°C for the bulk and binned method, and did not exceed 1°C in the alternative binned method. With the exception of the binned method in biome 9 for 10 bins, the CAS temperature was the lowest with the bulk method and the alternative binned method was the

closest in agreement with the explicit method. Diurnal plots for the grid averaged CAS relative humidity are shown in figures 4.25d, e, and f for all methods and biomes. Absolute errors were as high as 40% in the bulk method, 30% in the binned method, and less than 5% in the alternative binned method. Similar to the first precipitation experiment (section 4.15), the method with the lowest CAS temperature had the highest CAS relative humidity, as a result of having the highest LH flux. The highly spatially varying meteorology in this experiment resulted in larger differences (relative to the first precipitation experiment) in the CAS temperature and relative humidity between the explicit, binned and alternative binned method.

4.26 Total Plant Available Water Distribution Plots

As in section 4.16, the distribution of total plant available water for the explicit and alternative binned method was binned at hour 24 for selected days to produce PawTot distribution plots. Distribution plots for days 21 (hours 481-504), 23 (hours 529-552), and 25 (hours 577-600) for biome 6 (see figure 4.21a) are shown in figures 4.26a, b and c for the binned method for 10, 20, and 50 bins respectively, and in figures 4.26d, e and f for the alternative binned method for 10, 20, and 50 bins. Wet peaks and dry down periods are difficult to pick out because of the precipitation distribution in this method. For each day, precipitation occurred somewhere in the grid, but did not cover large fractions of the grid area as in the first precipitation experiment. Figures 4.26g, h, i, j, k, and l are similar plots for biome 6 (see figure 4.21a) for days 52 (hours 1225-1248), 54 (hours 1273-1296) and 56 (hours 1321-1344).

From the PawTot distribution plots, the alternative binned method better captured the spatial heterogeneity for the distribution of PawTot produced by the explicit method. The two

major problems with the binned method were the initialization issue and the precipitation distribution (see section 4.11) and were to blame for the poor performance. These findings were concluded for all biomes.

4.3 Chapter 4 Figures

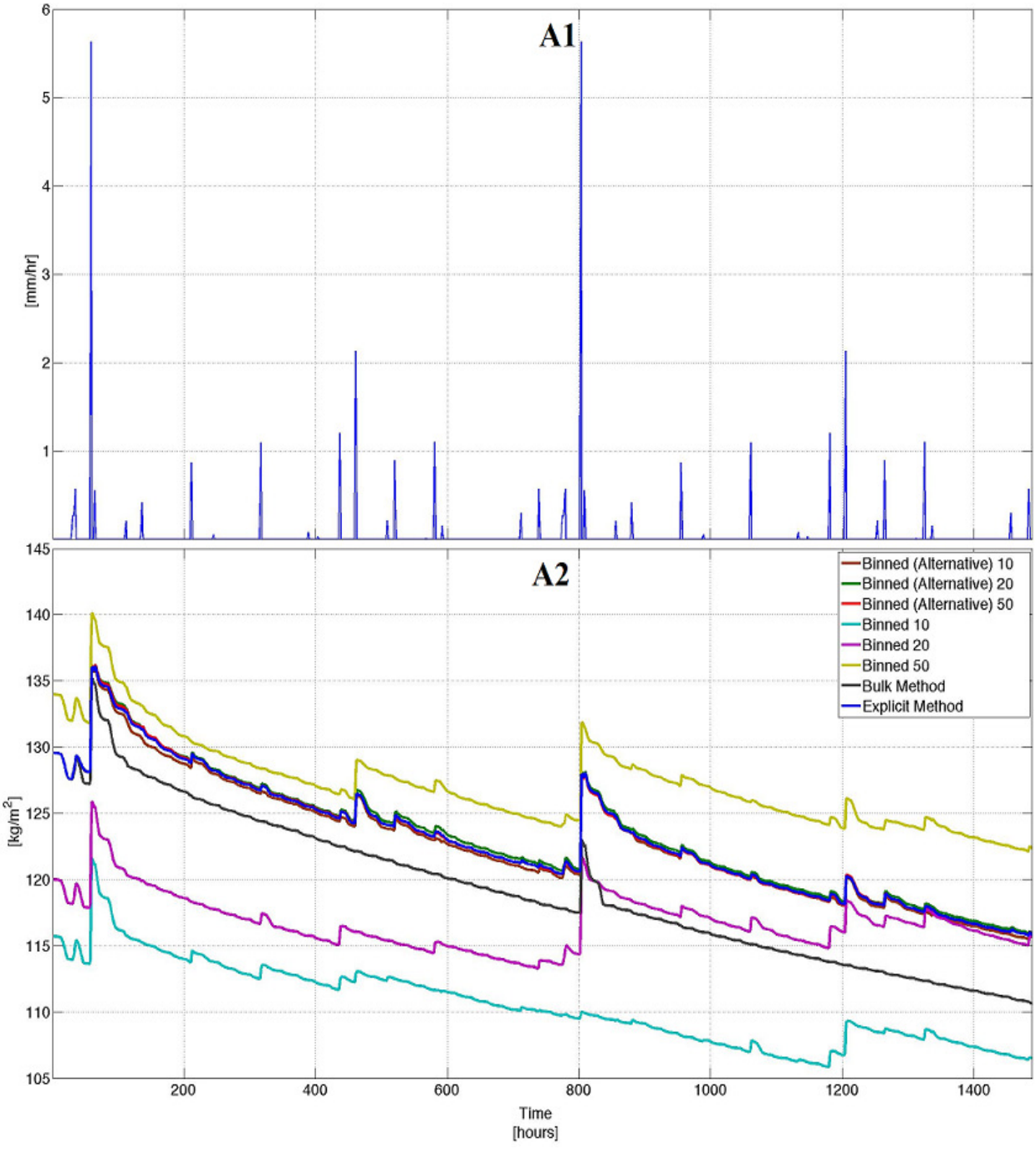

Figure 4.11a. Time series of the grid area averaged rainfall and total plant available water for biome 9, where panel A1 shows the grid area averaged rainfall rate and panel A2 is the grid area averaged total plant available water for the various methods.

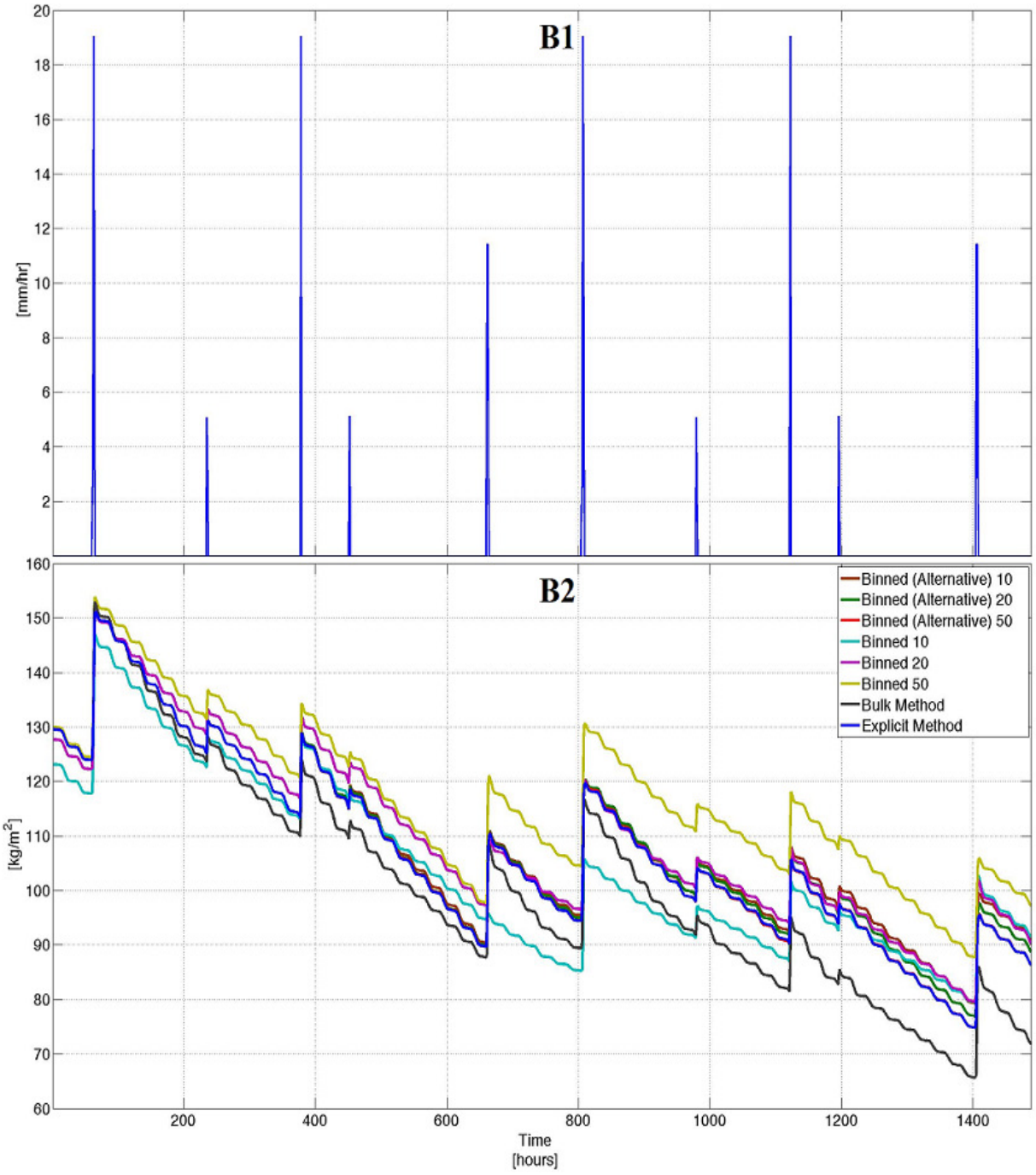

Figure 4.11b. Time series of the grid area averaged rainfall and total plant available water for biome 6, where panel B1 shows the grid area averaged rainfall rate and panel B2 is the gird area averaged total plant available water for the various methods.

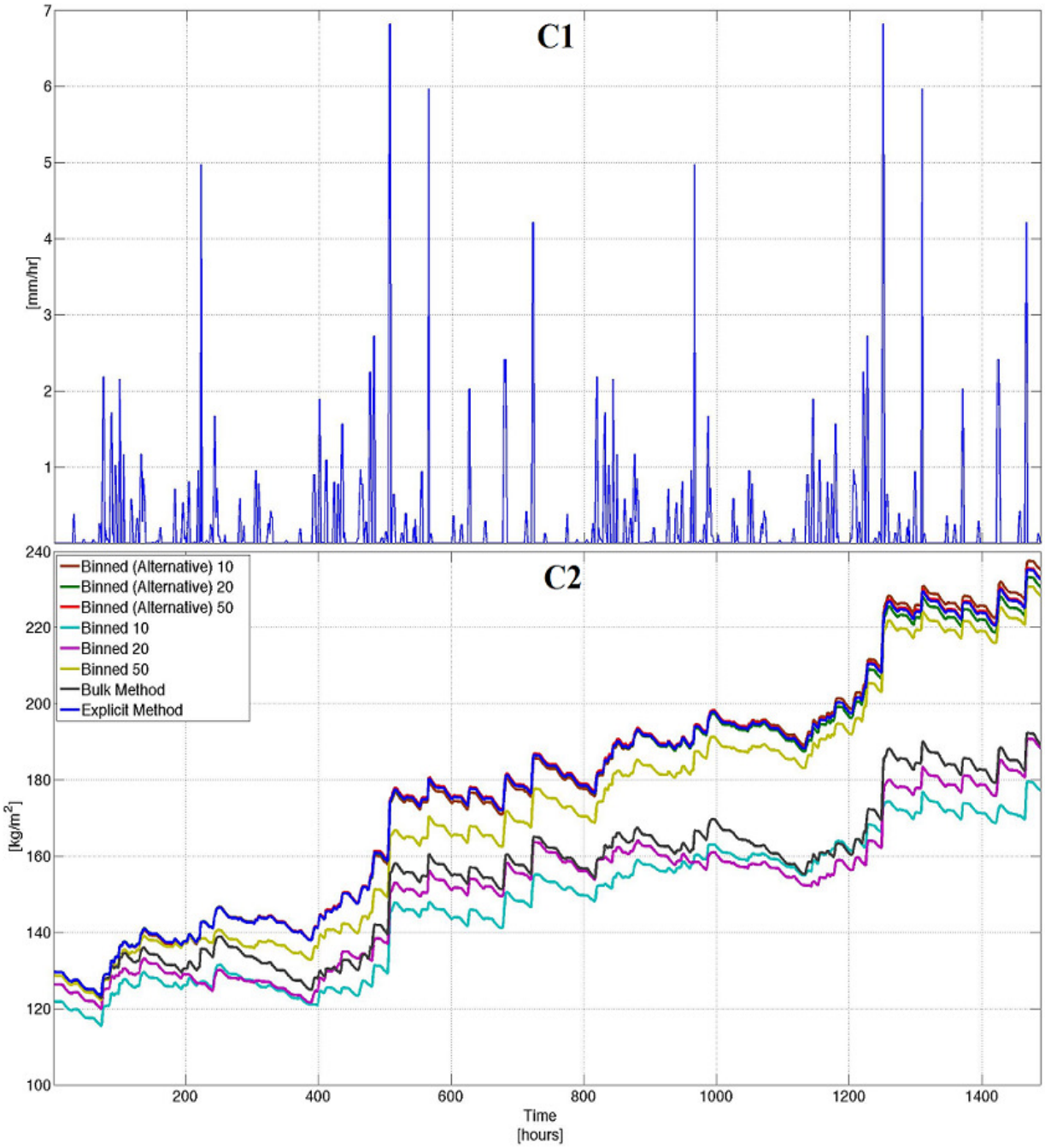

Figure 4.11c. Time series of the grid area averaged rainfall and total plant available water for biome 3, where panel C1 shows the grid area averaged rainfall rate and panel C2 is the grid area averaged total plant available water for the various methods.

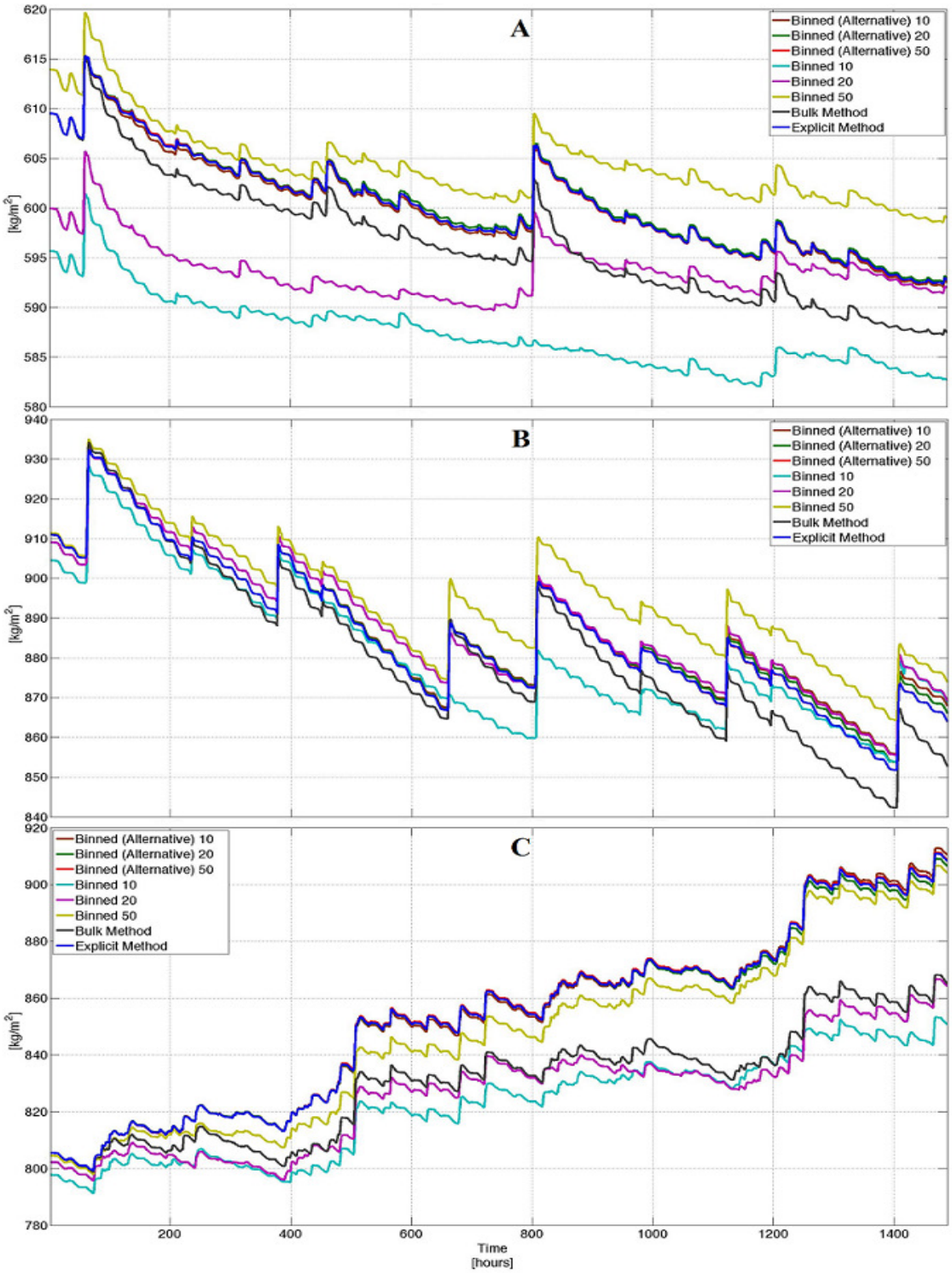

Figure 4.11d. Time series of the grid area averaged column integrated soil water mass for soil layers 1-8 for all methods, where panel A is biome 9, panel B is biome 6 and panel C is biome 3.

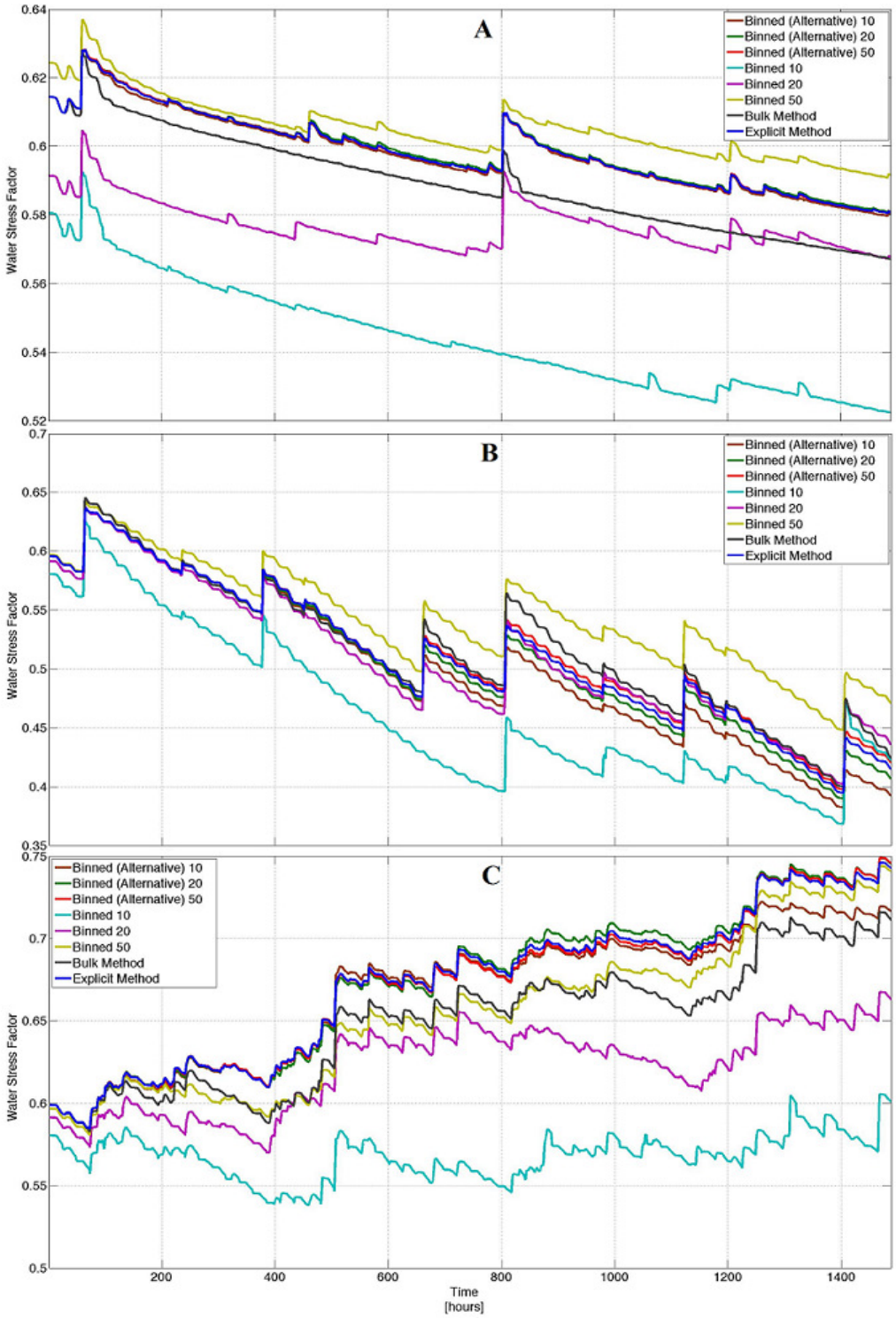

Figure 4.11e. Time series of the grid area averaged water stress factor for all methods, where panel A is biome 9, panel B is biome 6, and panel C is biome 3.

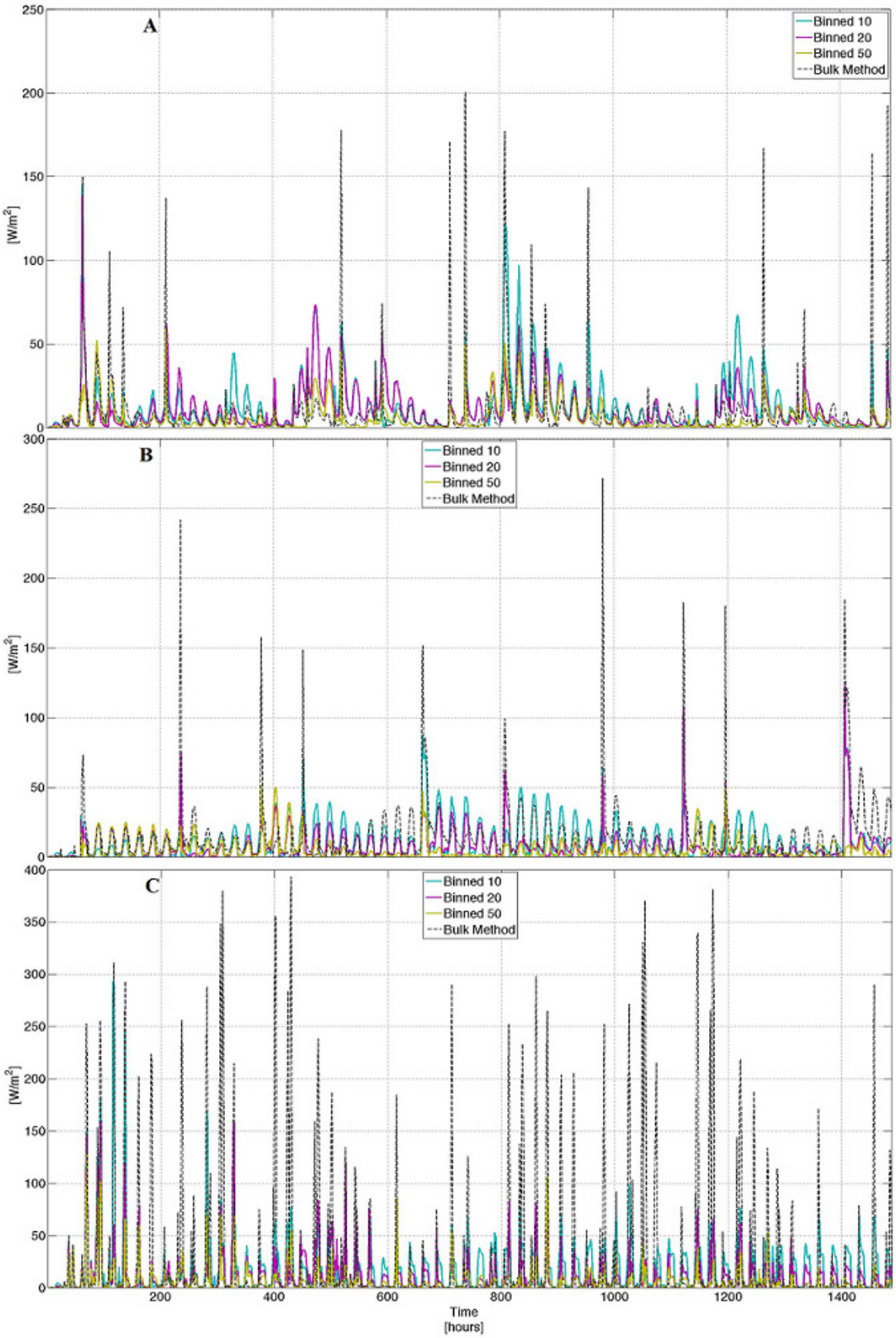

Figure 4.12a. Time series of absolute errors for the grid averaged LH flux for the binned and bulk method, where panel A is biome 9, panel B is biome 6, and panel C is biome 3.

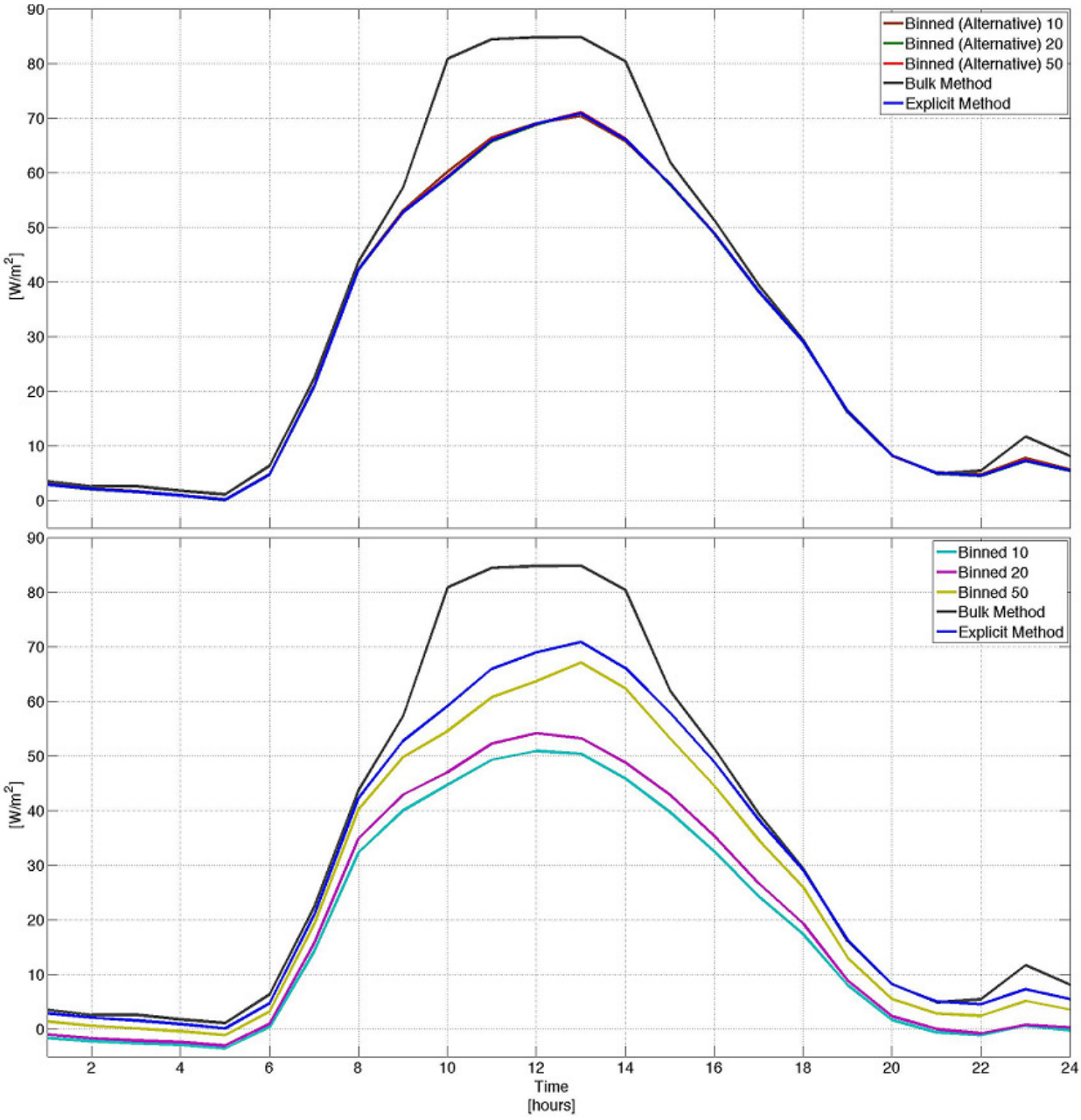

Figure 4.12b. Diurnal composites of the grid area averaged LH flux for all methods in biome 9.

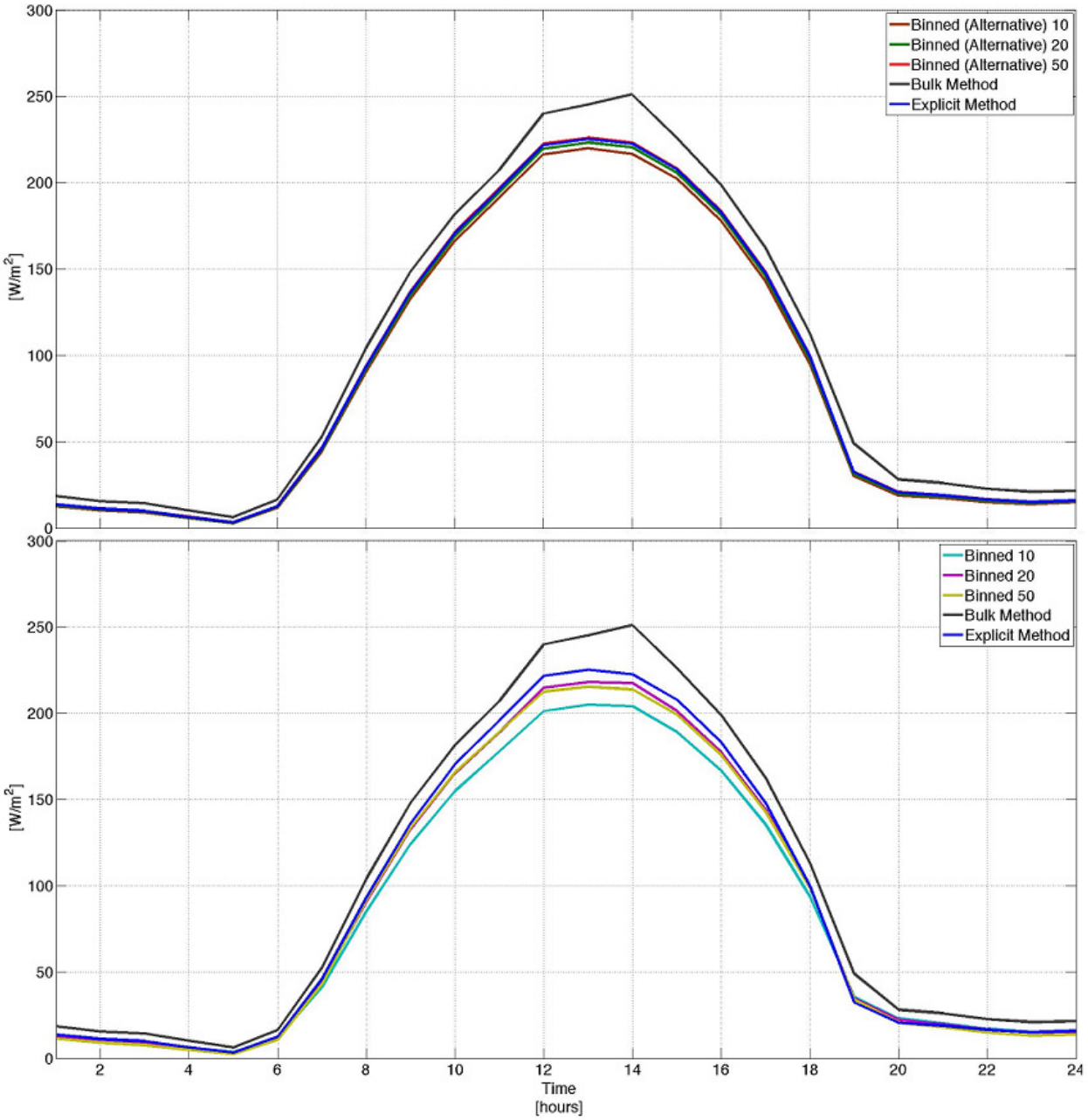

Figure 4.12c. Diurnal composites of the grid area averaged LH flux for all methods in biome 6.

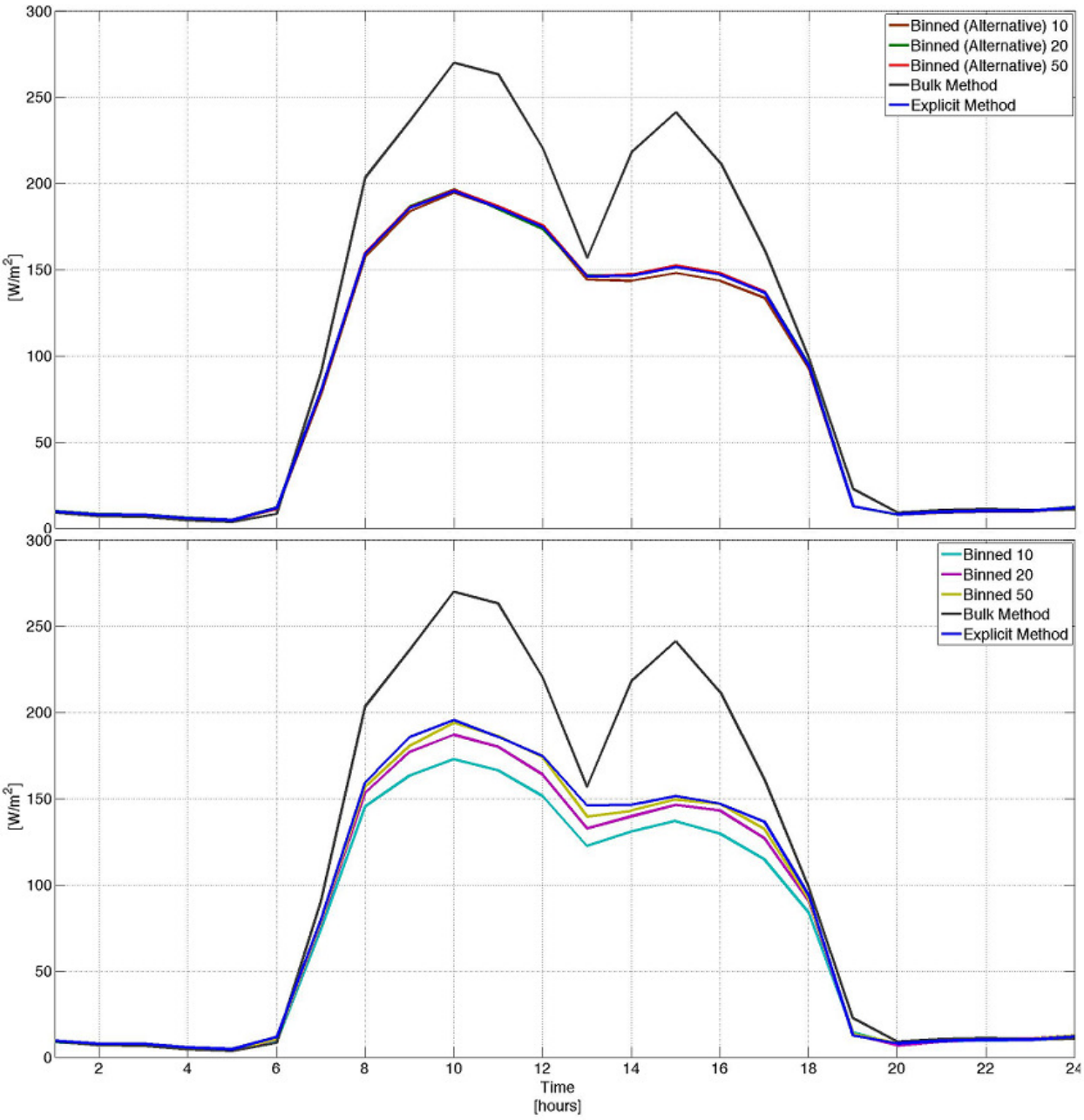

Figure 4.12d. Diurnal composites of the grid area averaged LH flux for all methods in biome 3.

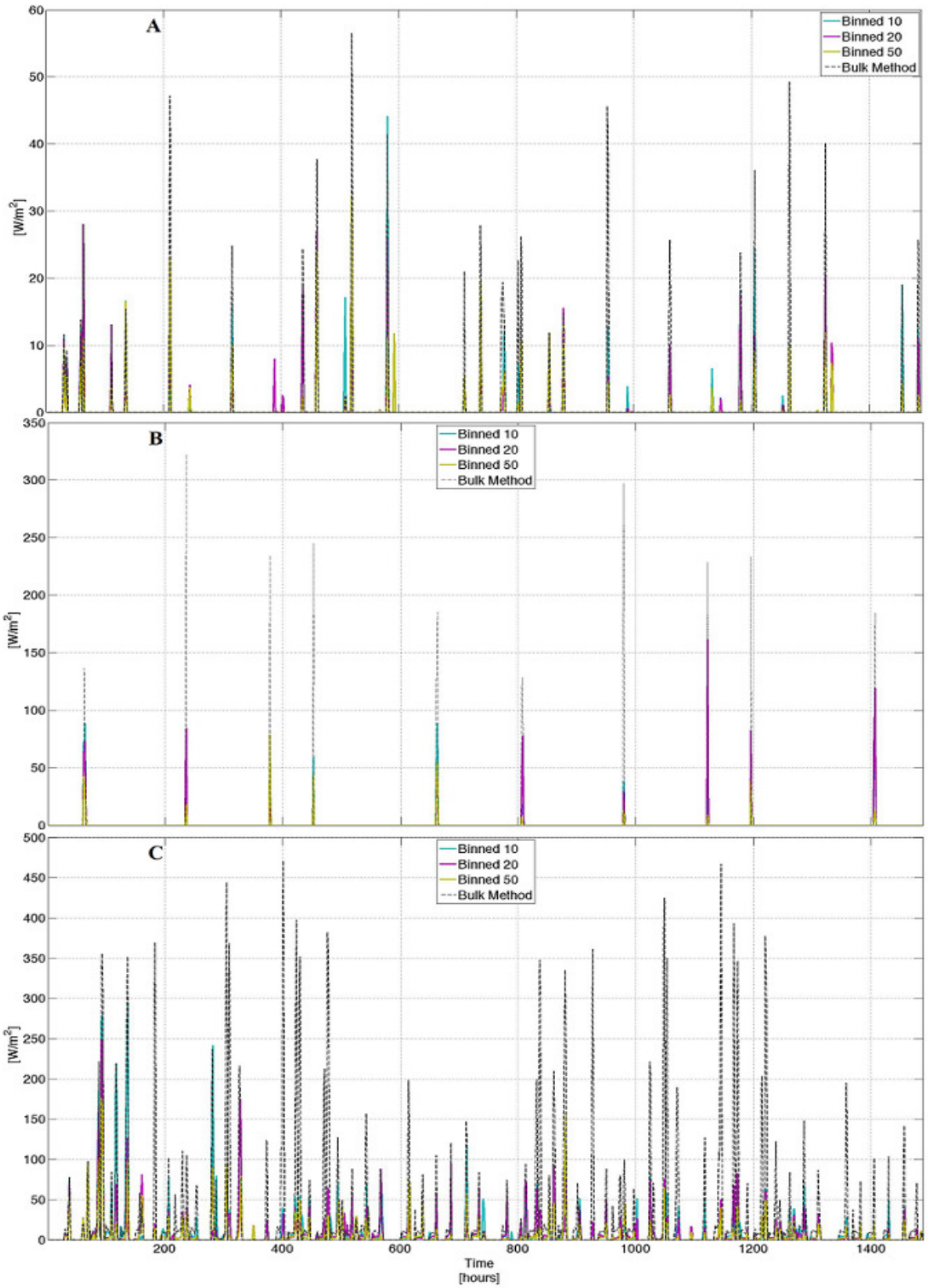

Figure 4.12e. Time series of absolute errors for the grid area averaged canopy intercepted LH flux for the binned and bulk method, where panel A is biome 9, panel B is biome 6, and panel C is biome 3.

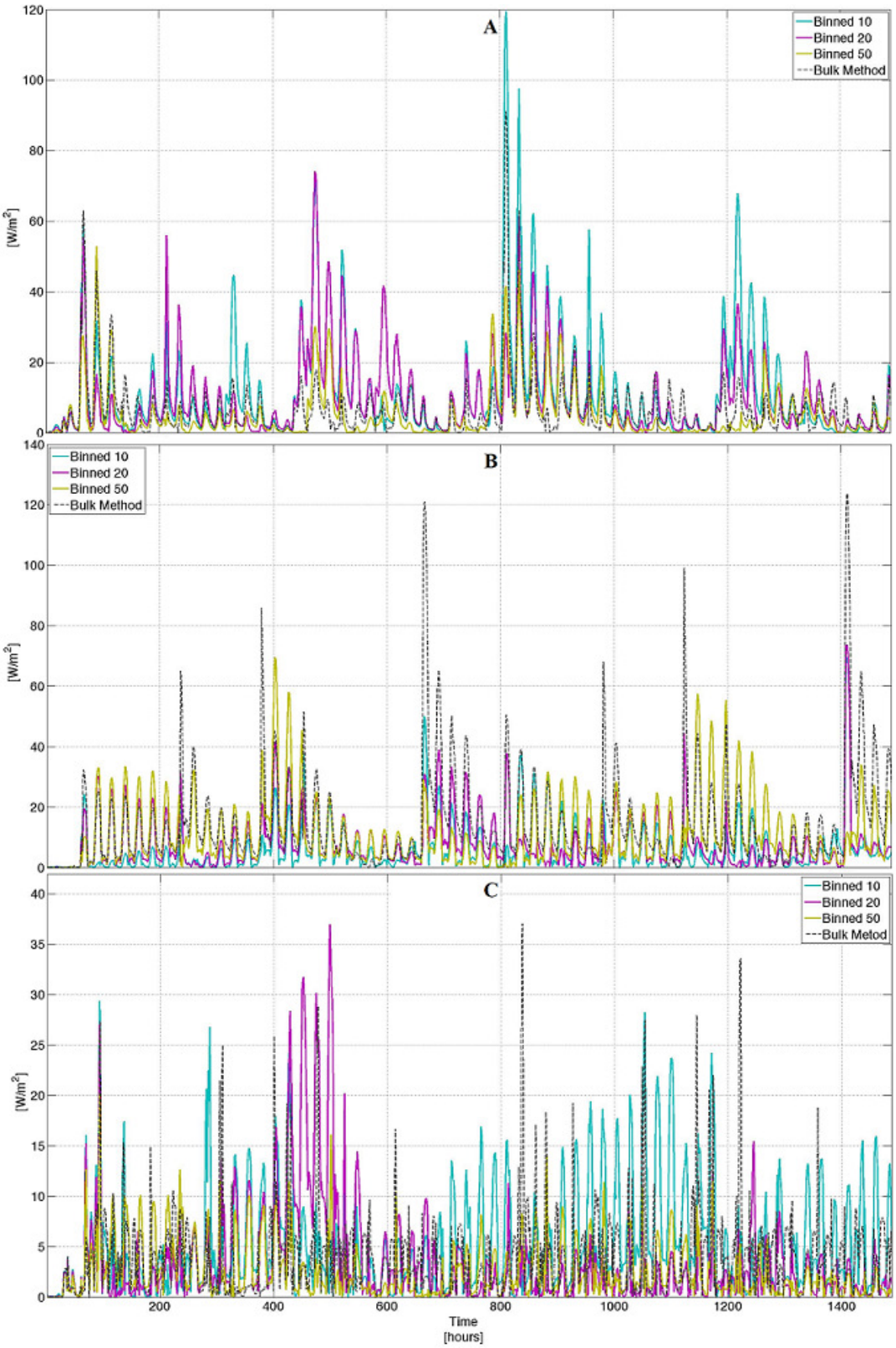

Figure 4.12f. Time series of absolute errors for the grid area averaged ground LH flux for the binned and bulk method, where panel A is biome 9, panel B is biome 6, and panel C is biome 3.

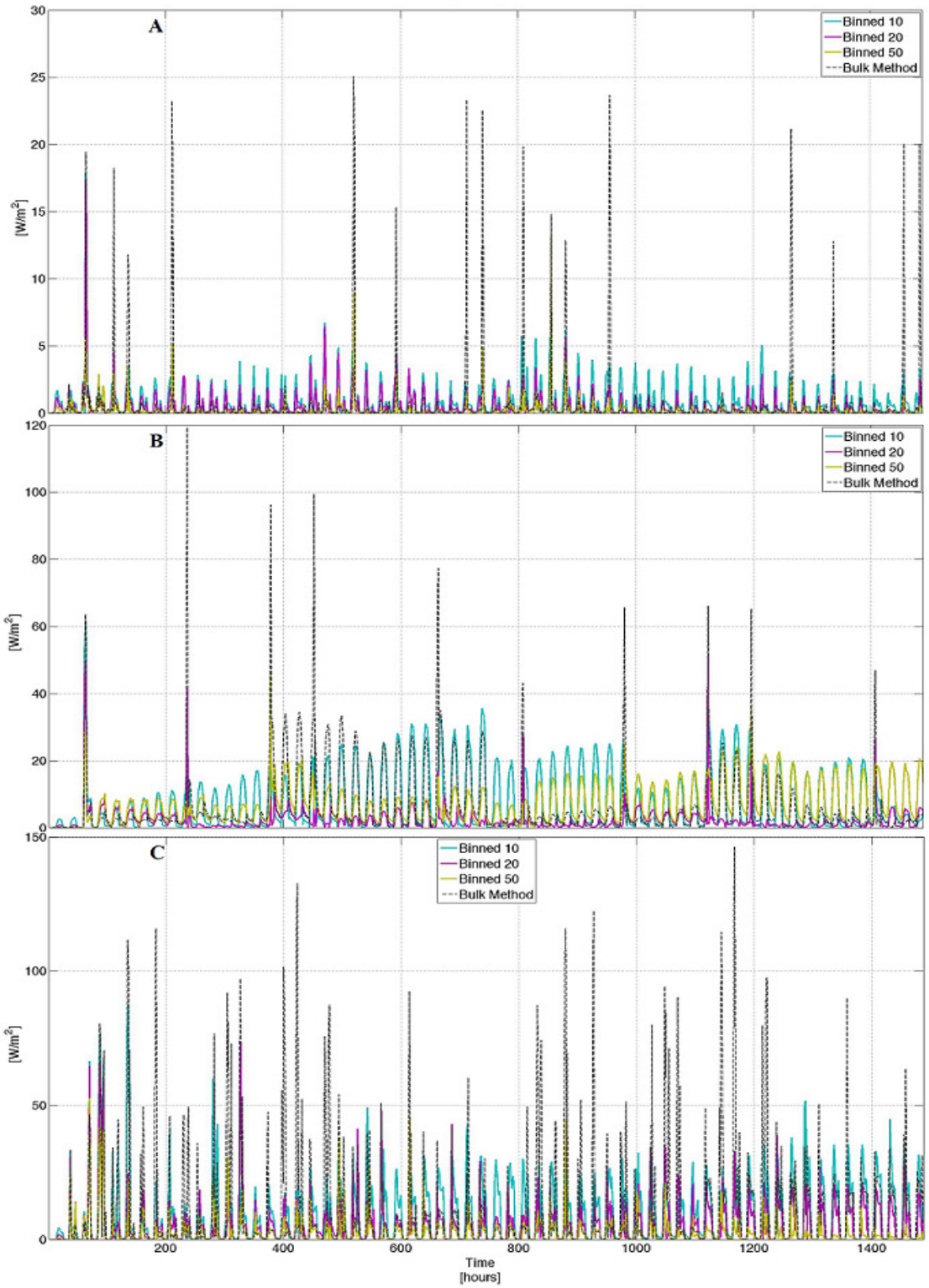

Figure 4.12g. Time series of absolute errors for the grid area averaged canopy transpiration for the binned and bulk method, where panel A is biome 9, panel B is biome 6, and panel C is biome 3.

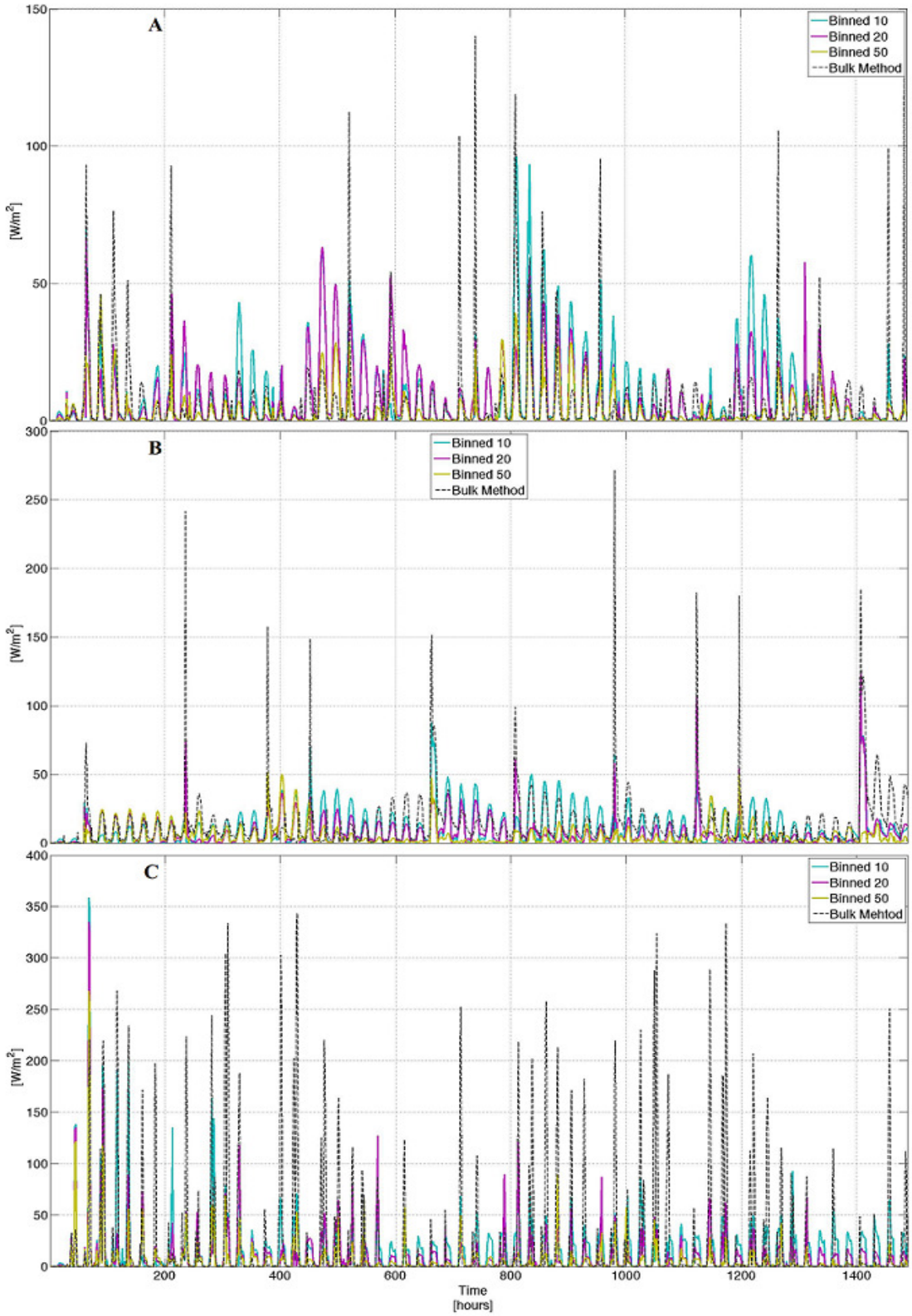

Figure 4.13a. Time series of absolute errors for the grid area averaged SH flux for the binned and bulk method, where panel A is biome 9, panel B is biome 6, and panel C is biome 3.

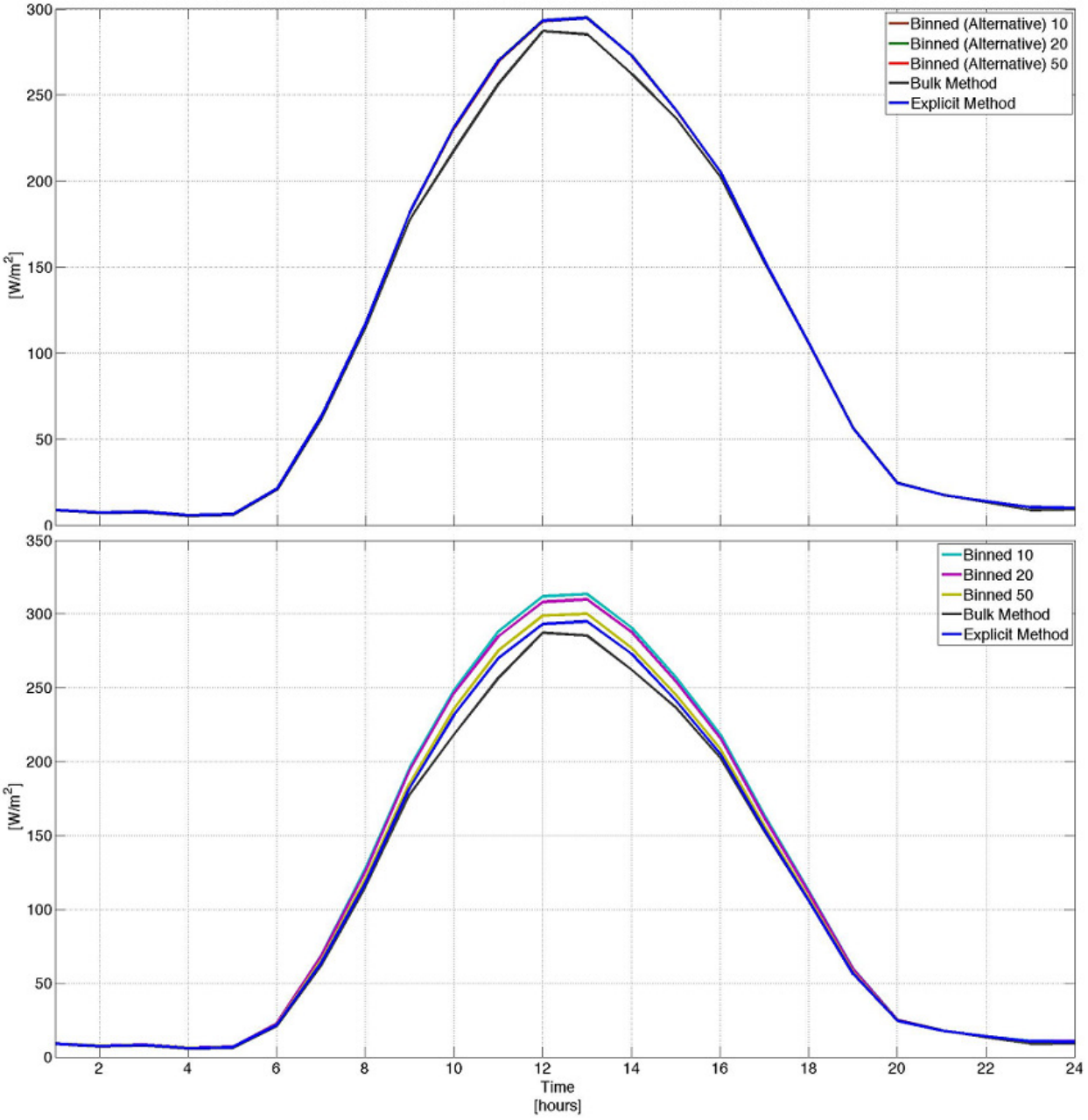

Figure 4.13b. Diurnal composites of the grid area averaged SH flux for all methods in biome 9.

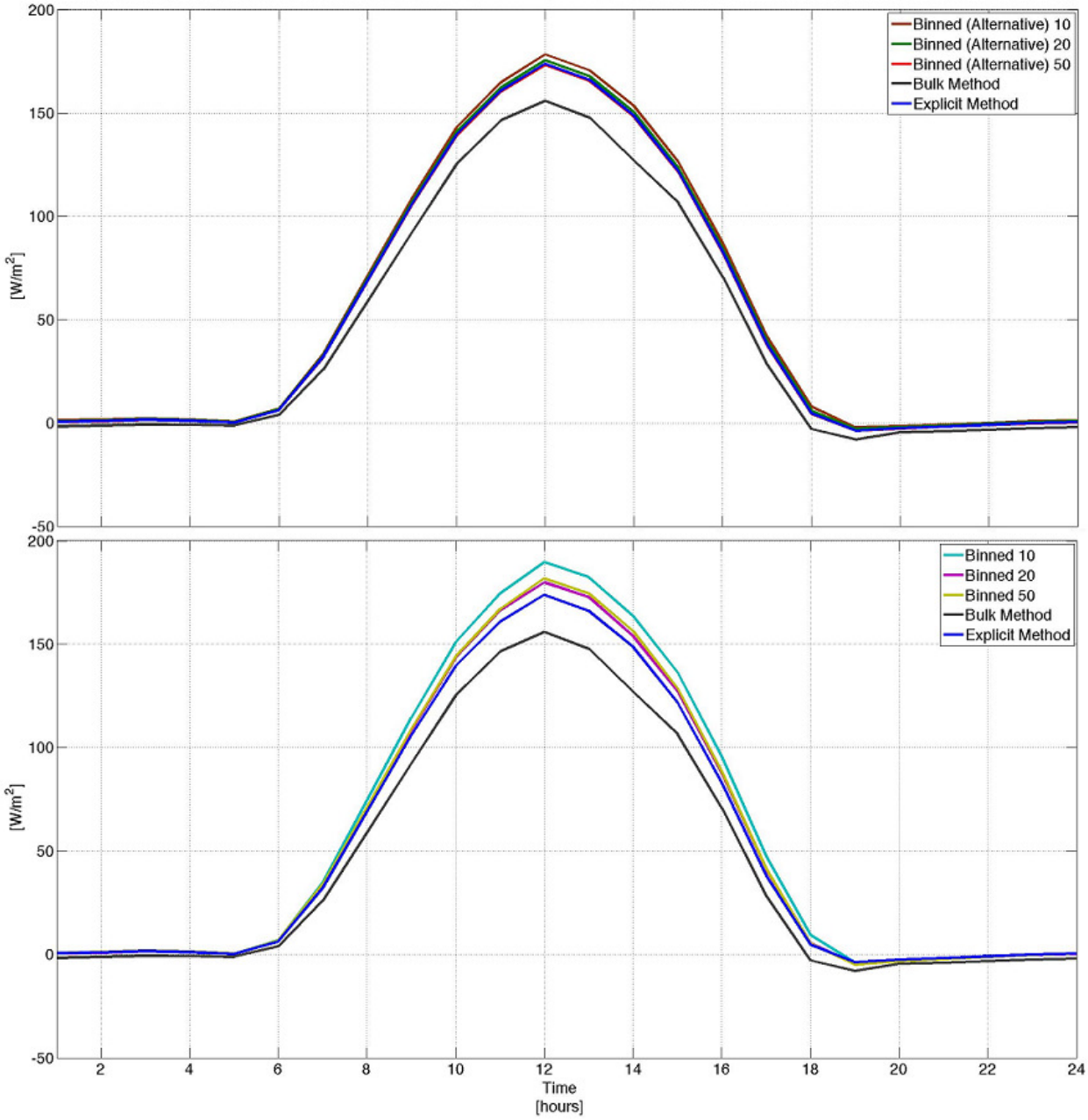

Figure 4.13c. Diurnal composites of the grid area averaged SH flux for all methods in biome 6.

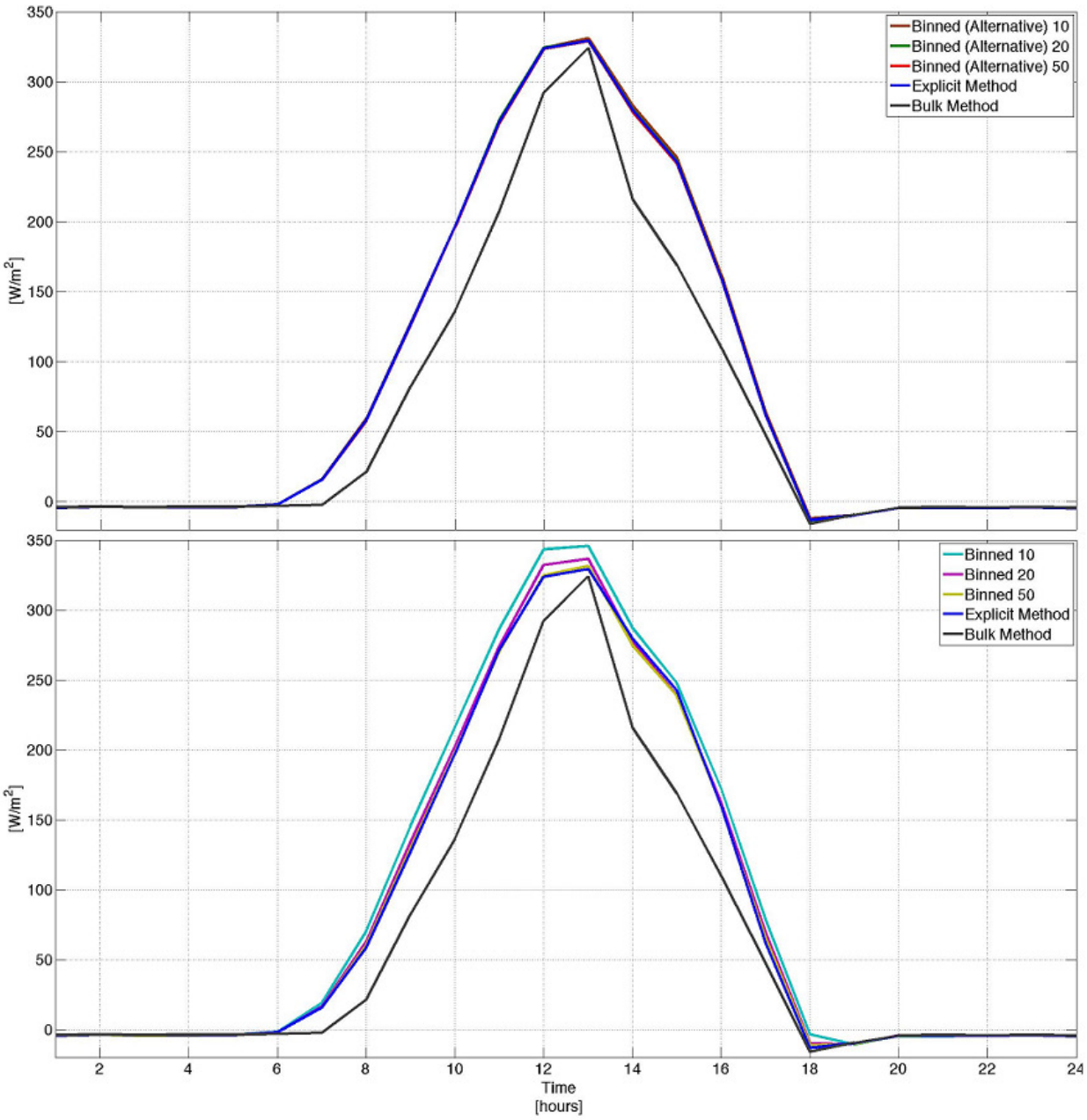

Figure 4.13d. Diurnal composites of the grid area averaged SH flux for all methods in biome 3.

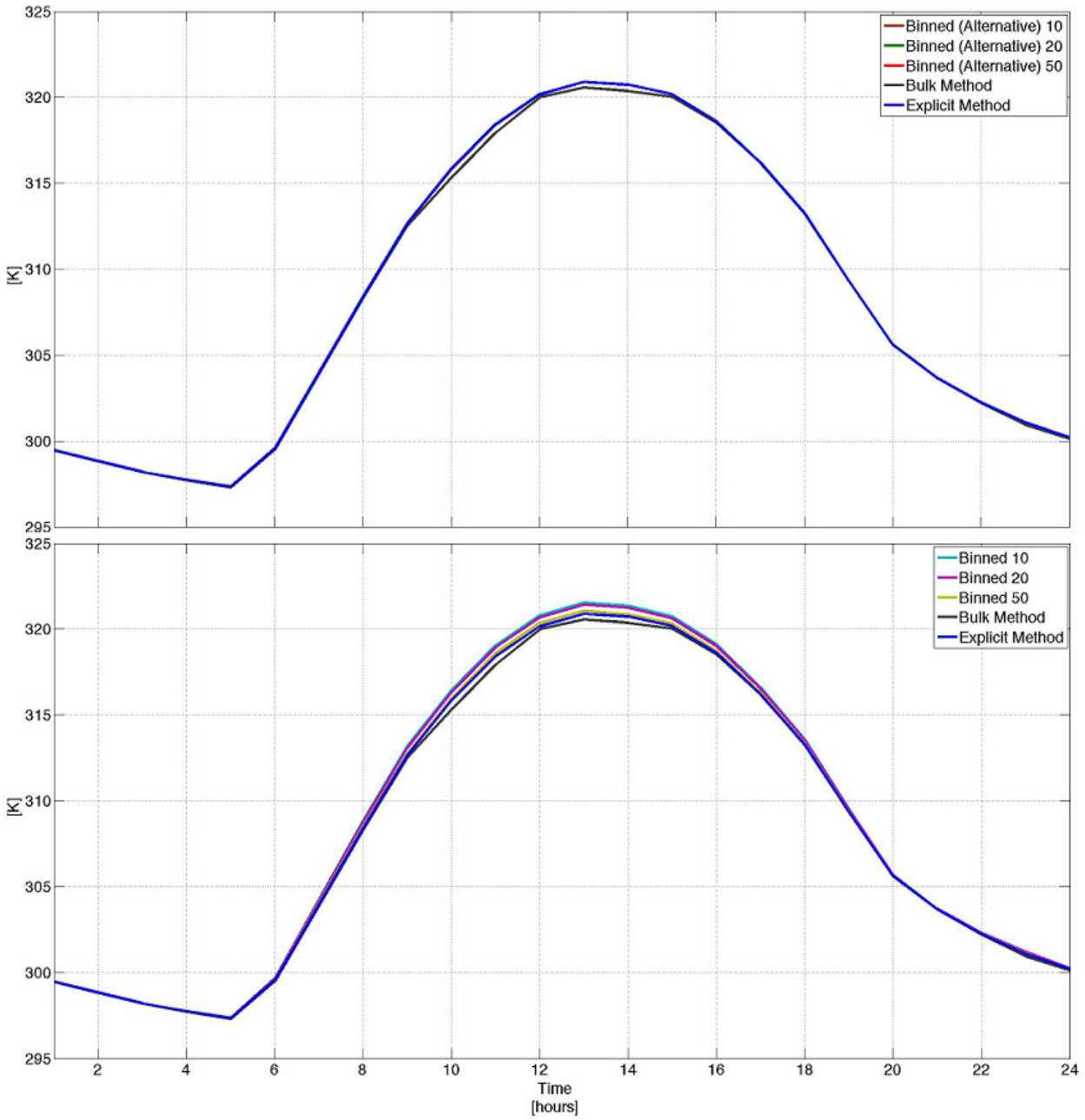

Figure 4.15a. Diurnal composites of the grid area averaged CAS temperature for all methods in biome 9.

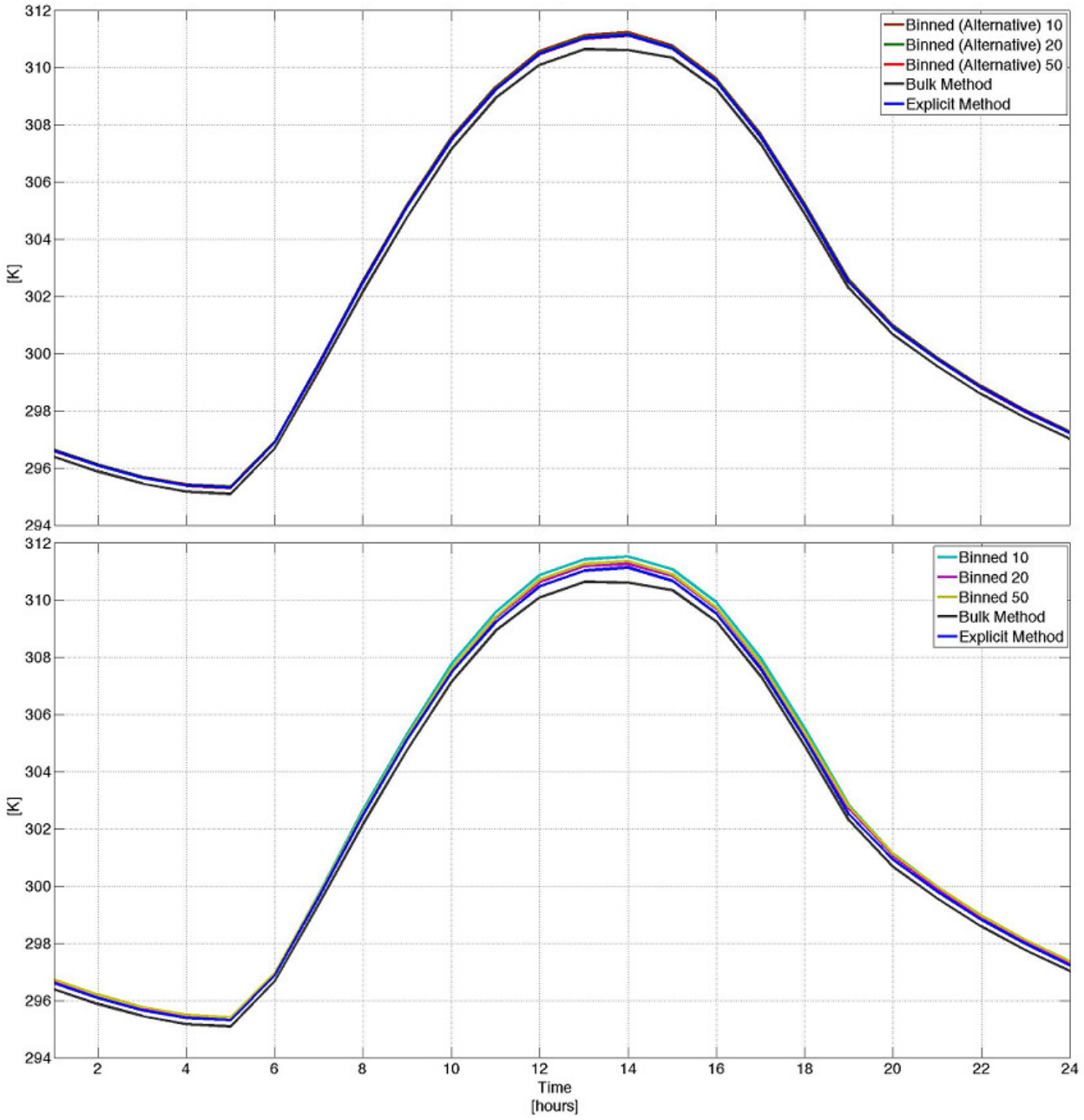

Figure 4.15b. Diurnal composites of the grid area averaged CAS temperature for all methods in biome 6.

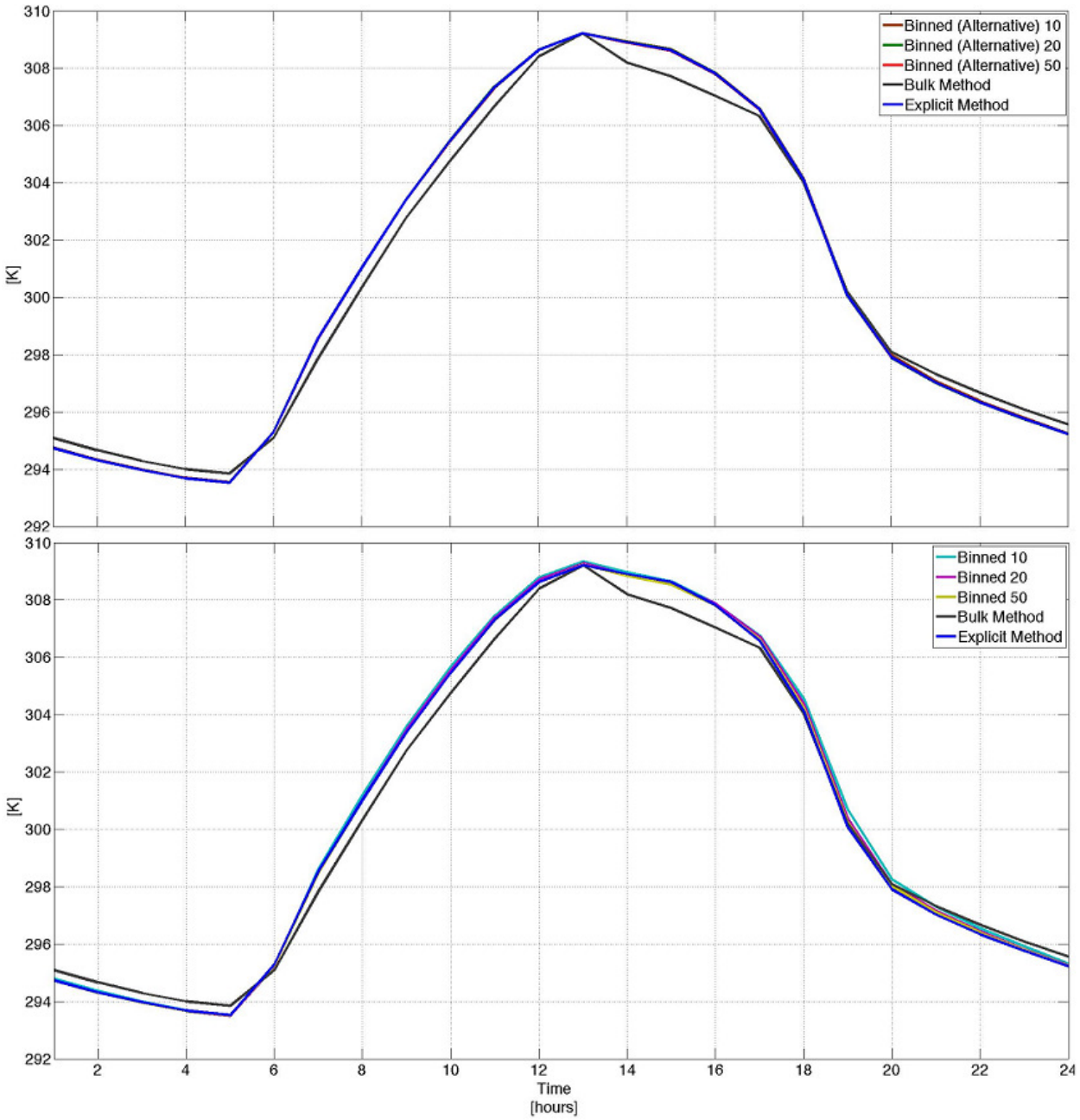

Figure 4.15c. Diurnal composites of the grid area averaged CAS temperature for all methods in biome 3.

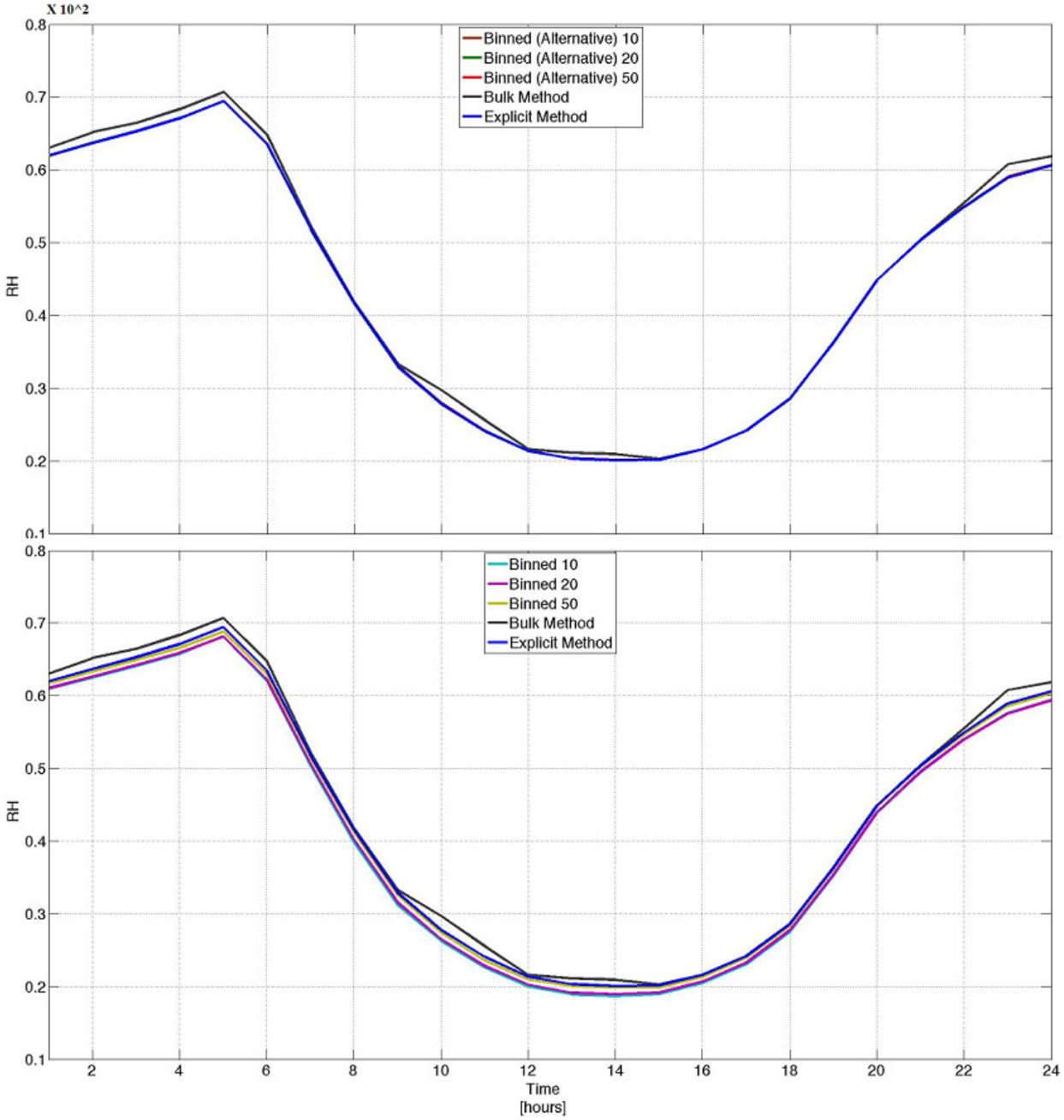

Figure 4.15d. Diurnal composites of the grid area averaged CAS relative humidity for all methods in biome 9.

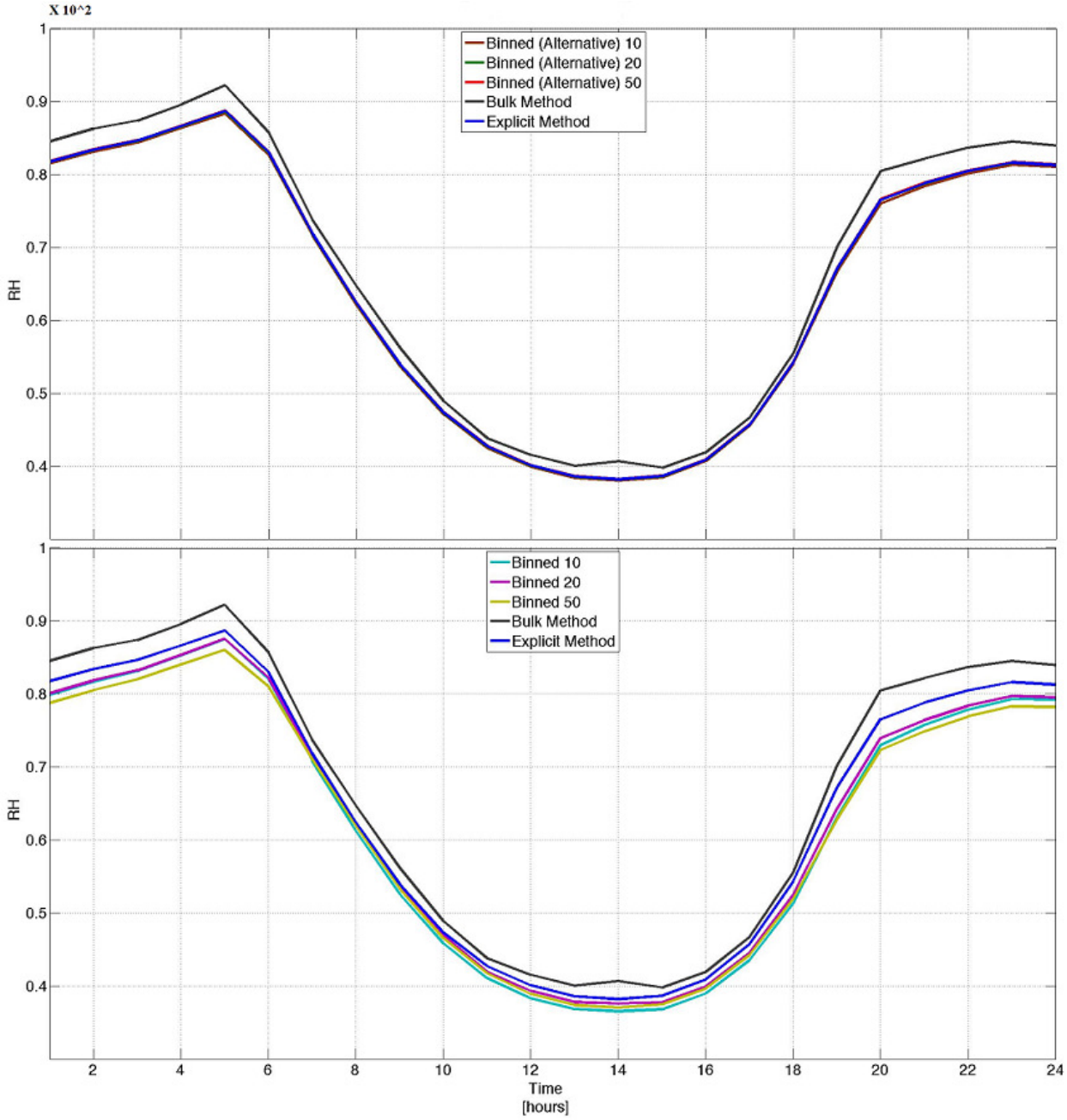

Figure 4.15e. Diurnal composites of the grid area averaged CAS relative humidity for all methods in biome 6.

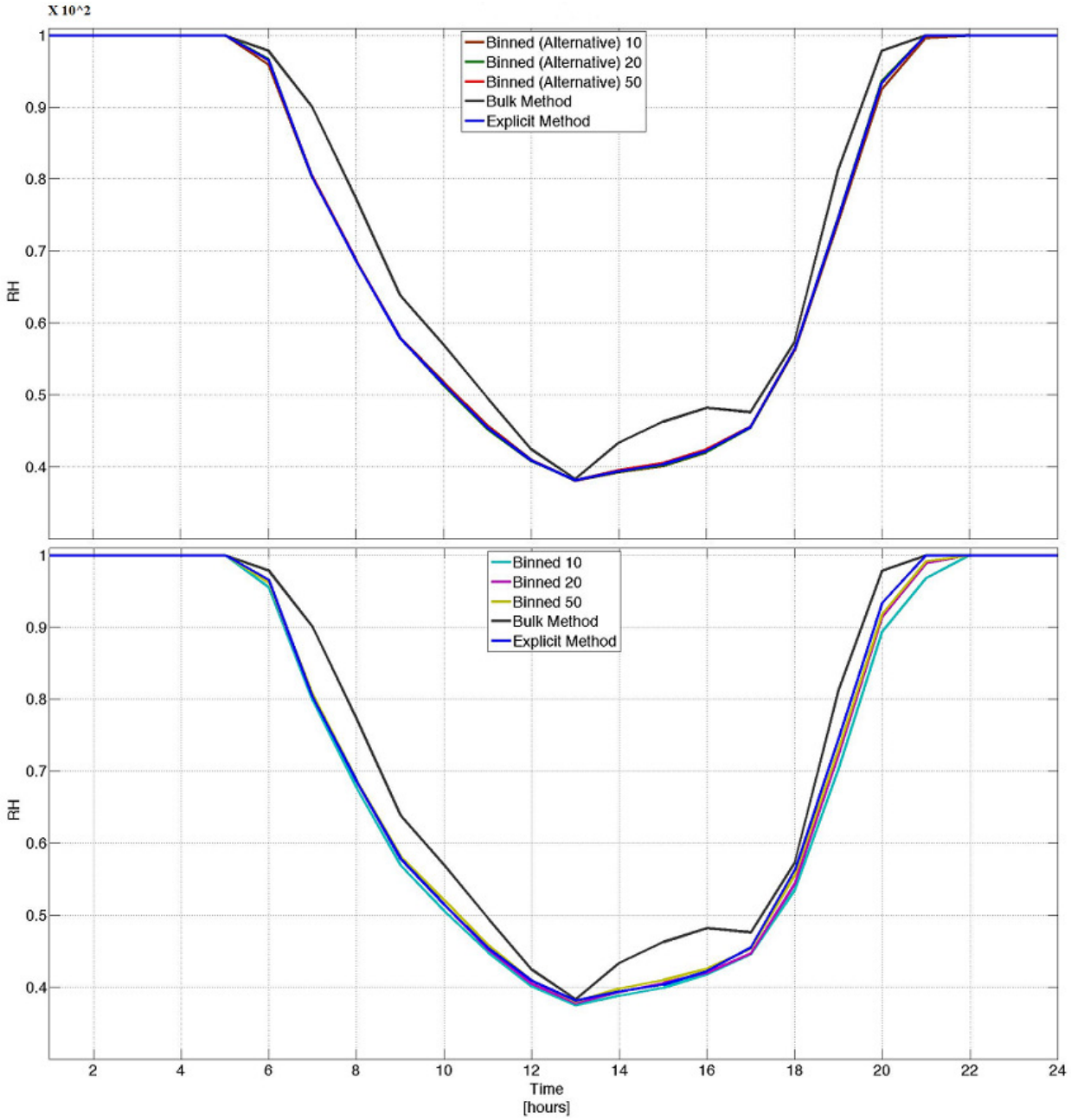

Figure 4.15f. Diurnal composites of the grid area averaged CAS relative humidity for all methods in biome 3.

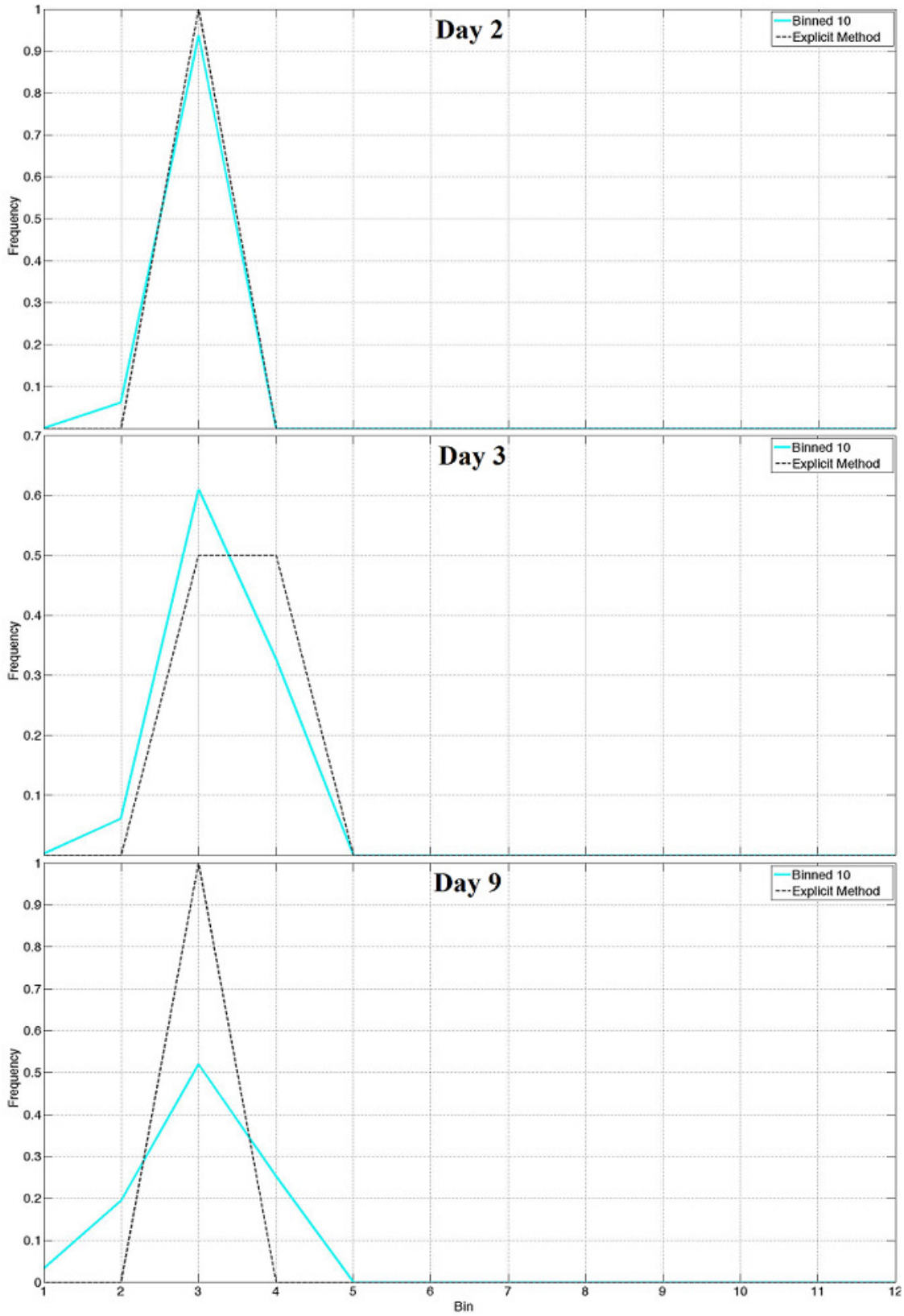

Figure 4.16a. Total plant available water distribution plots for the explicit and binned (10 bins) method, where days 2 and 9 are dry and day 3 has a precipitation event (bin wetness increases to the right).

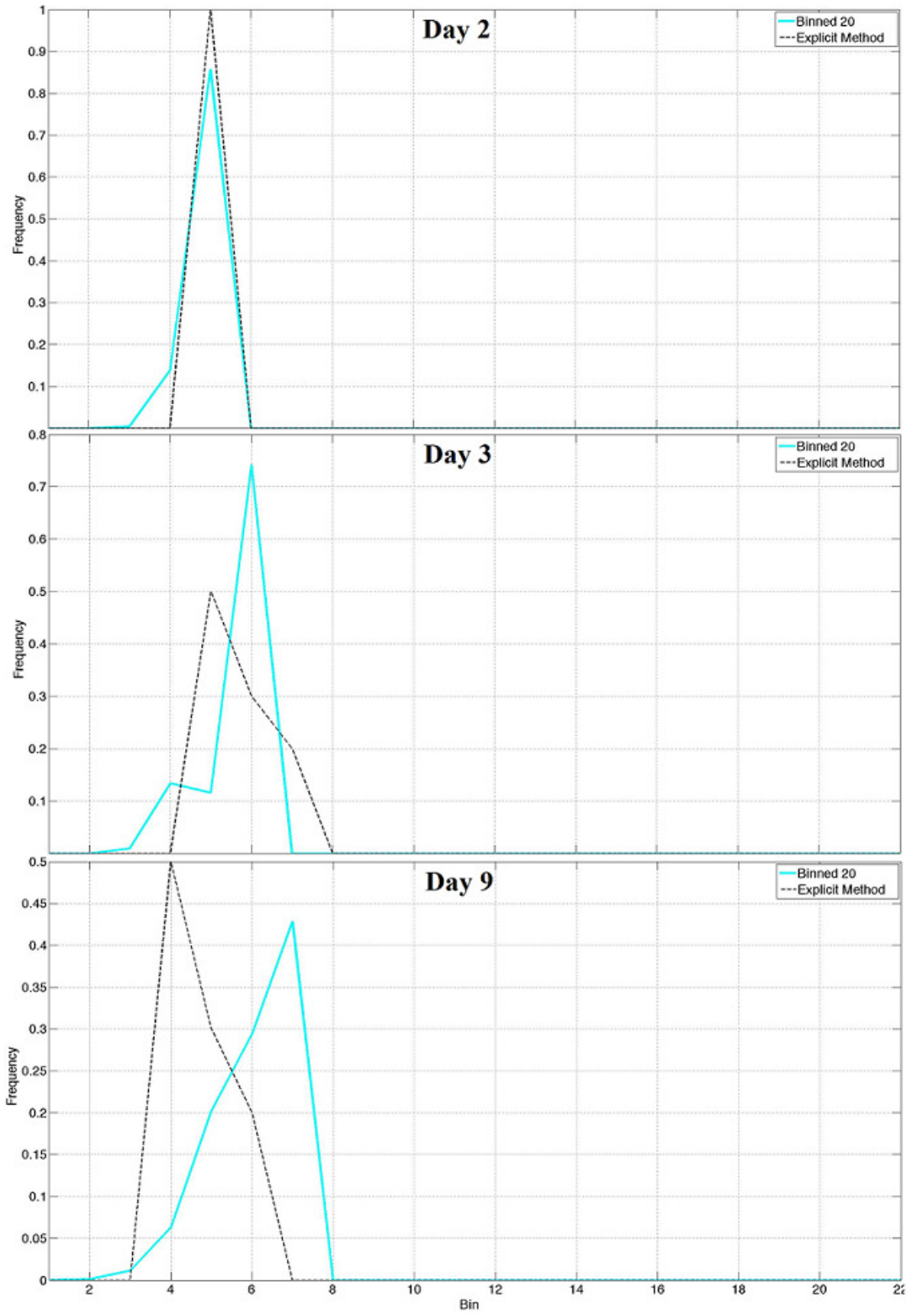

Figure 4.16b. Total plant available water distribution plots for the explicit and binned (20 bins) method, where days 2 and 9 are dry and day 3 has a precipitation event (bin wetness increases to the right).

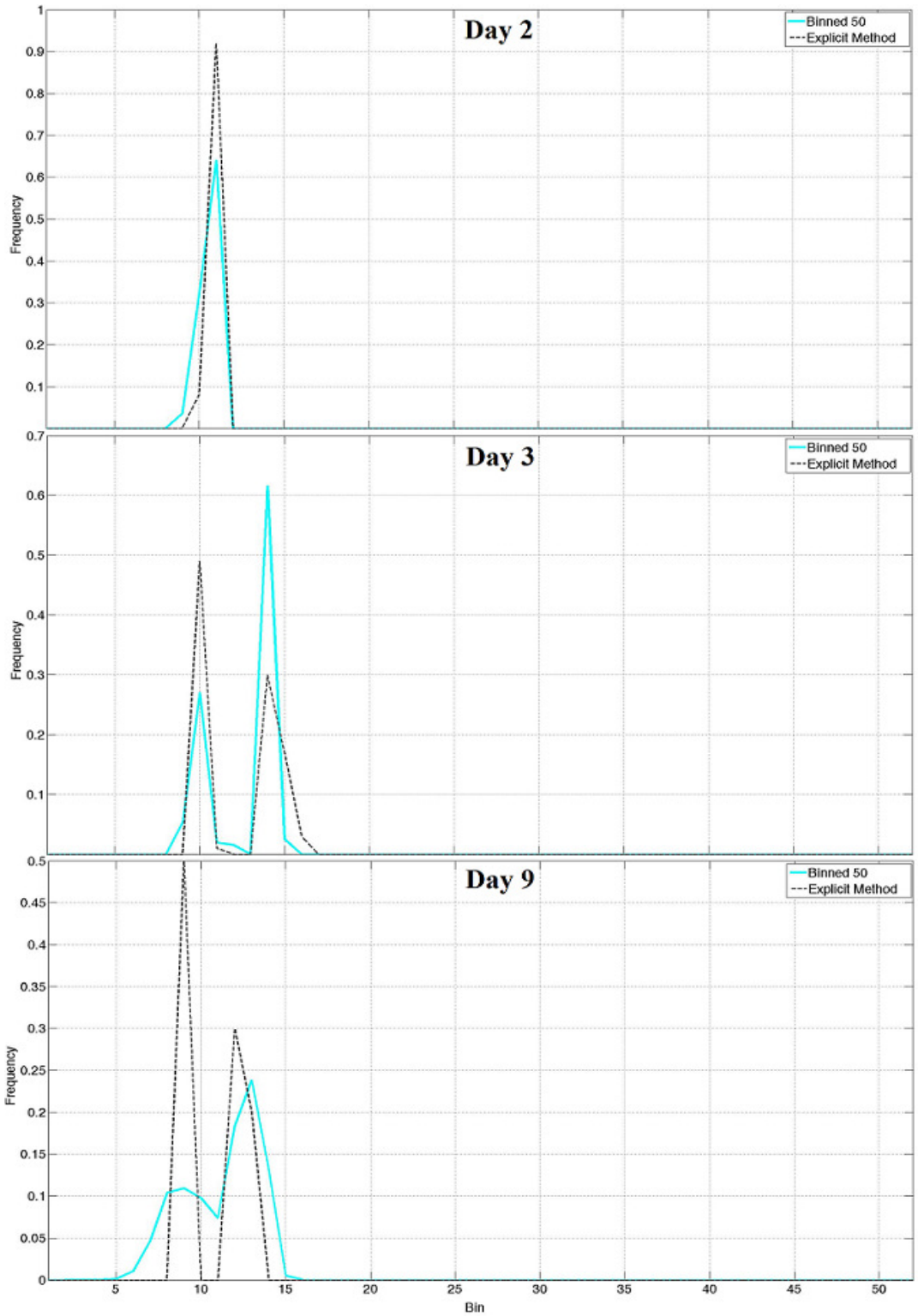

Figure 4.16c. Total plant available water distribution plots for the explicit and binned (50 bins) method, where days 2 and 9 are dry and day 3 has a precipitation event (bin wetness increases to the right).

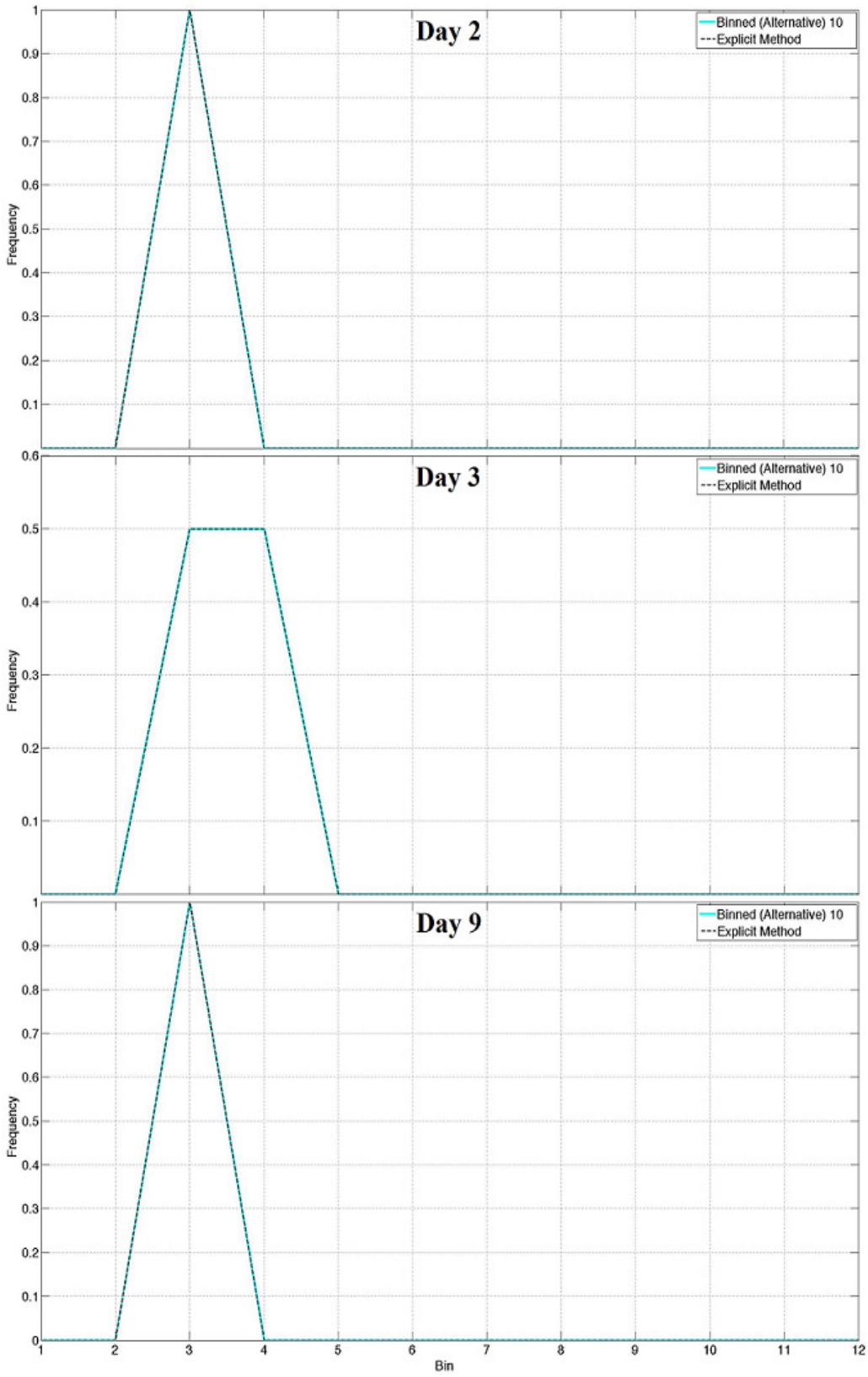

Figure 4.16d. Total plant available water distribution plots for the explicit and alternative binned (10 bins) method, where days 2 and 9 are dry and day 3 has a precipitation event (bin wetness increases to the right).

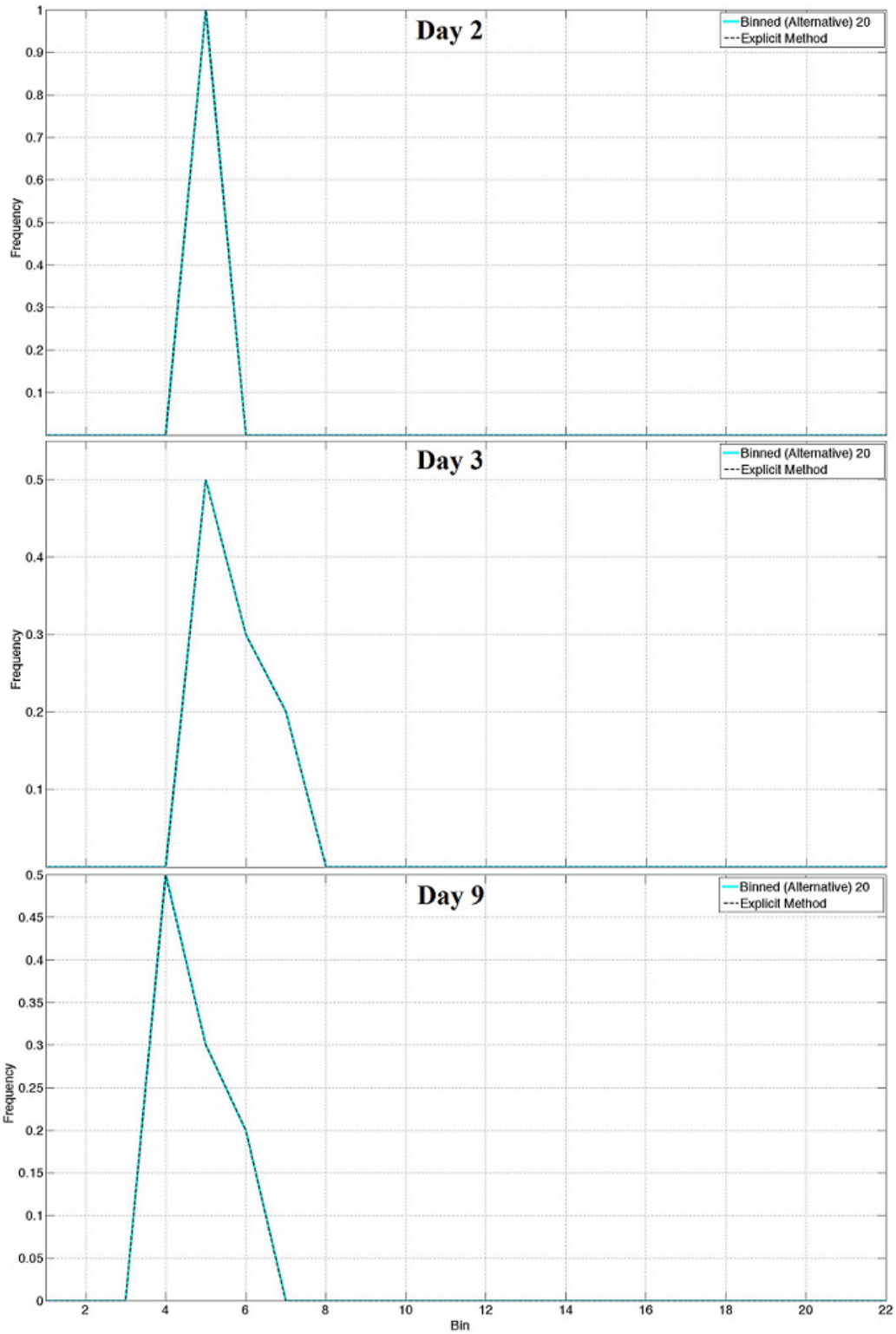

Figure 4.16e. Total plant available water distribution plots for the explicit and alternative binned (20 bins) method, where days 2 and 9 are dry and day 3 has a precipitation event (bin wetness increases to the right).

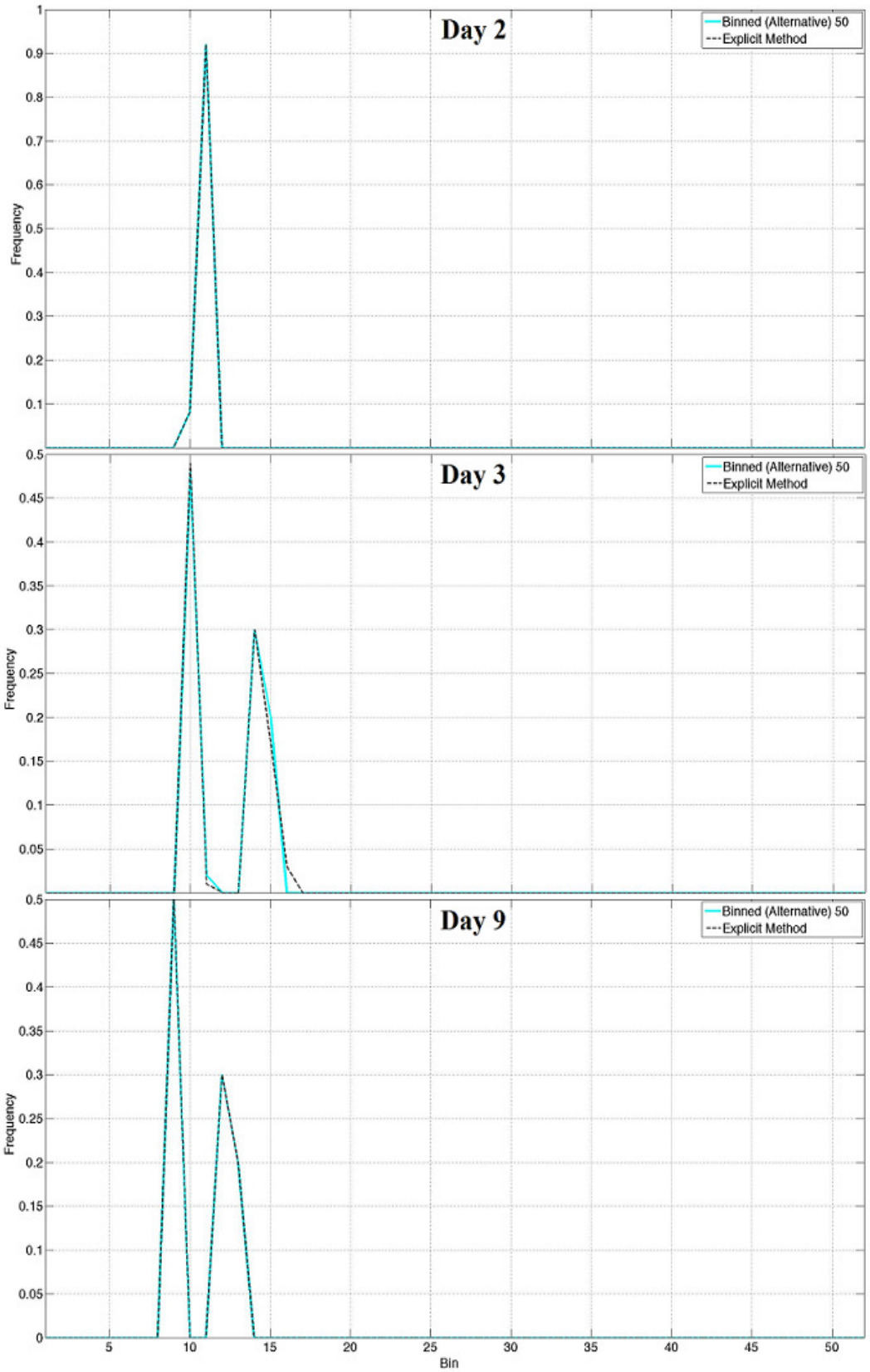

Figure 4.16f. Total plant available water distribution plots for the explicit and alternative binned (50 bins) method, where days 2 and 9 are dry and day 3 has a precipitation event (bin wetness increases to the right).

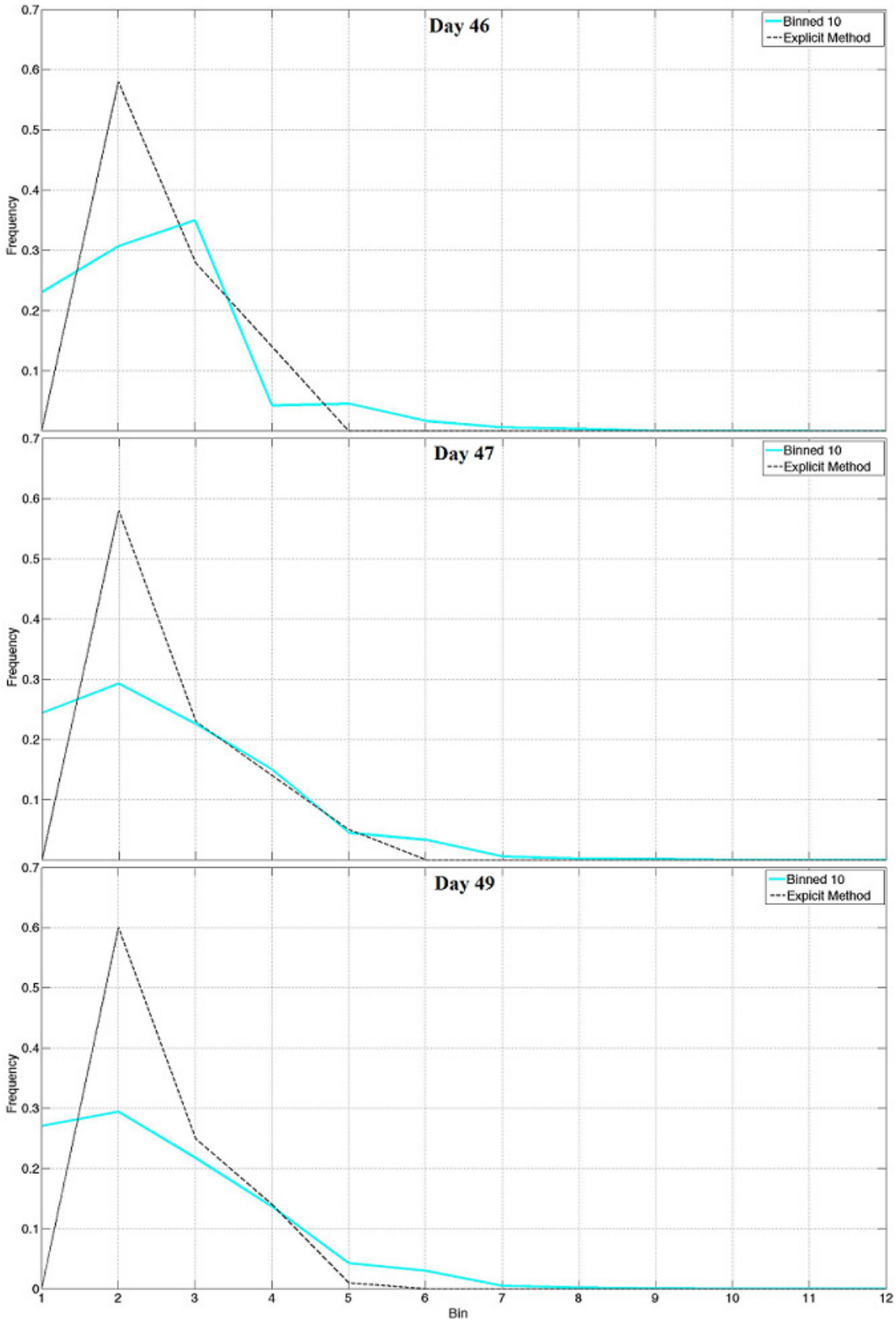

Figure 4.16g. Total plant available water distribution plots for the explicit and binned (10 bins) method, where days 46 and 49 are dry and day 47 has a precipitation event (bin wetness increases to the right).

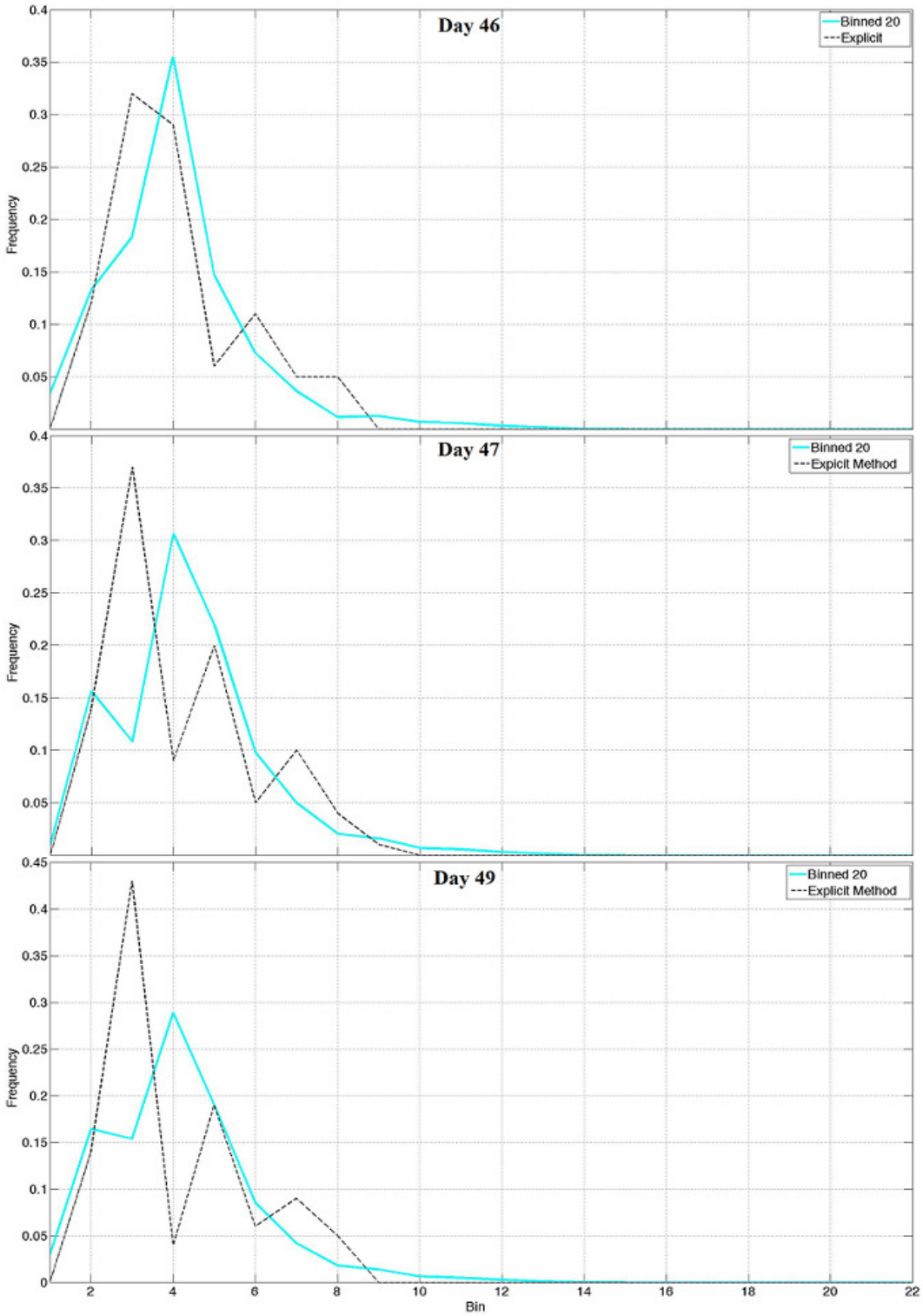

Figure 4.16h. Total plant available water distribution plots for the explicit and binned (20 bins) method, where days 46 and 49 are dry and day 47 has a precipitation event (bin wetness increases to the right).

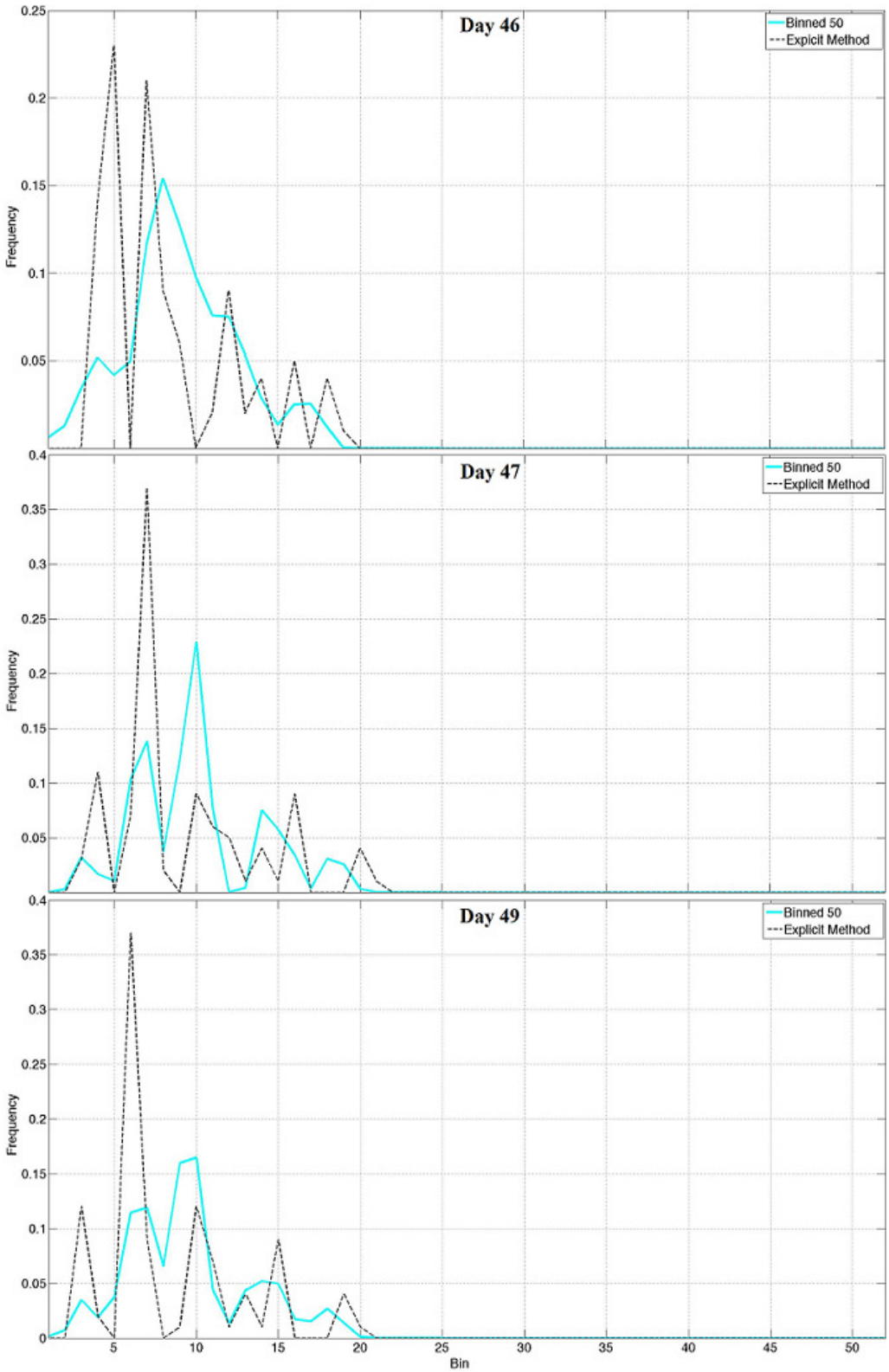

Figure 4.16i. Total plant available water distribution plots for the explicit and binned (50 bins) method, where days 46 and 49 are dry and day 47 has a precipitation event (bin wetness increases to the right).

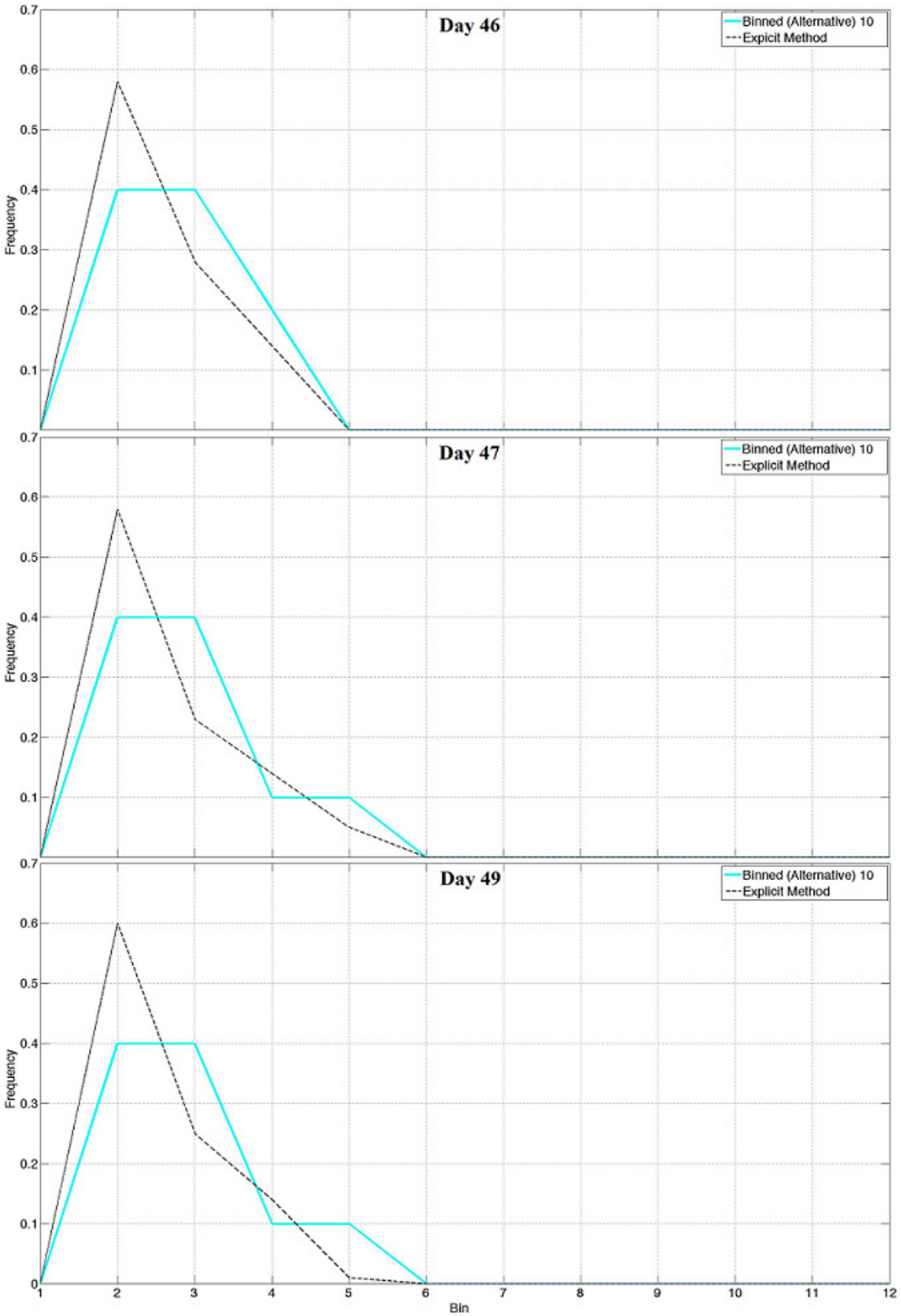

Figure 4.16j. Total plant available water distribution plots for the explicit and alternative binned (10 bins) method, where days 46 and 49 are dry and day 47 has a precipitation event (bin wetness increases to the right).

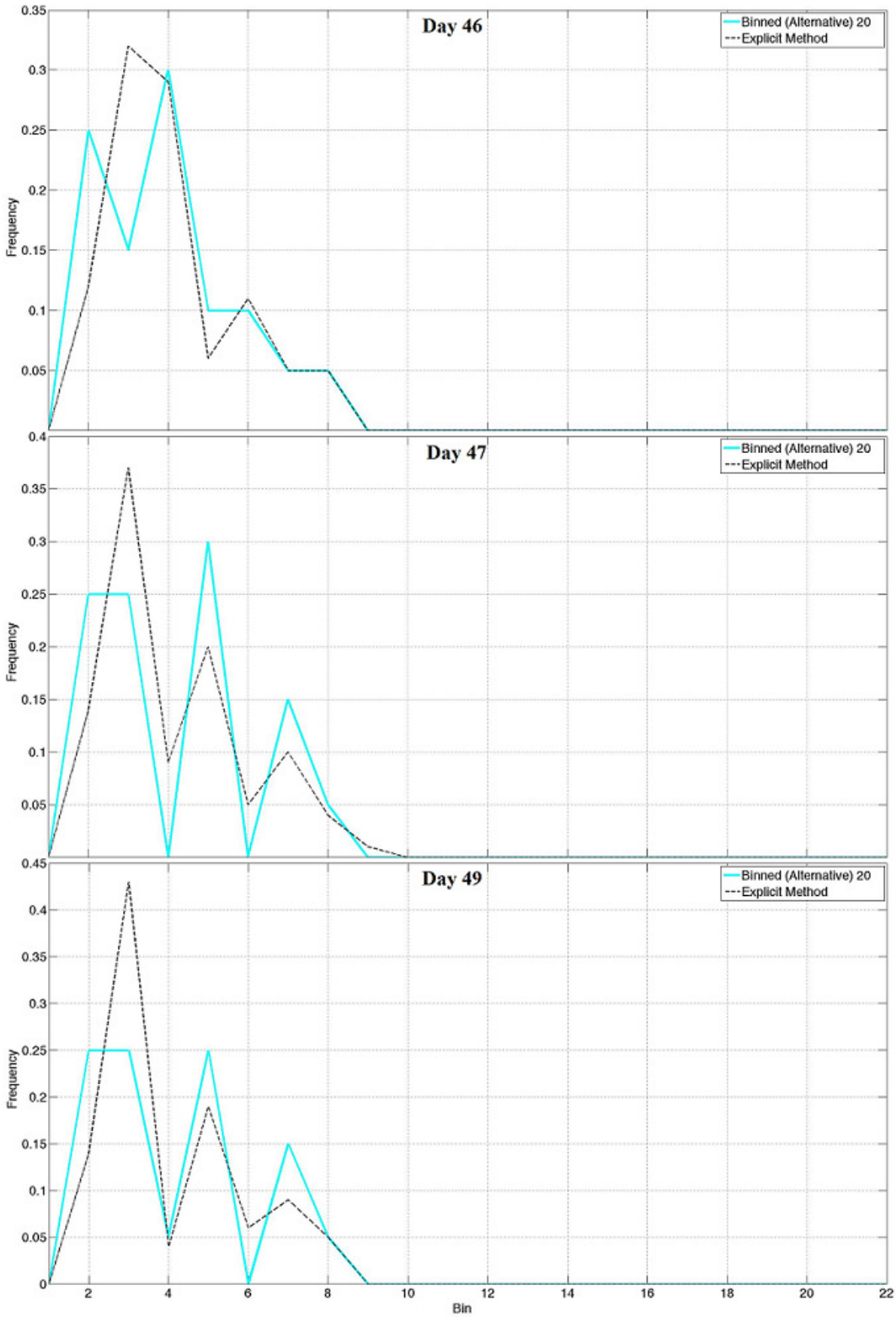

Figure 4.16k. Total plant available water distribution plots for the explicit and alternative binned (20 bins) method, where days 46 and 49 are dry and day 47 has a precipitation event (bin wetness increases to the right).

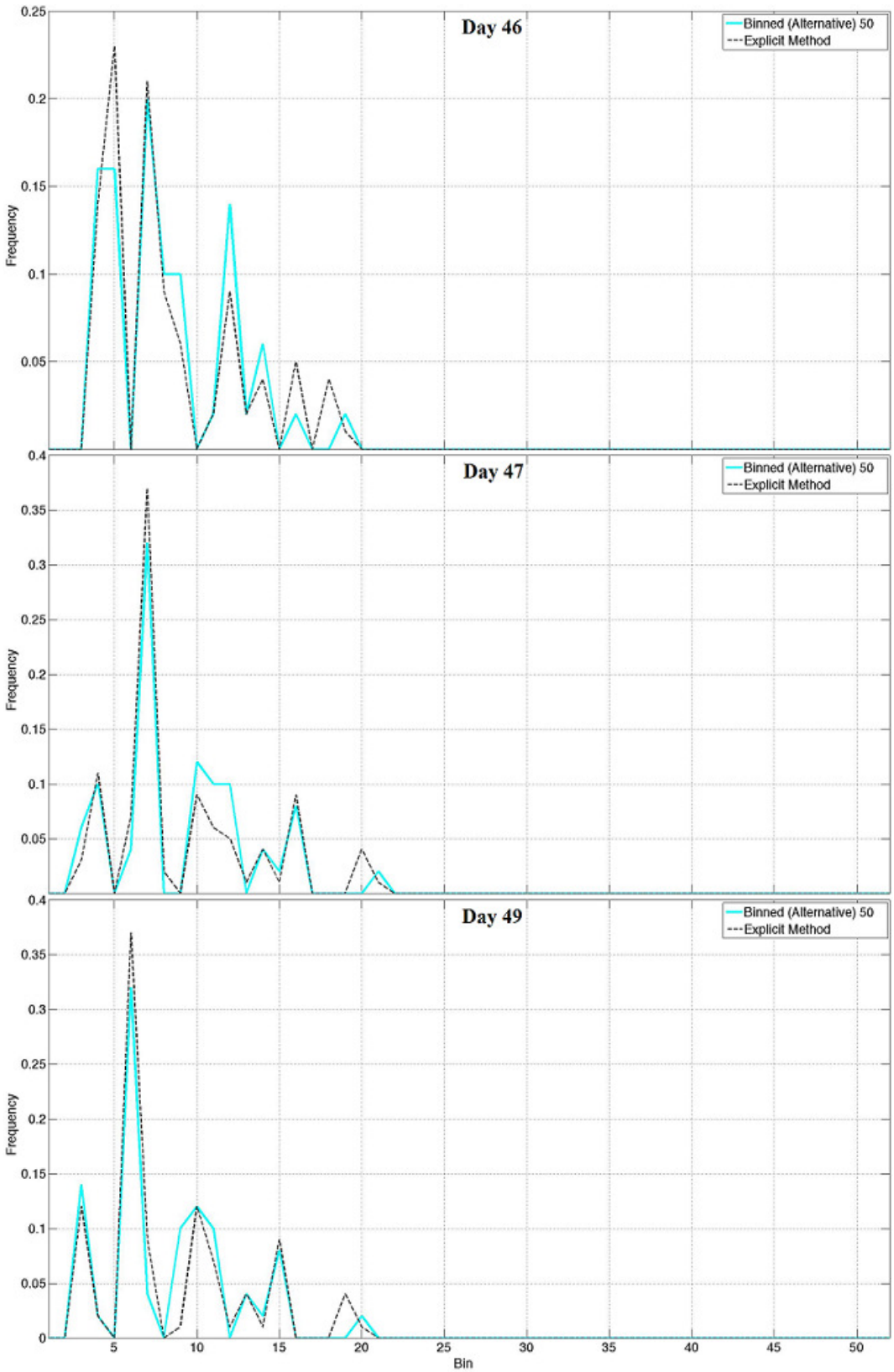

Figure 4.16l. Total plant available water distribution plots for the explicit and alternative binned (50 bins) method, where days 46 and 49 are dry and day 47 has a precipitation event (bin wetness increases to the right).

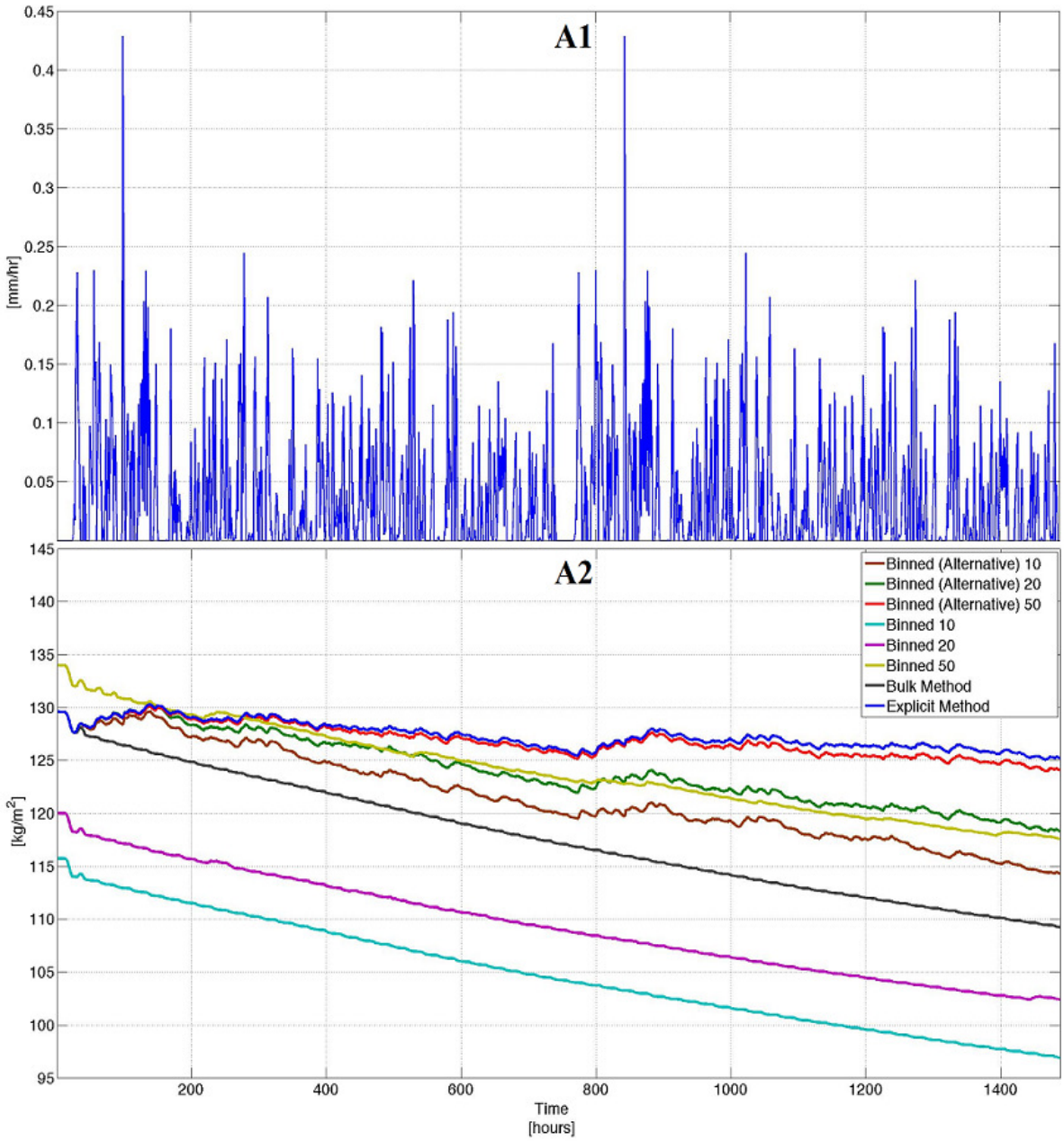

Figure 4.21a. Time series of the grid area averaged rainfall and total plant available water for biome 9, where panel A1 shows the grid area averaged rainfall rate and panel A2 is the grid area averaged total plant available water for the various methods.

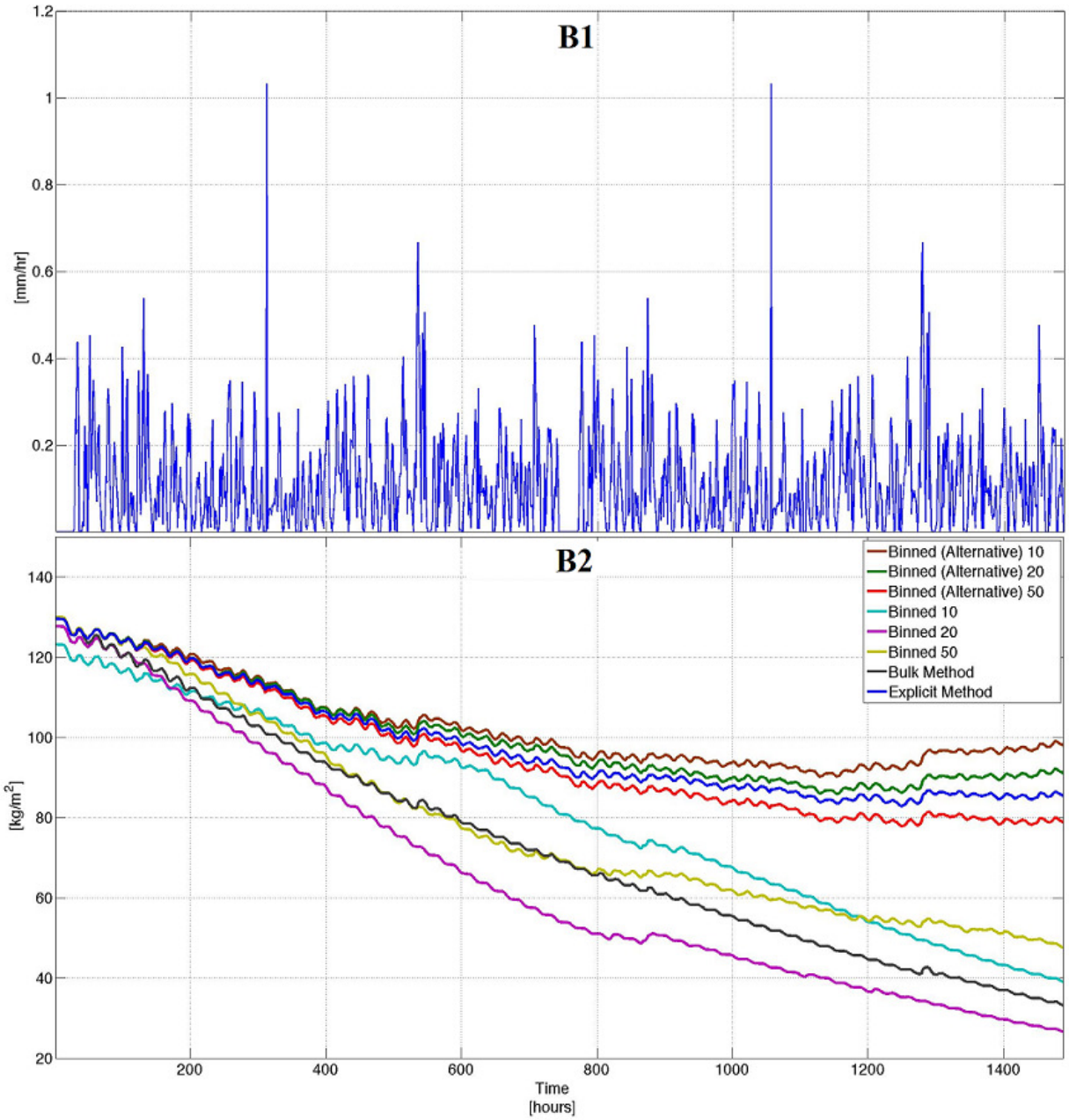

Figure 4.21b. Time series of the grid area averaged rainfall and total plant available water for biome 6, where panel B1 shows the grid area averaged rainfall rate and panel B2 is the gird area averaged total plant available water for the various methods.

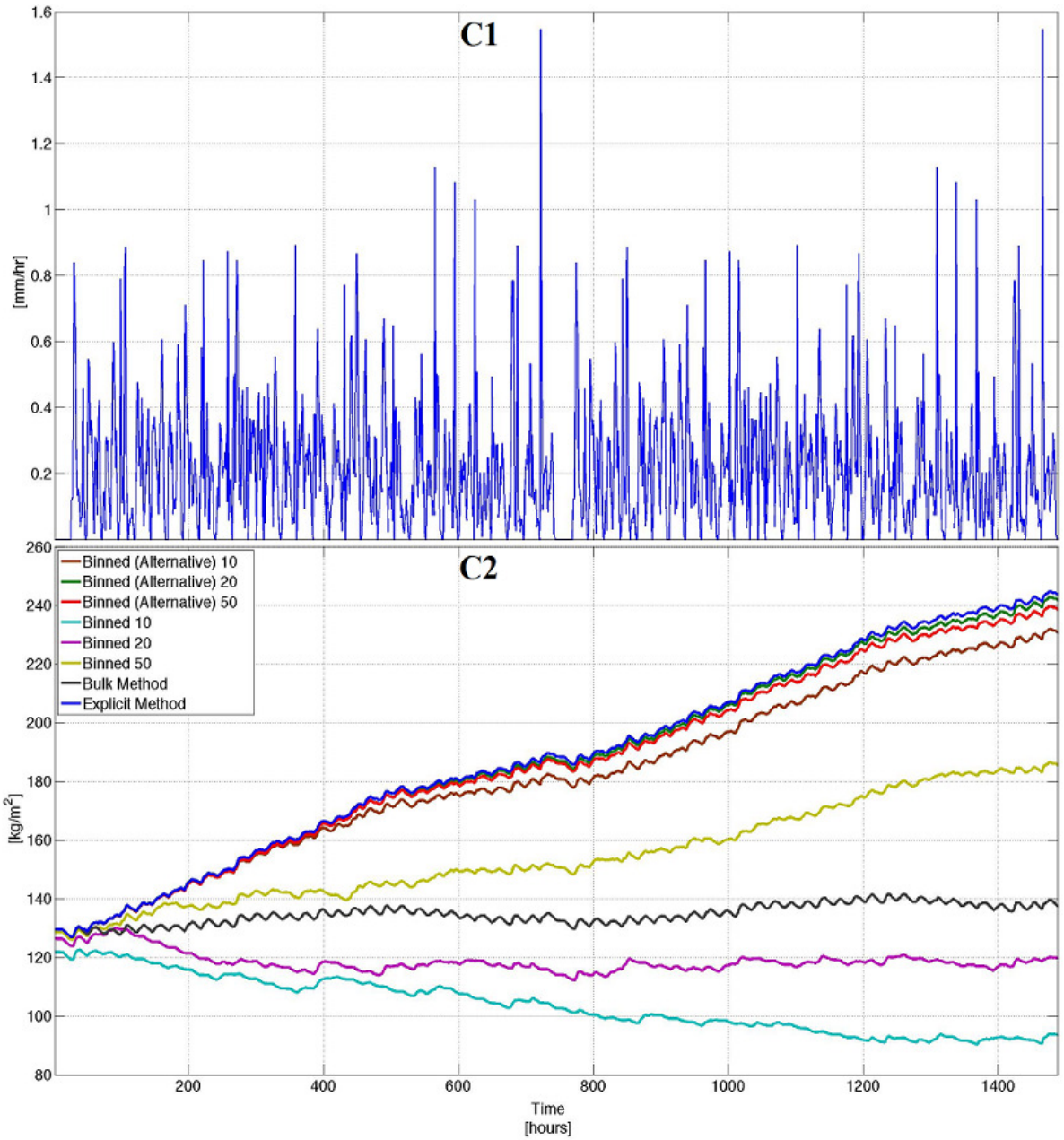

Figure 4.21c. Time series of the grid area averaged rainfall and total plant available water for biome 3, where panel C1 shows the grid area averaged rainfall rate and panel C2 is the grid area averaged total plant available water for the various methods.

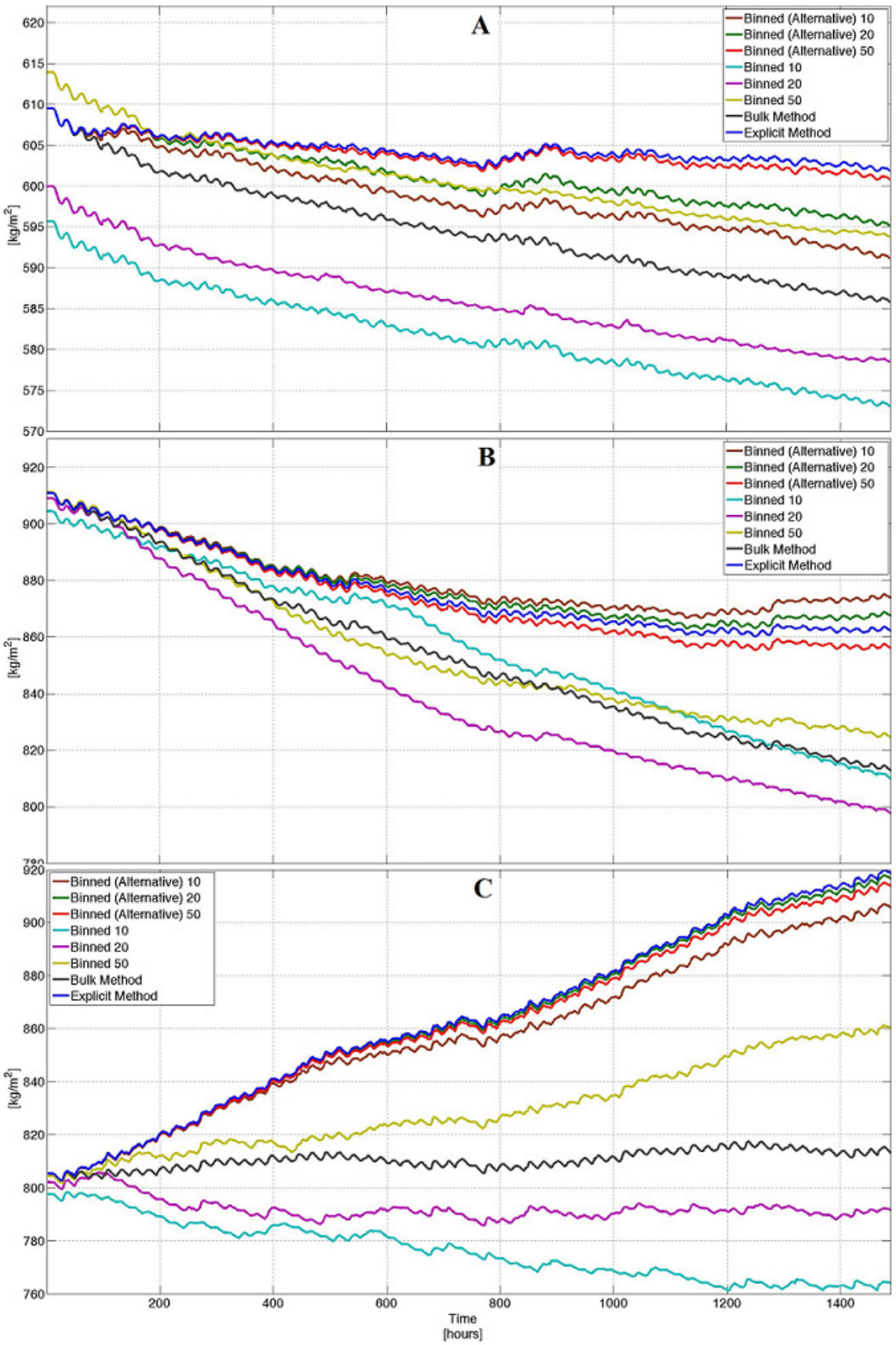

Figure 4.21d. Time series of the grid area averaged column integrated soil water mass for soil layers 1-8 for all methods, where panel A is biome 9, panel B is biome 6 and panel C is biome 3.

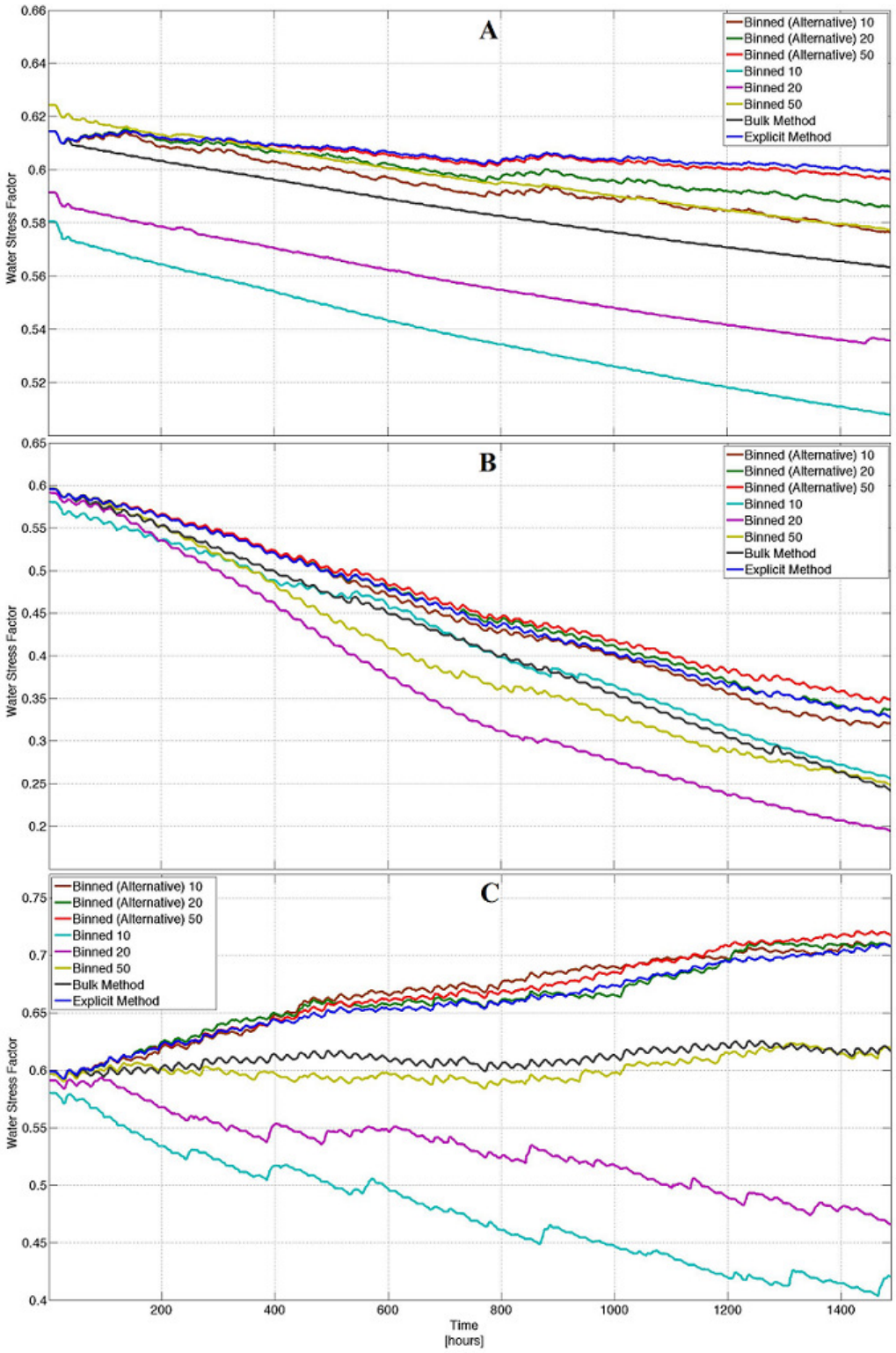

Figure 4.21e. Time series of the grid area averaged water stress factor for all methods, where panel A is biome 9, panel B is biome 6, and panel C is biome 3.

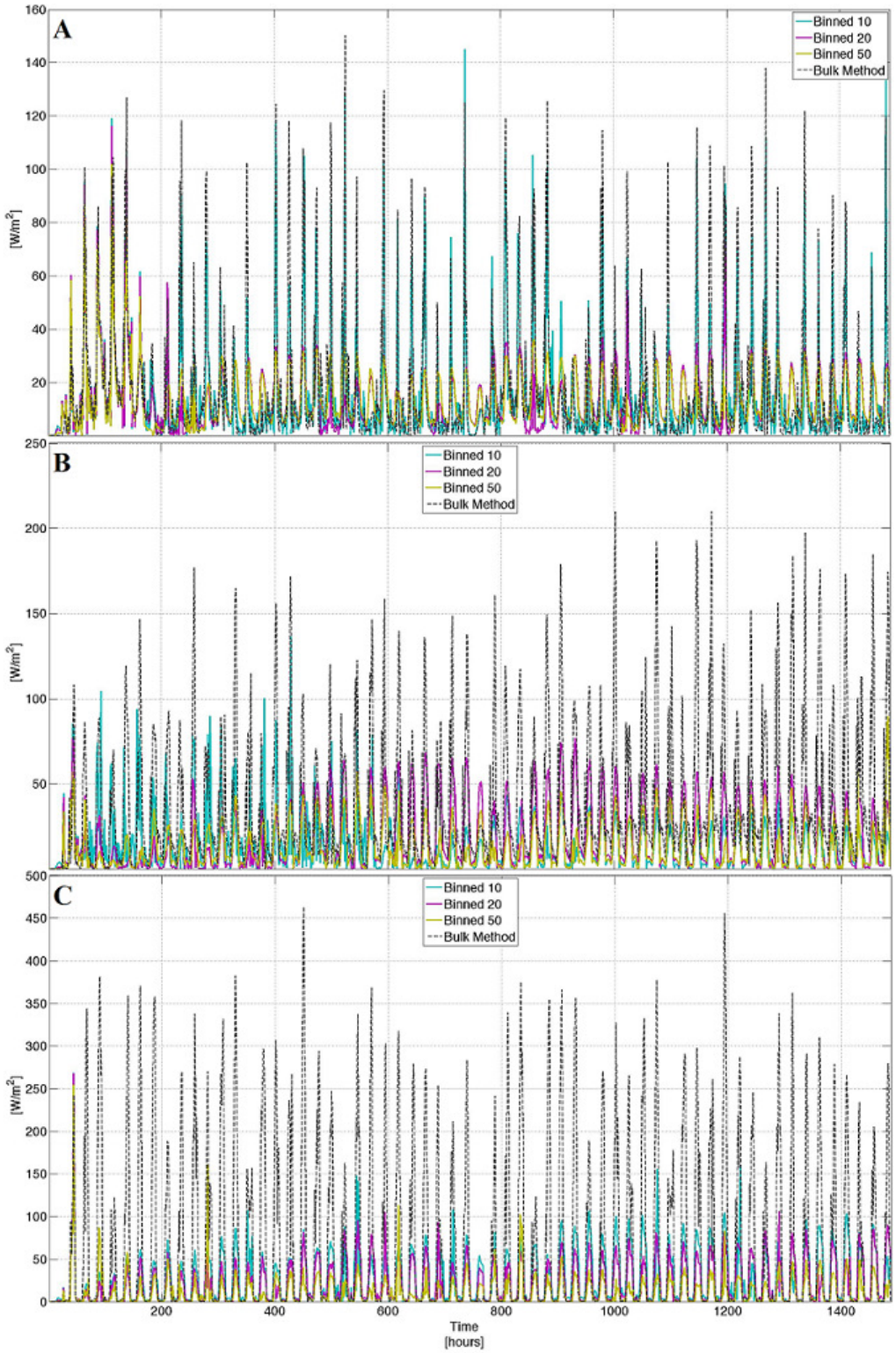

Figure 4.22a. Time series of absolute errors for the grid area averaged LH flux for the binned and bulk method, where panel A is biome 9, panel B is biome 6, and panel C is biome 3.

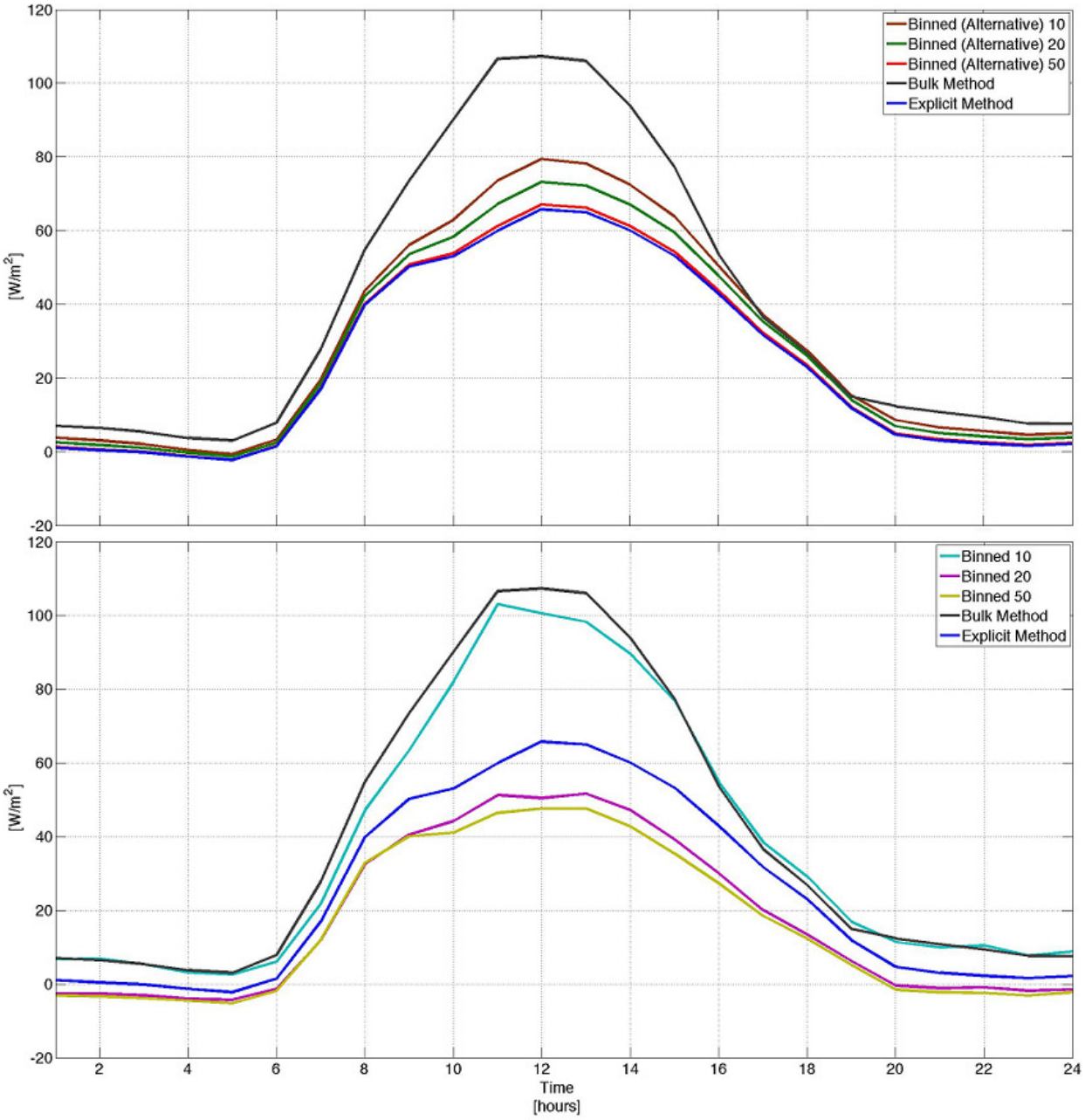

Figure 4.22b. Diurnal composites of the grid area averaged LH flux for all methods in biome 9.

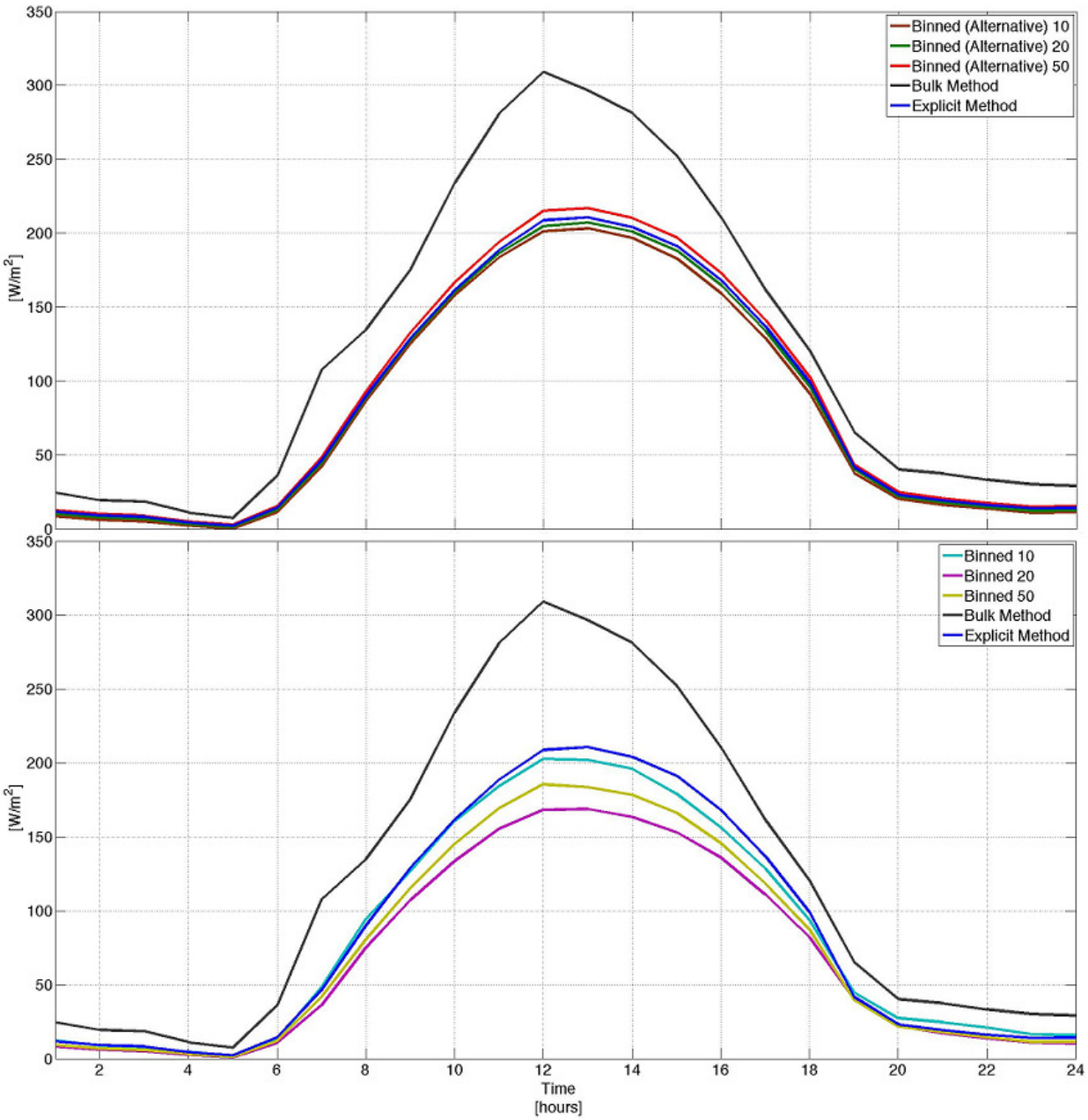

Figure 4.22c. Diurnal composites of the grid area averaged LH flux for all methods in biome 6.

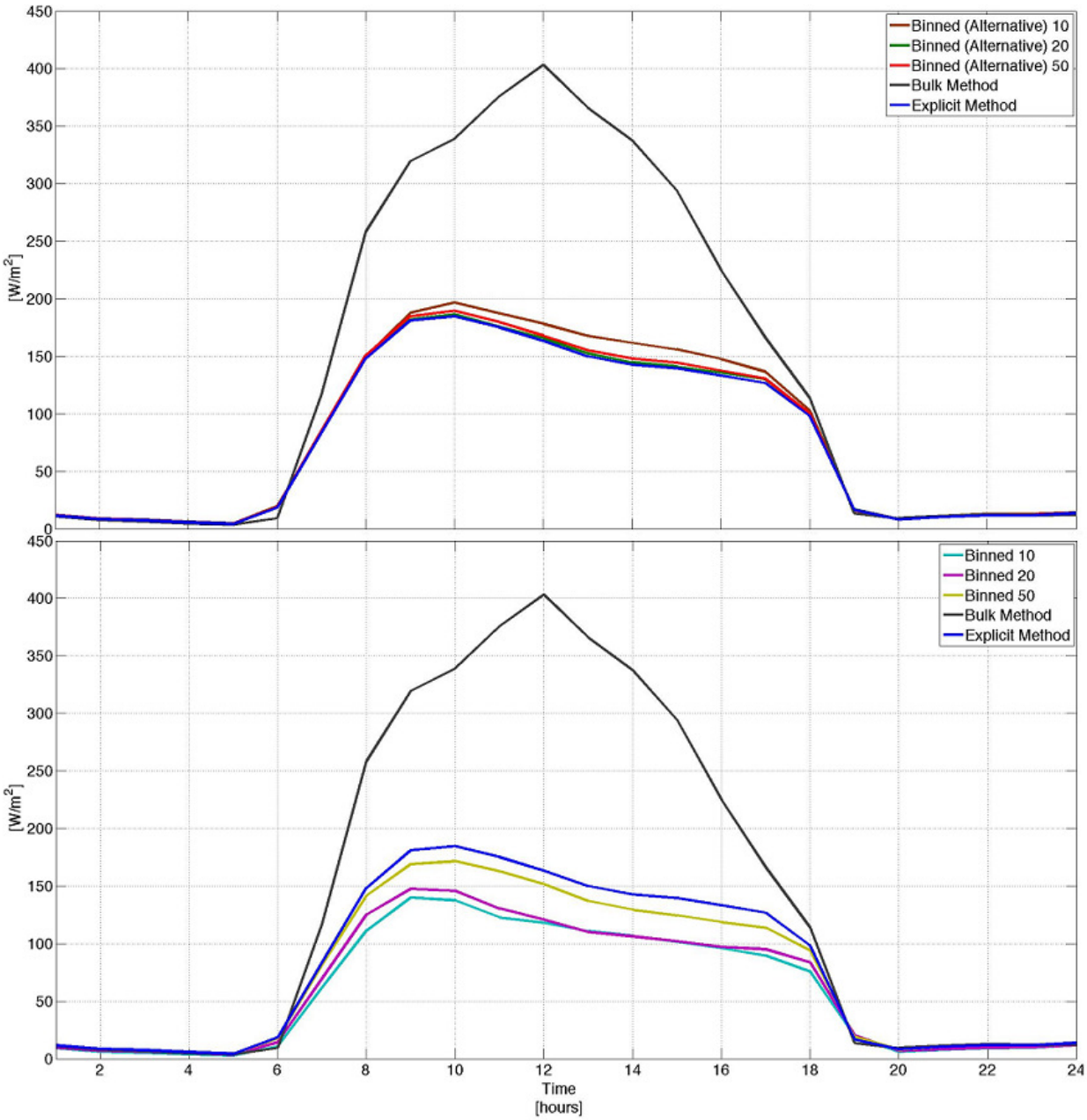

Figure 4.22d. Diurnal composites of the grid area averaged LH flux for all methods in biome 3.

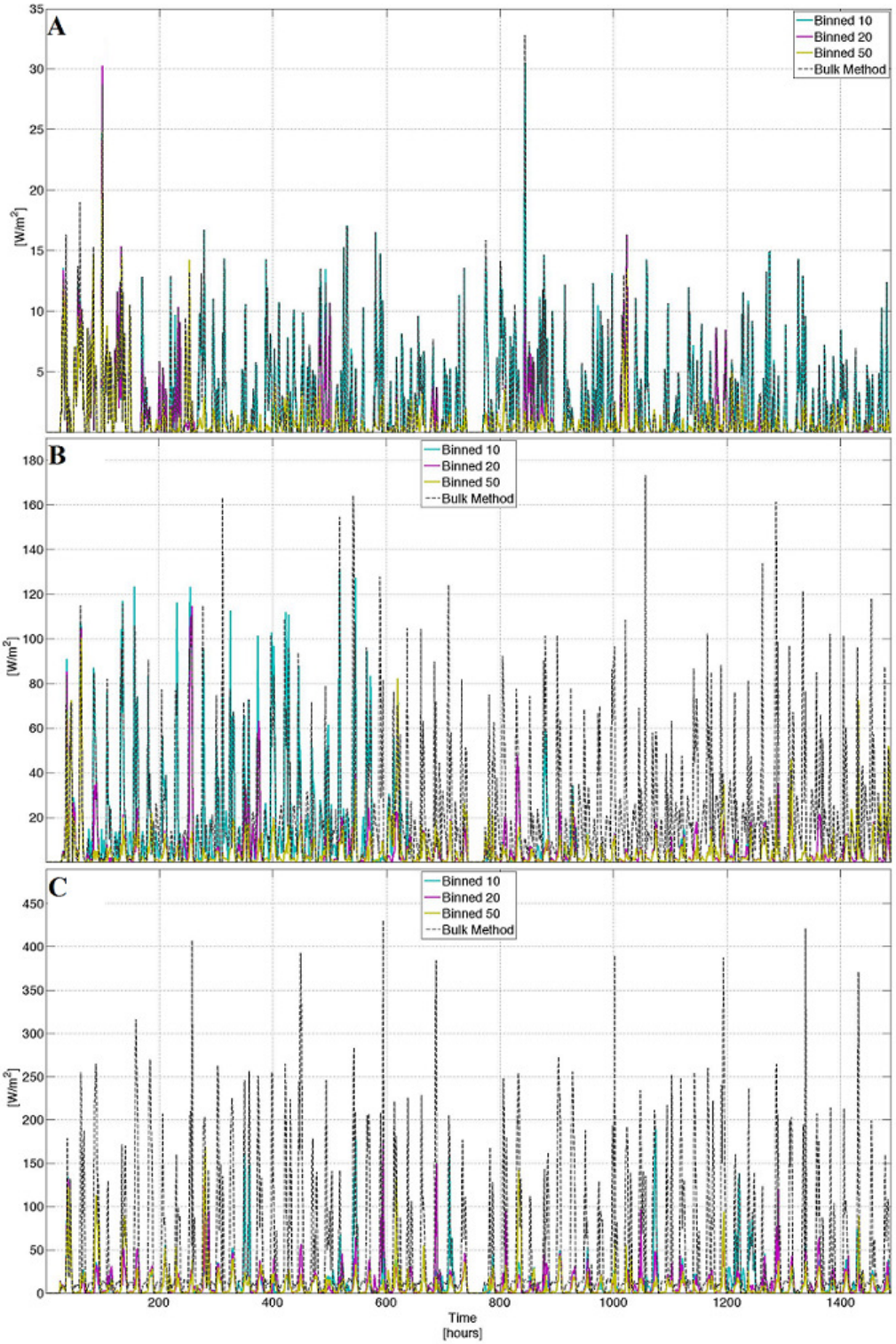

Figure 4.22e. Time series of absolute errors for the grid area averaged canopy intercepted LH flux for the binned and bulk method, where panel A is biome 9, panel B is biome 6, and panel C is biome 3.

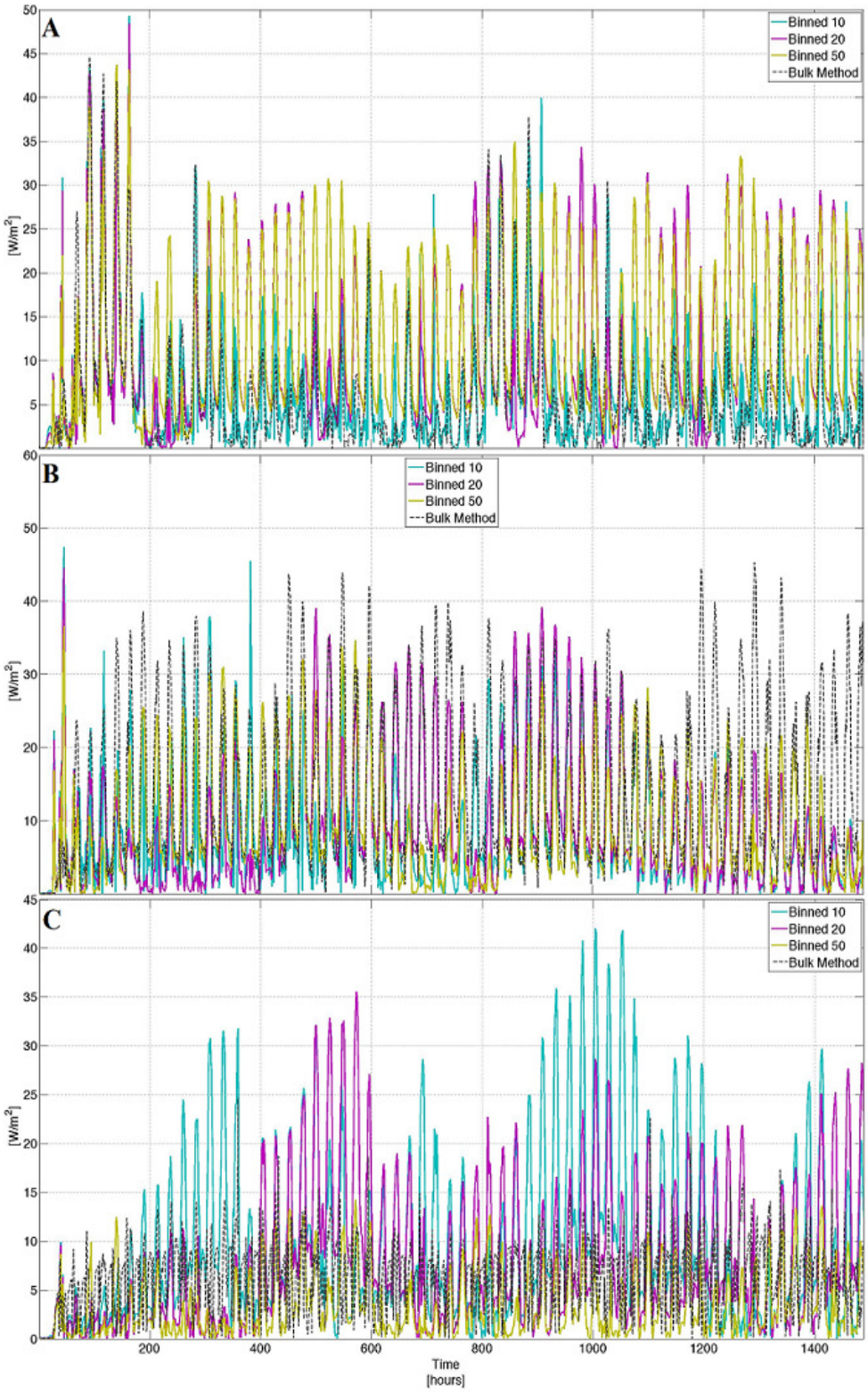

Figure 4.22f. Time series of absolute errors for the grid area averaged ground LH flux for the binned and bulk method, where panel A is biome 9, panel B is biome 6, and panel C is biome 3.

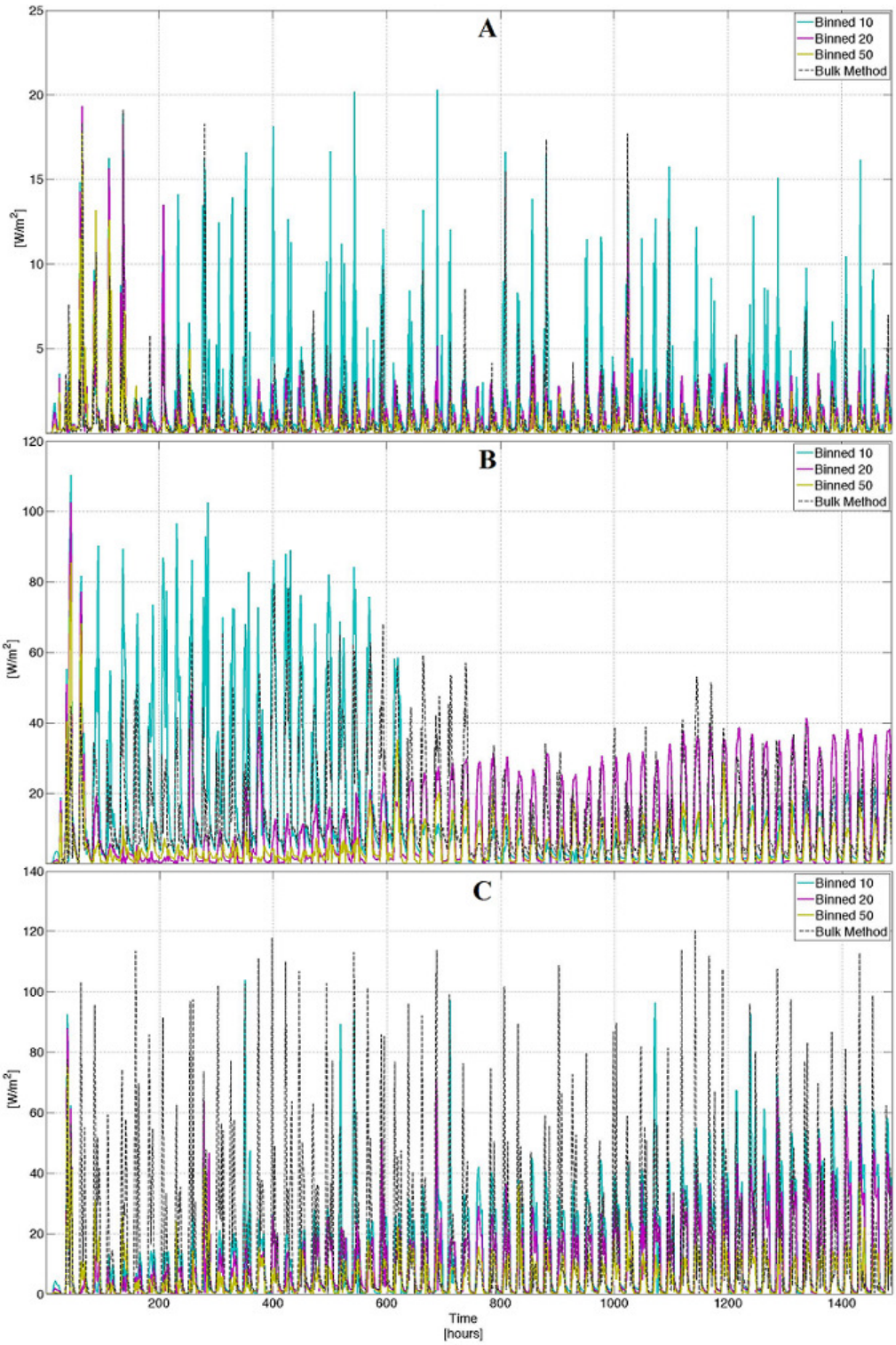

Figure 4.22g. Time series of absolute errors for the grid area averaged transpiration for the binned and bulk method, where panel A is biome 9, panel B is biome 6, and panel C is biome 3.

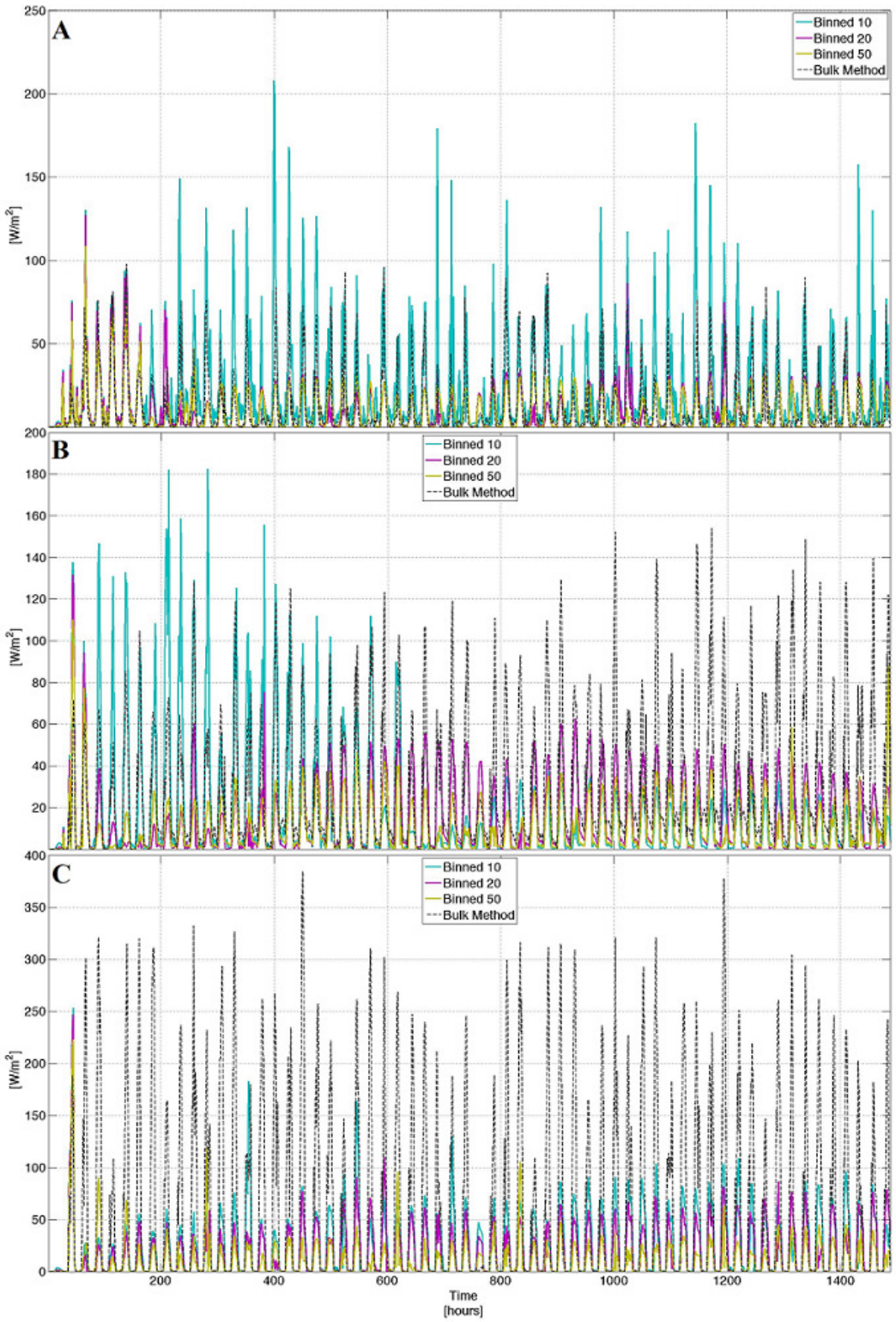

Figure 4.23a. Time series of absolute errors for the grid area averaged SH flux for the binned and bulk method, where panel A is biome 9, panel B is biome 6, and panel C is biome 3.

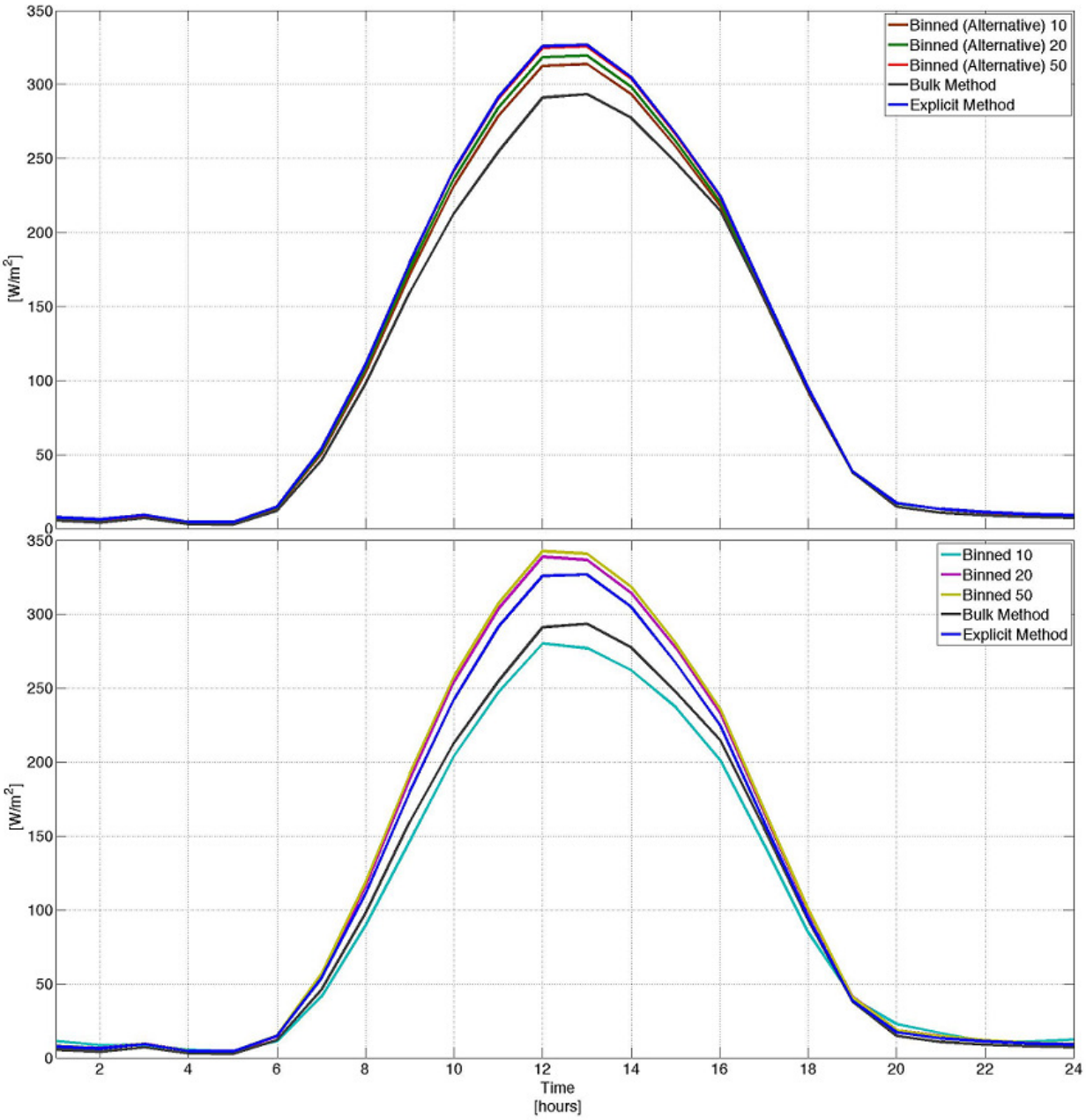

Figure 4.23b. Diurnal composites of the grid area averaged SH flux for all methods in biome 9.

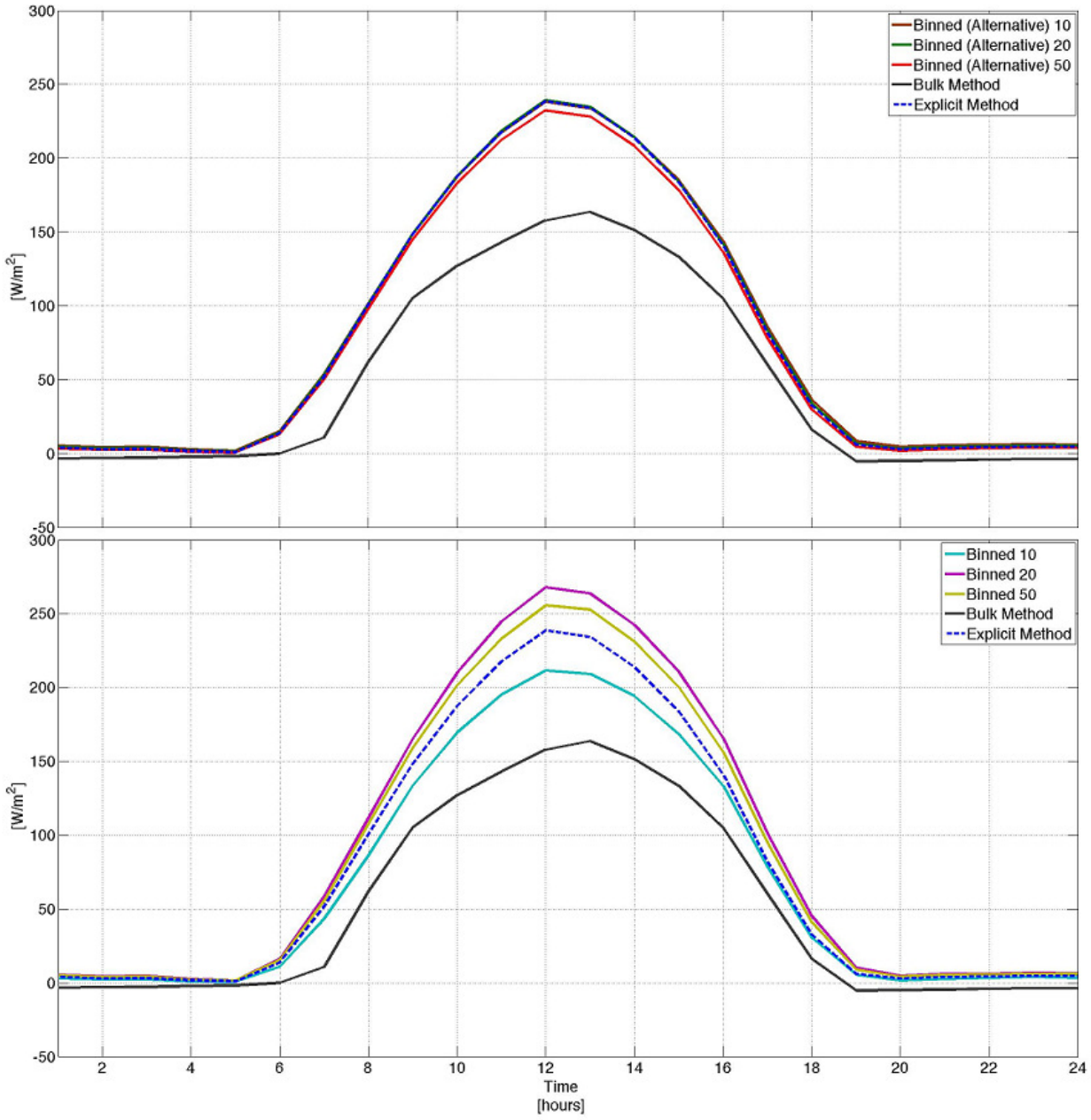

Figure 4.23c. Diurnal composites of the grid area averaged SH flux for all methods in biome 6.

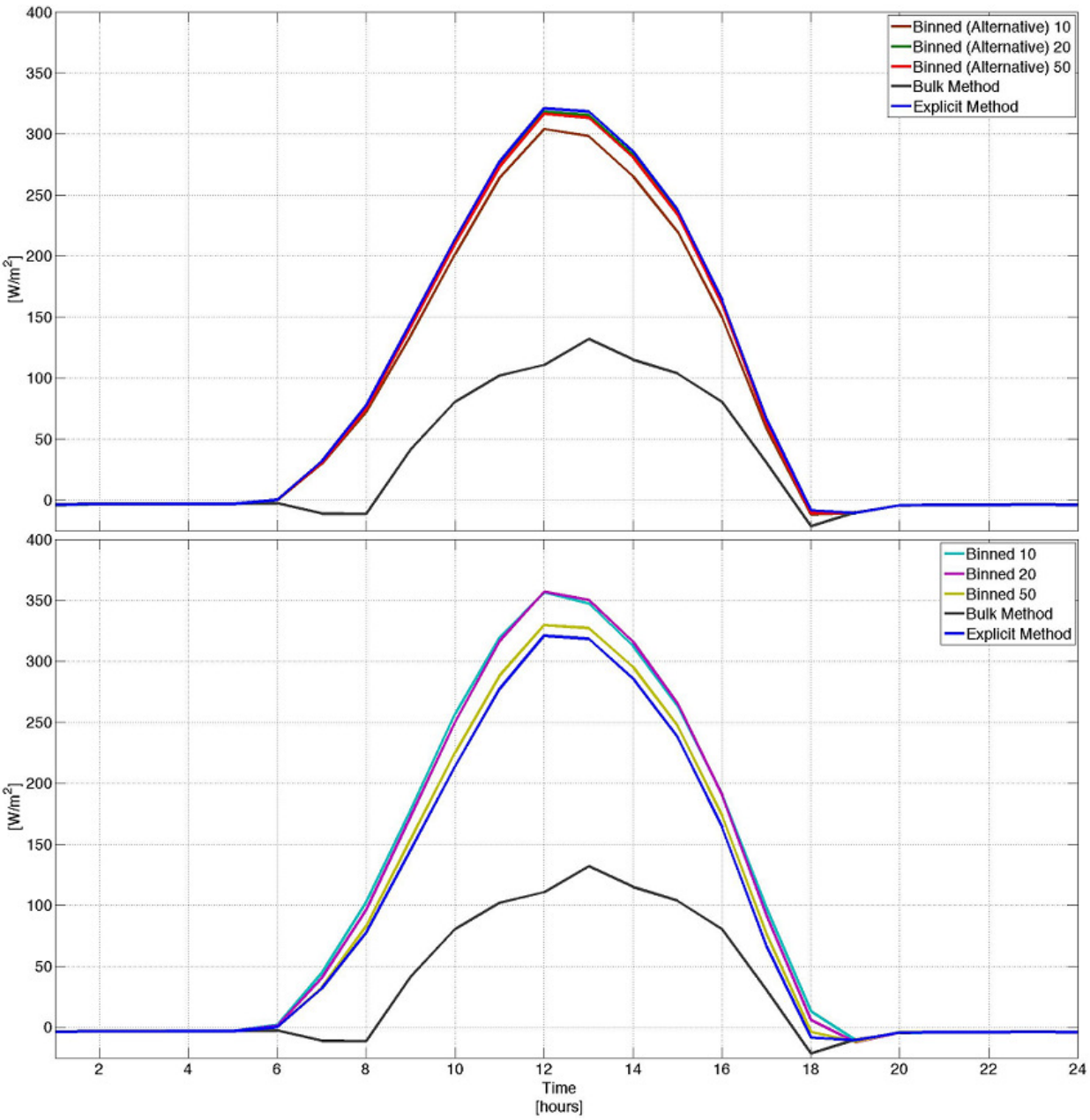

Figure 4.23d. Diurnal composites of the grid area averaged SH flux for all methods in biome 3.

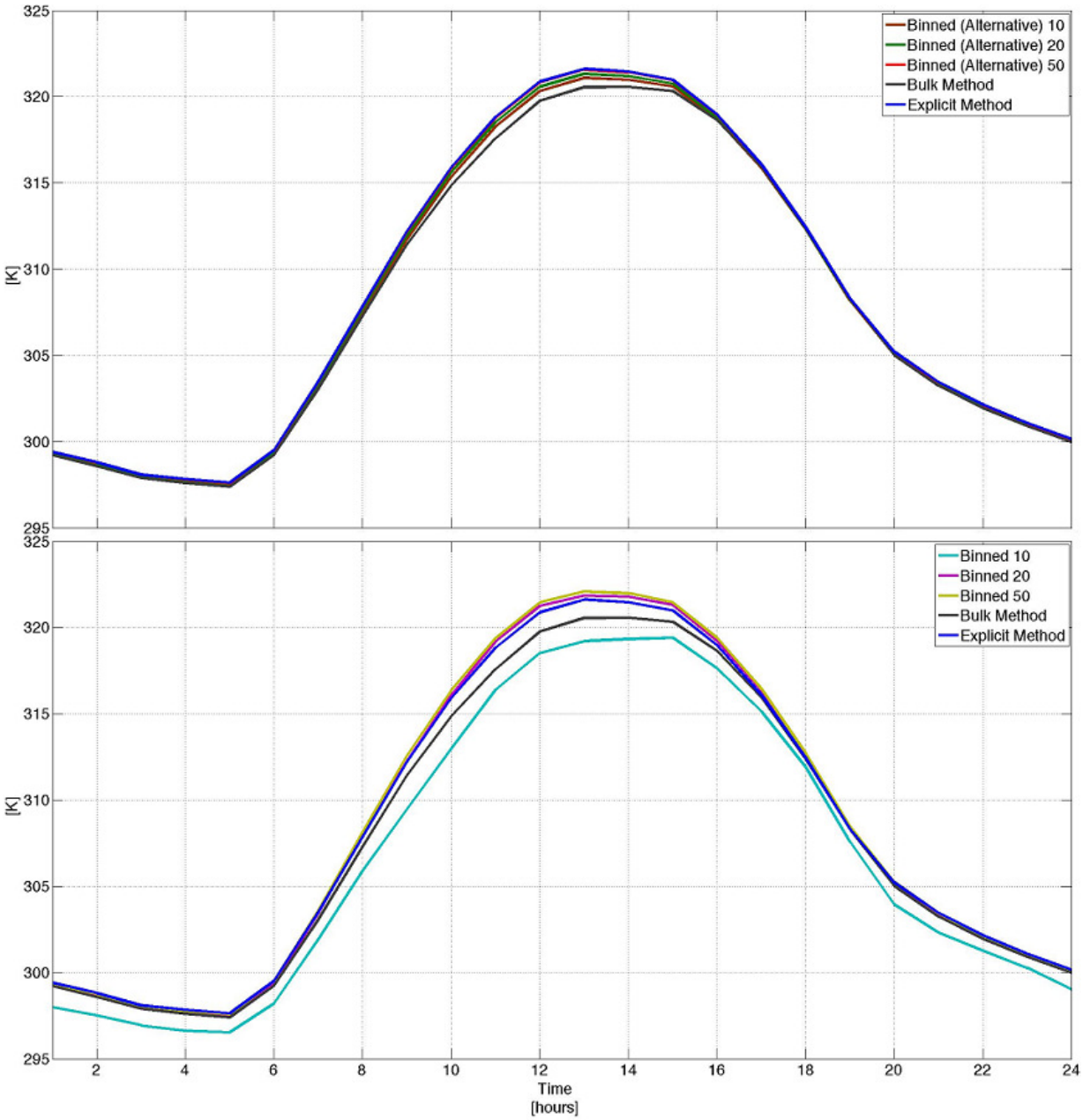

Figure 4.25a. Diurnal composites of the grid area averaged CAS temperature for all methods in biome 9.

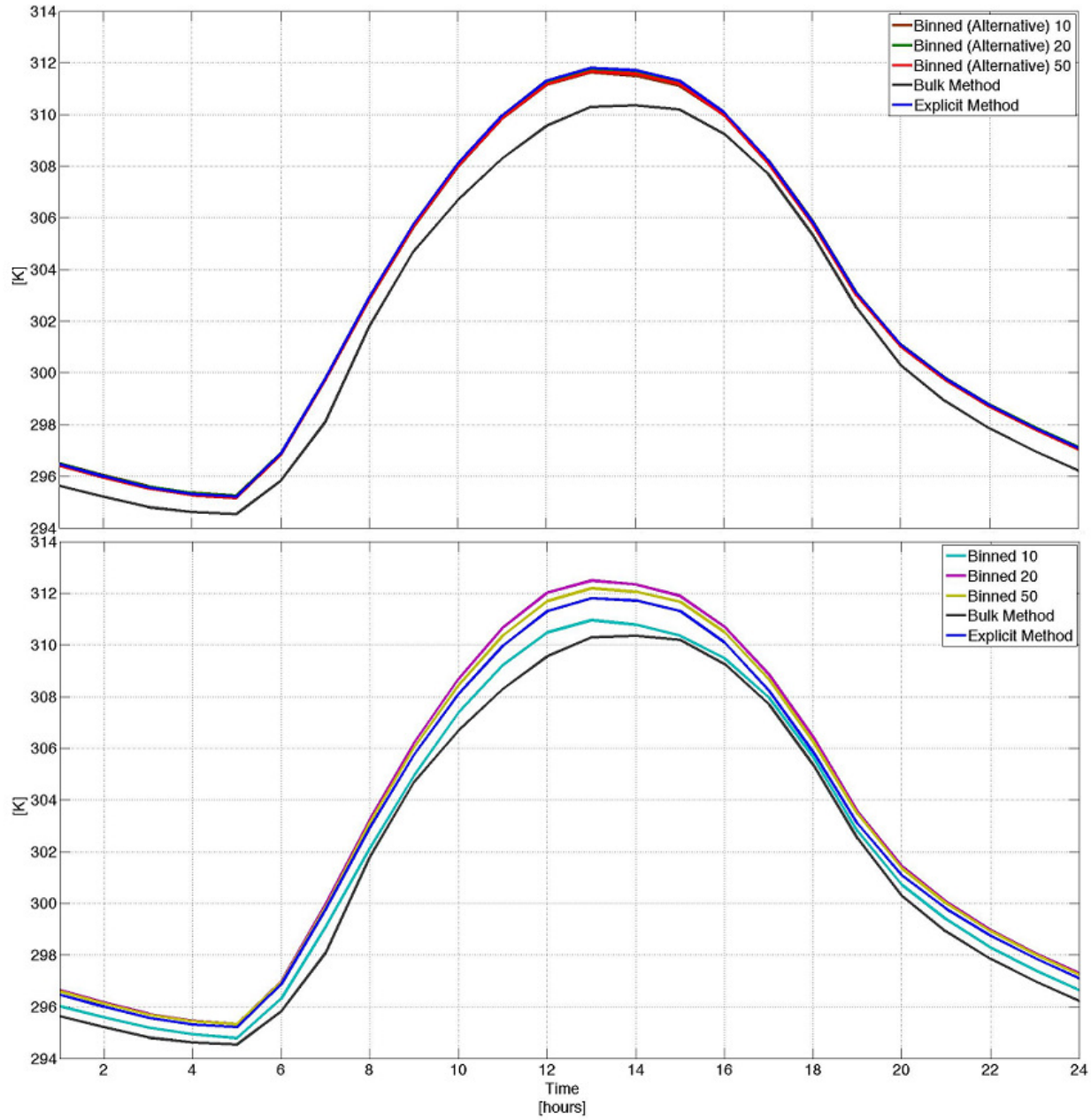

Figure 4.25b. Diurnal composites of the grid area averaged CAS temperature for all methods in biome 6.

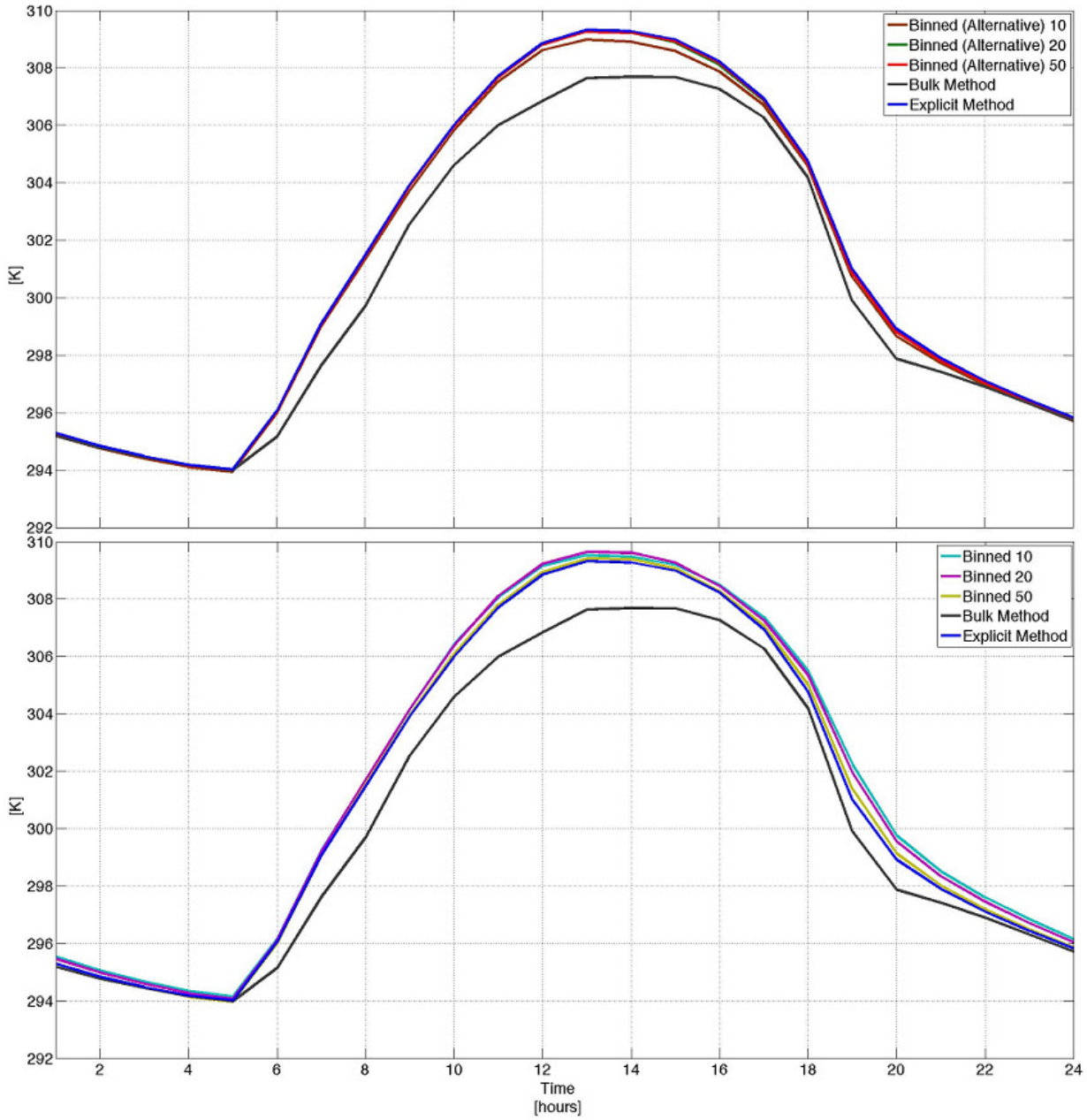

Figure 4.25c. Diurnal composites of the grid area averaged CAS temperature for all methods in biome 3.

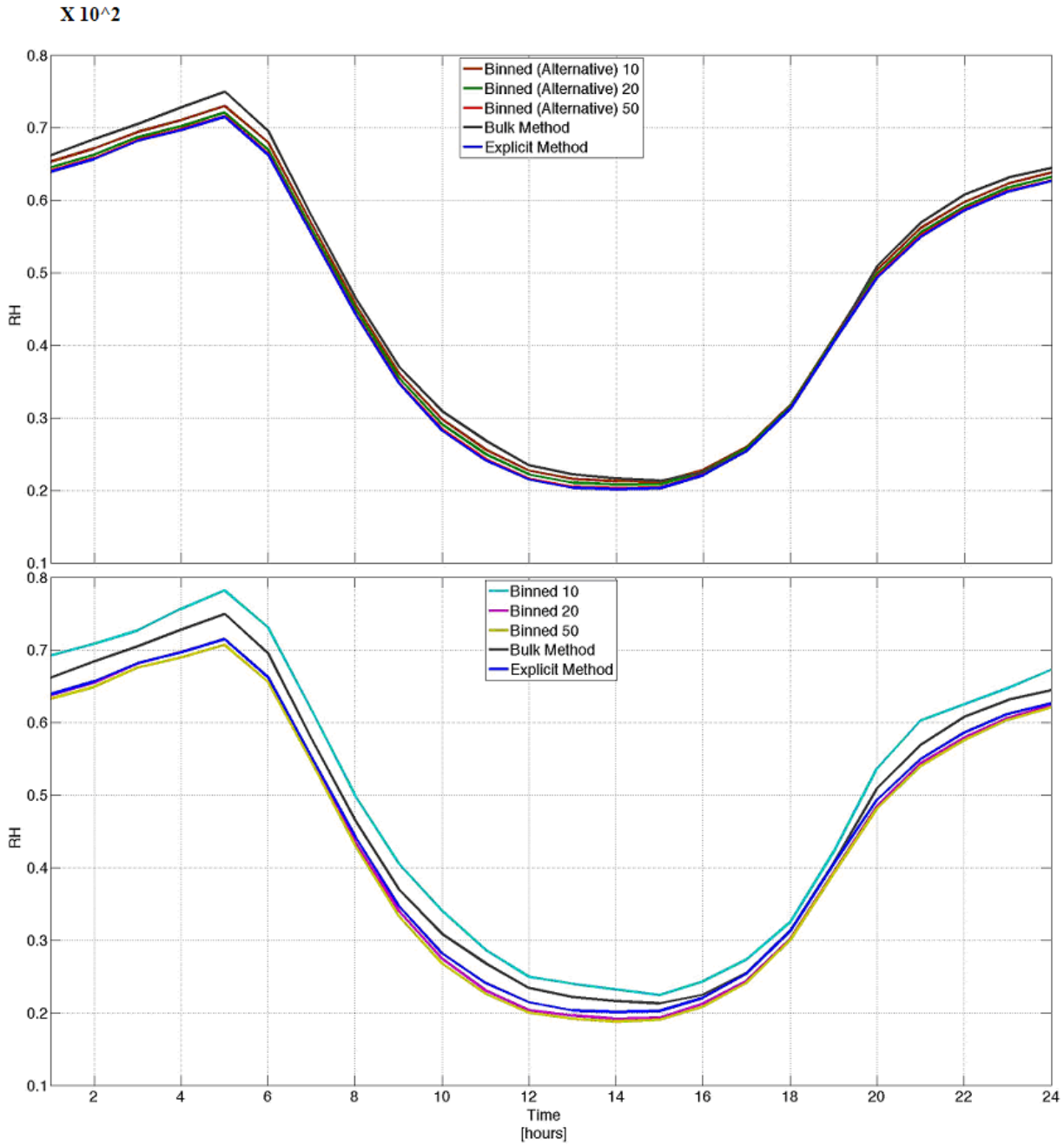

Figure 4.25d. Diurnal composites of the grid area averaged CAS relative humidity for all methods in biome 9.

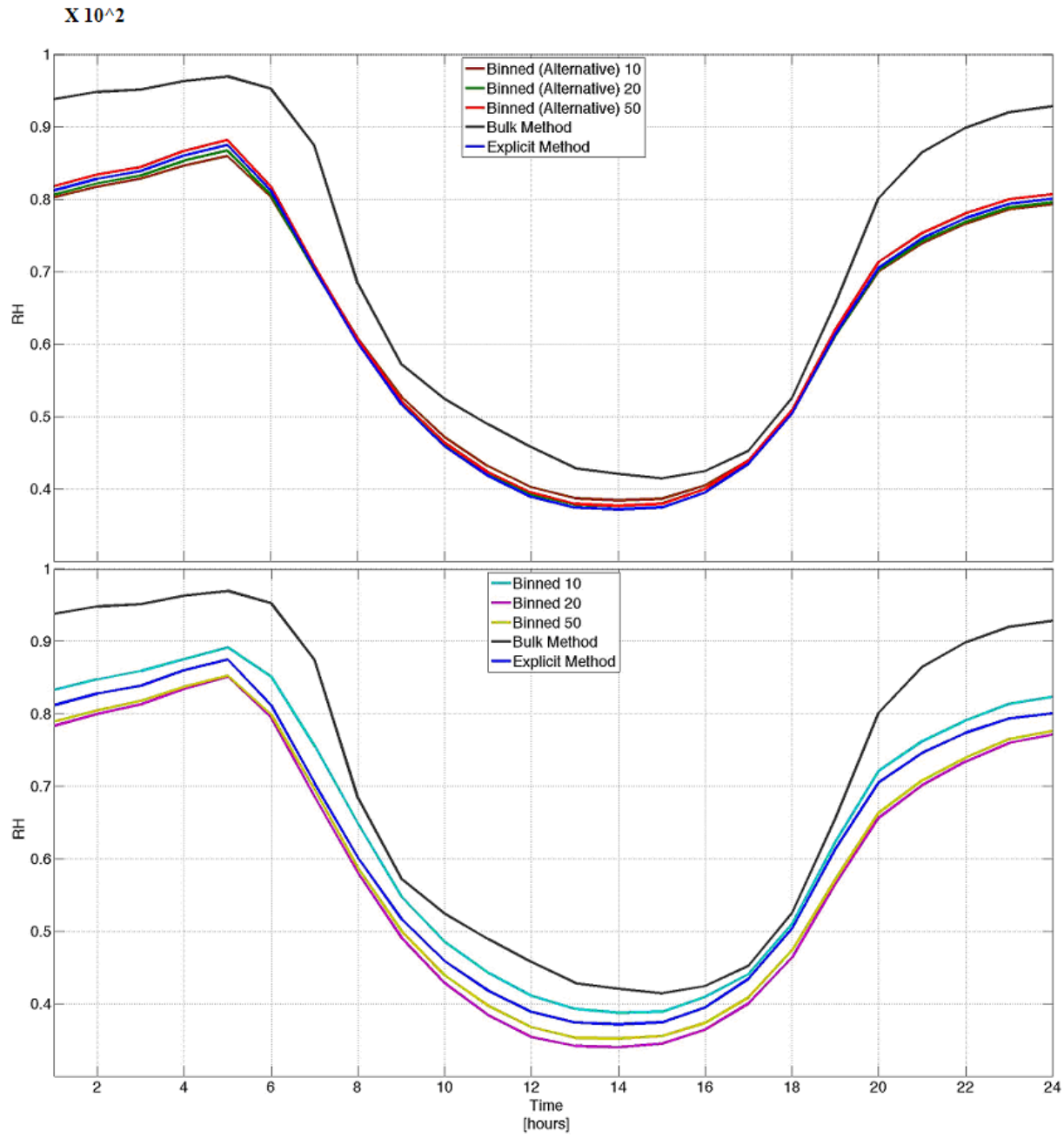

Figure 4.25e. Diurnal composites of the grid area averaged CAS relative humidity for all methods in biome 6.

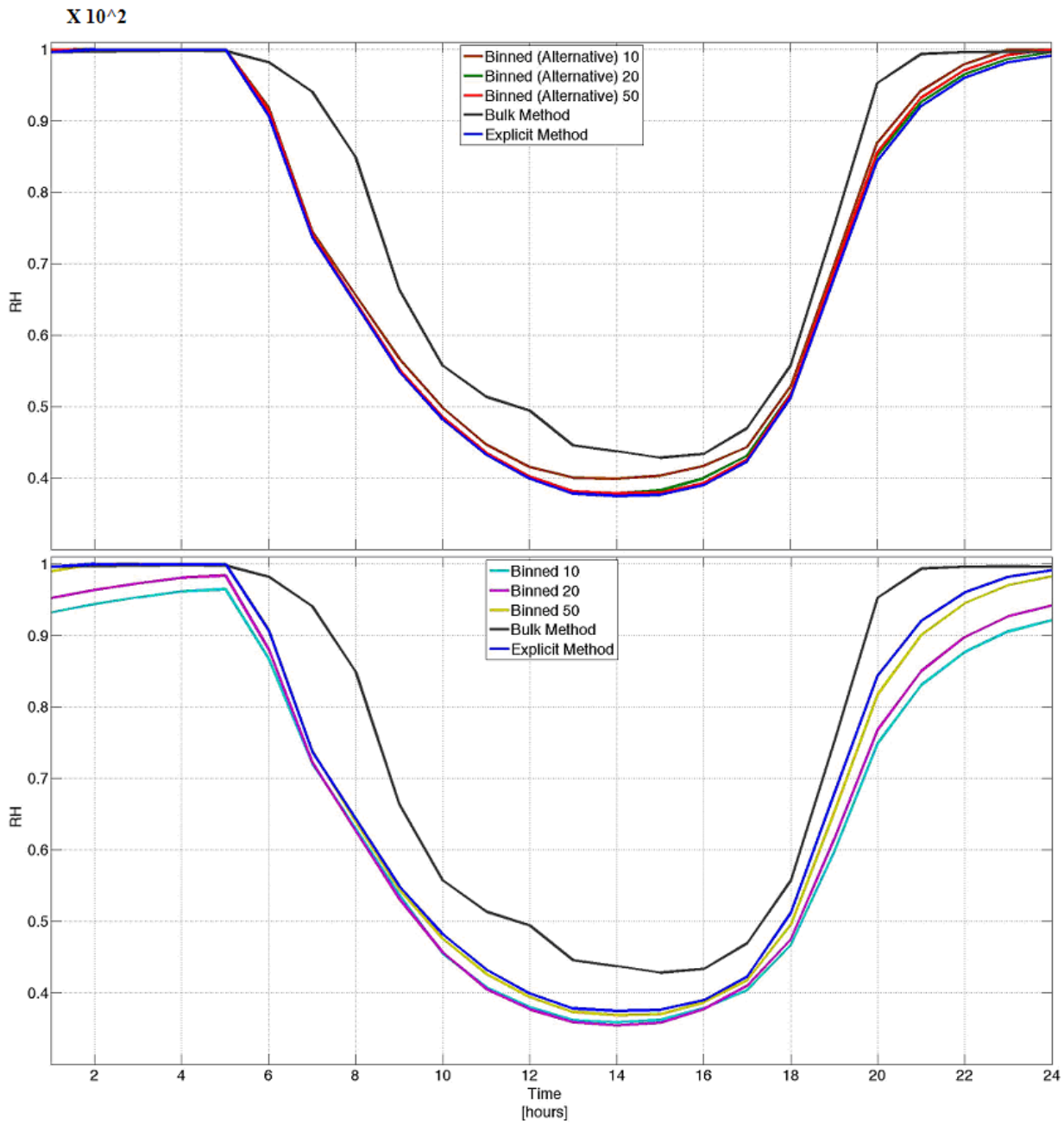

Figure 4.25f. Diurnal composites of the grid area averaged CAS relative humidity for all methods in biome 3.

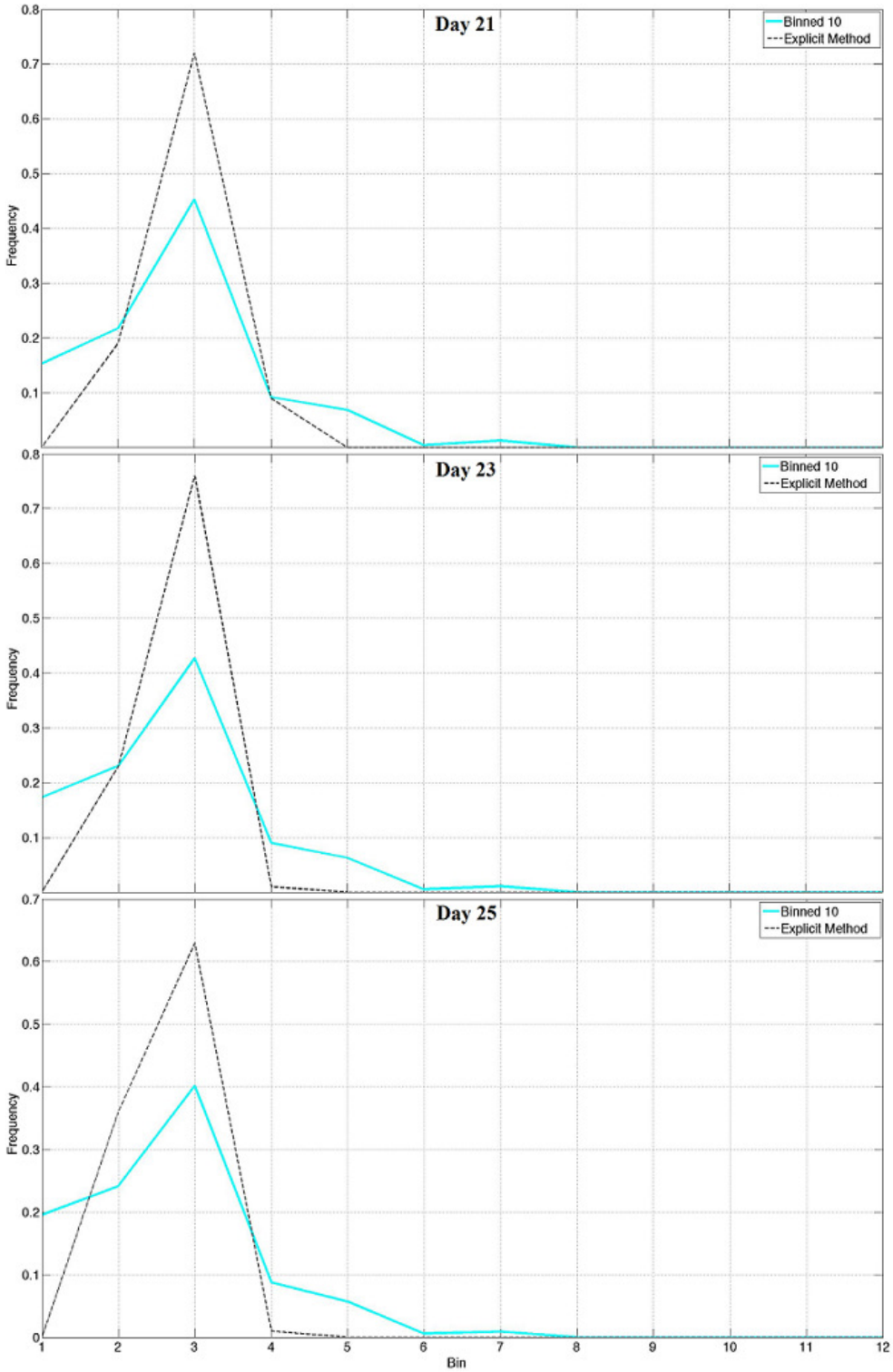

Figure 4.26a. Total plant available water distribution plots for the explicit and binned (10 bins) method, where precipitation events occur each day somewhere over the grid area as a result of the highly spatially varying precipitation distribution (bin wetness increases to the right).

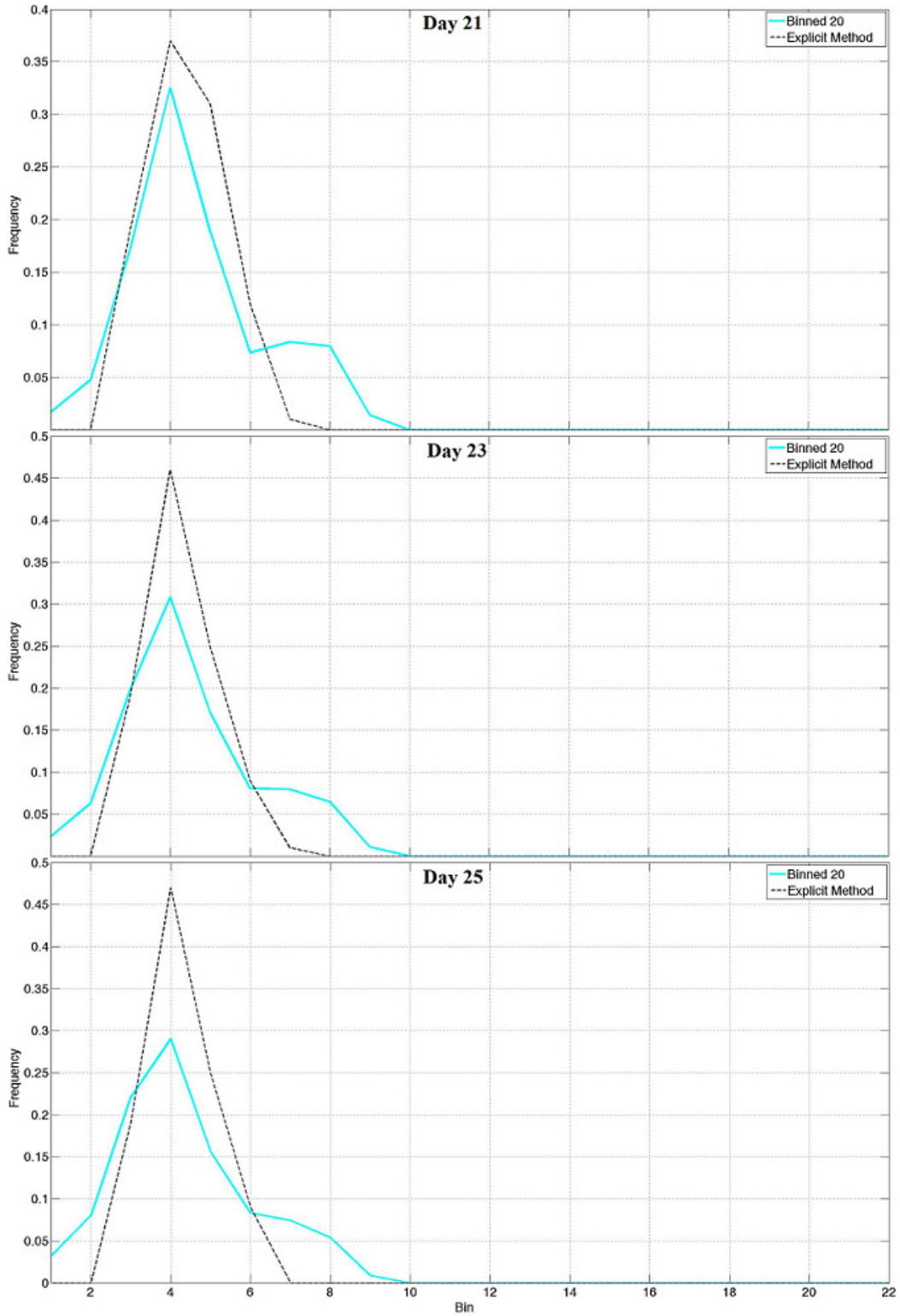

Figure 4.26b. Total plant available water distribution plots for the explicit and binned (20 bins) method, where precipitation events occur each day somewhere over the grid area as a result of the highly spatially varying precipitation distribution (bin wetness increases to the right).

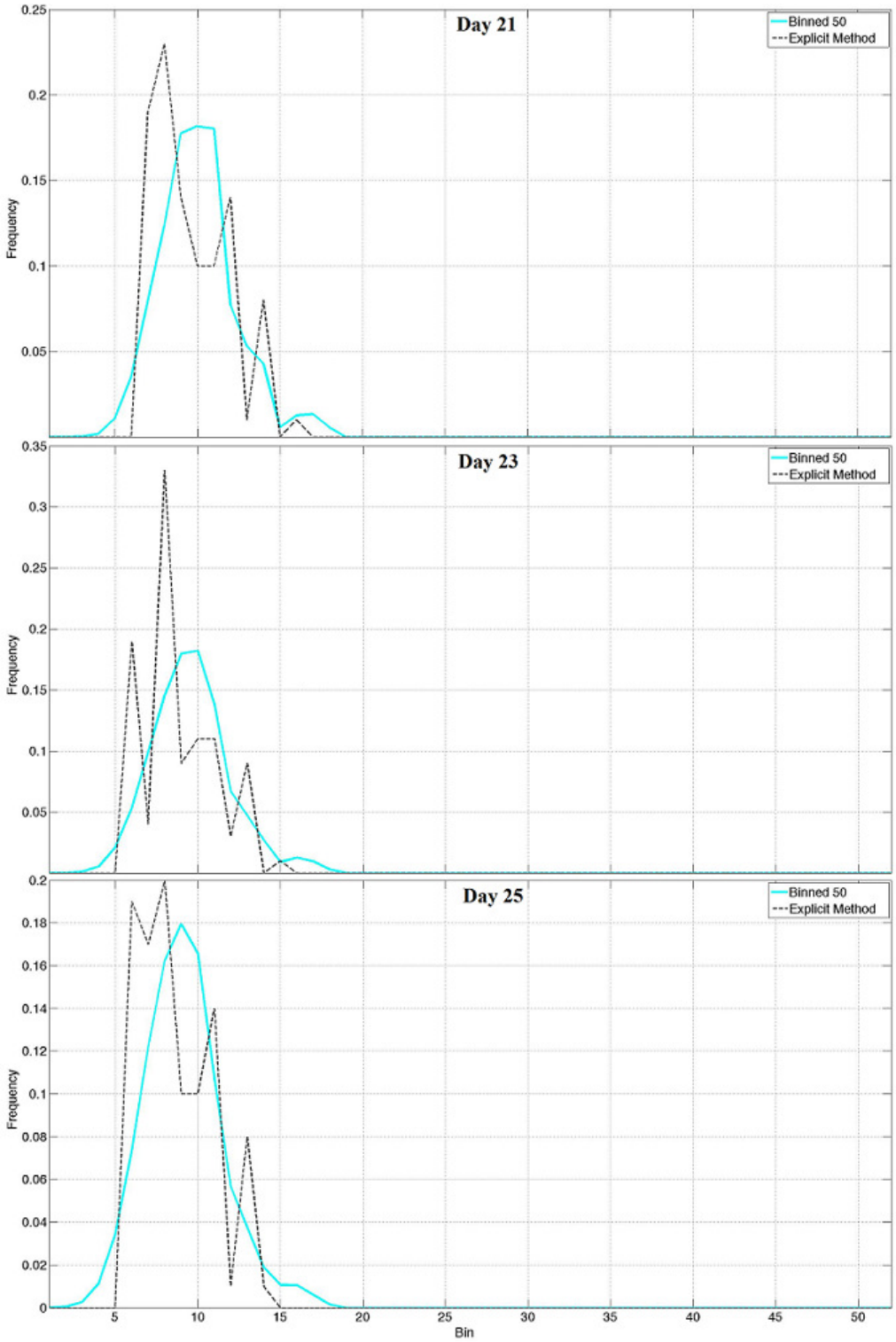

Figure 4.26c. Total plant available water distribution plots for the explicit and binned (50 bins) method, where precipitation events occur each day somewhere over the grid area as a result of the highly spatially varying precipitation distribution (bin wetness increases to the right).

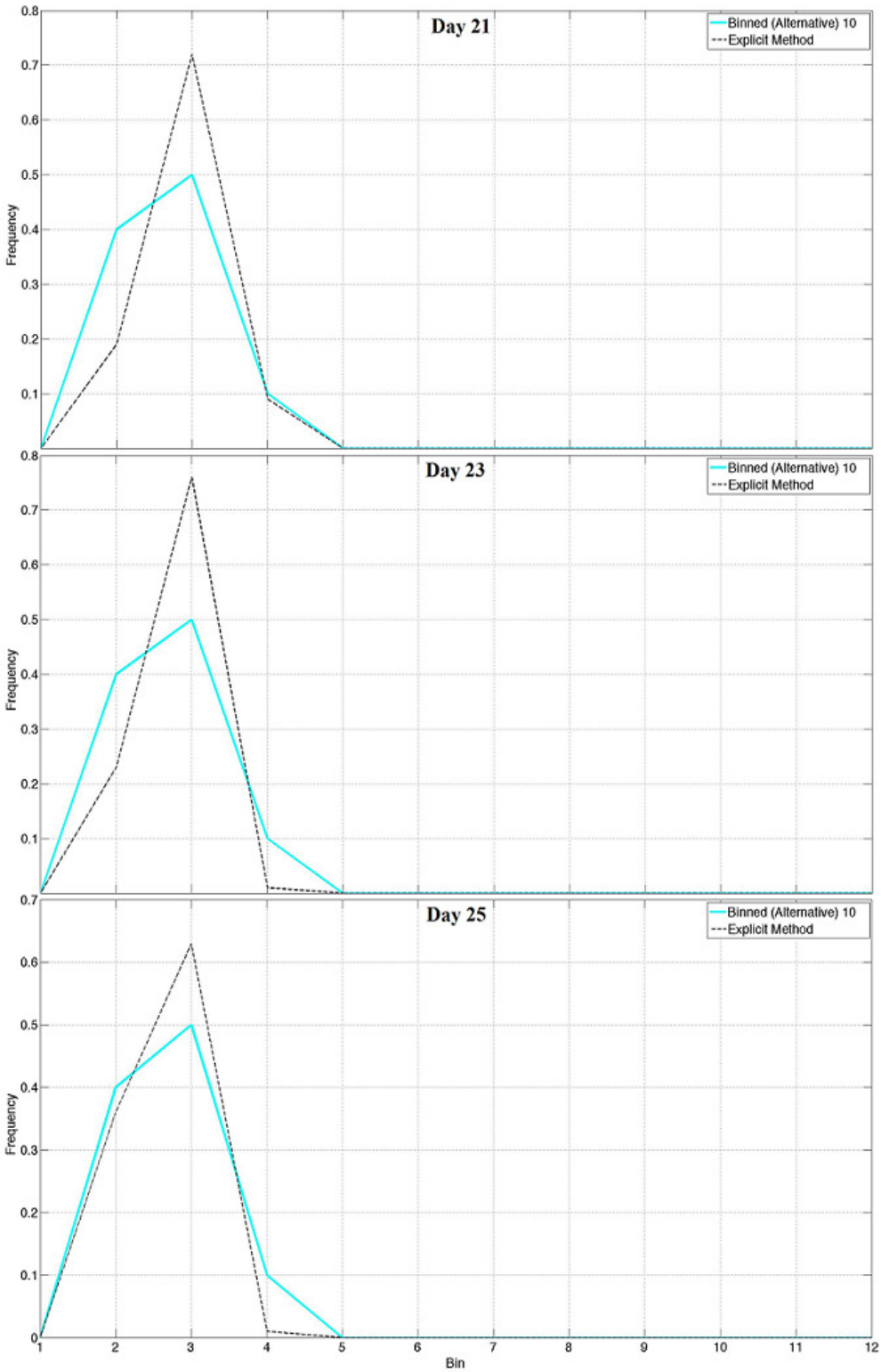

Figure 4.26d. Total plant available water distribution plots for the explicit and alternative binned (10 bins) method, where precipitation events occur each day somewhere over the grid area as a result of the highly spatially varying precipitation distribution (bin wetness increases to the right).

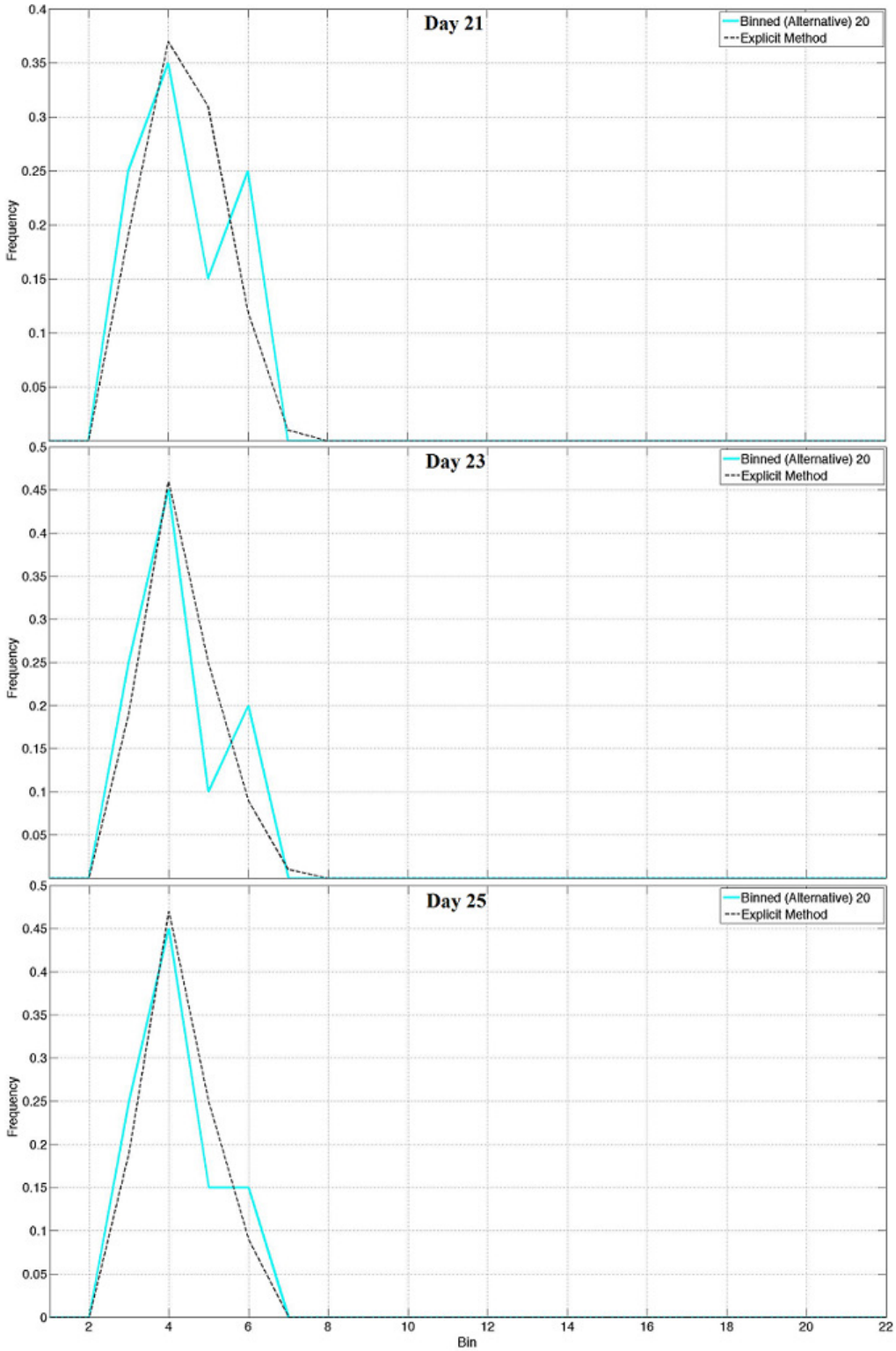

Figure 4.26e. Total plant available water distribution plots for the explicit and alternative binned (20 bins) method, where precipitation events occur each day somewhere over the grid area as a result of the highly spatially varying precipitation distribution (bin wetness increases to the right).

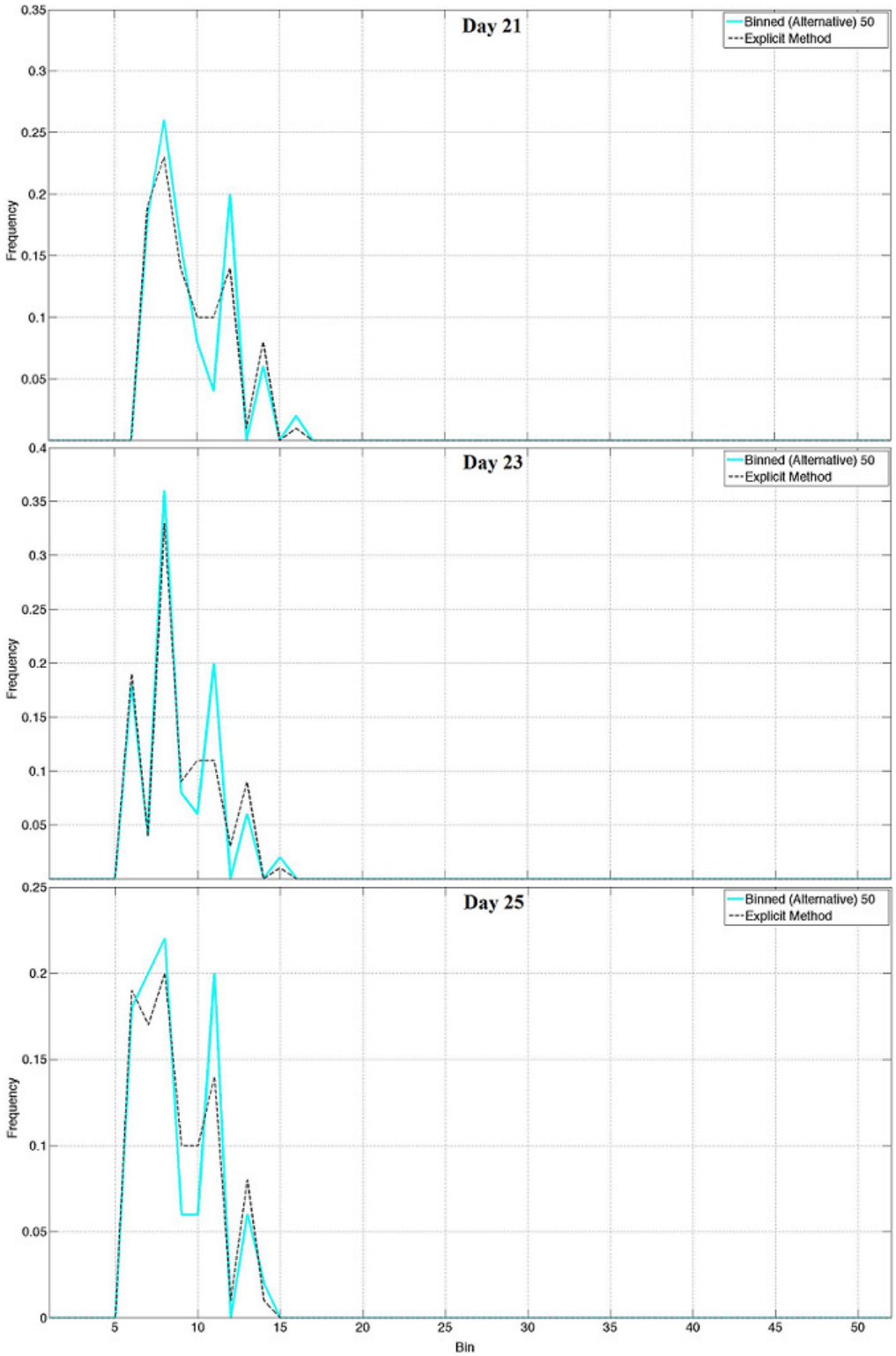

Figure 4.26f. Total plant available water distribution plots for the explicit and alternative binned (50 bins) method, where precipitation events occur each day somewhere over the grid area as a result of the highly spatially varying precipitation distribution (bin wetness increases to the right).

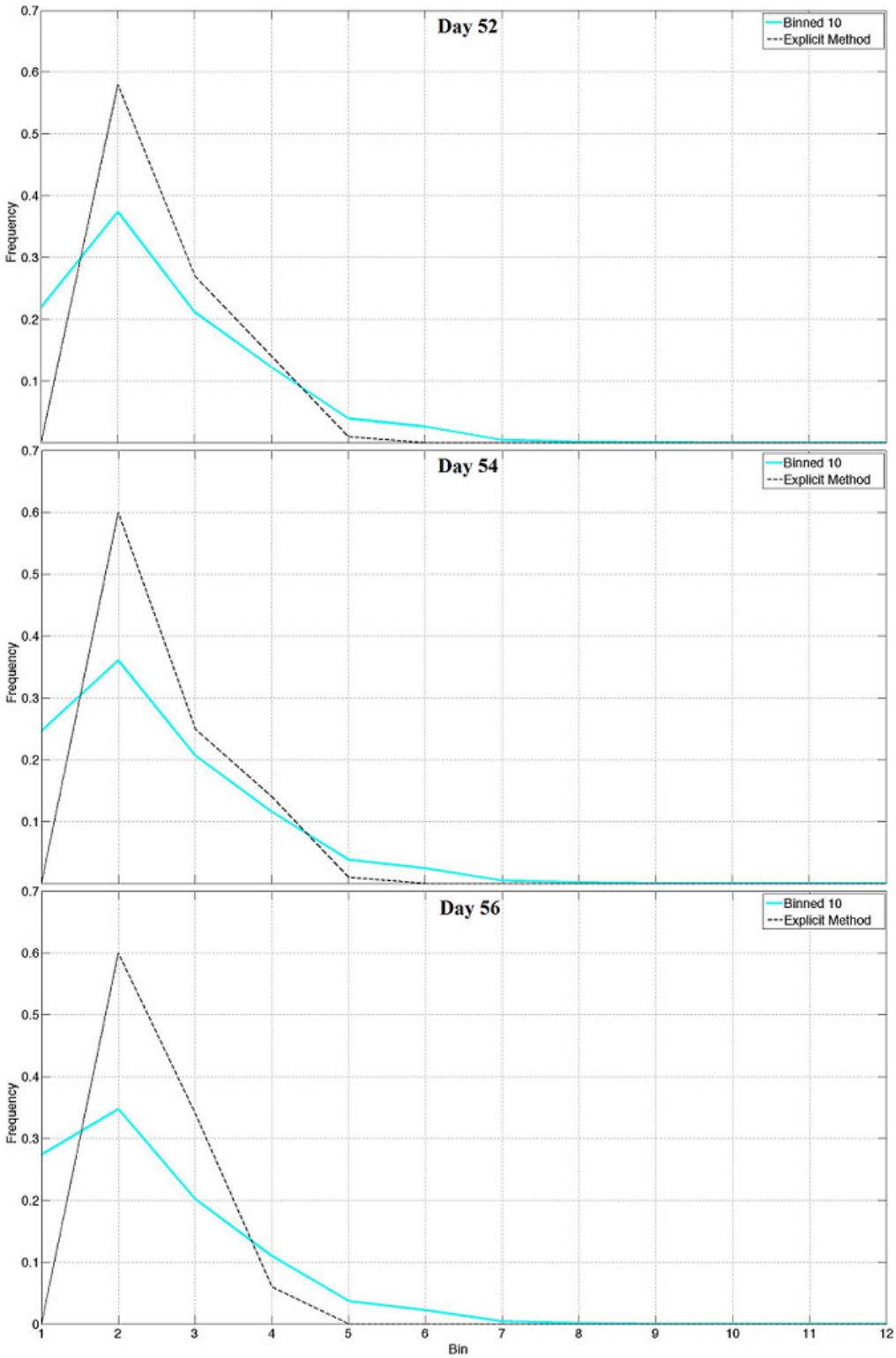

Figure 4.26g. Total plant available water distribution plots for the explicit and binned (10 bins) method, where precipitation events occur each day somewhere over the grid area as a result of the highly spatially varying precipitation distribution (bin wetness increases to the right).

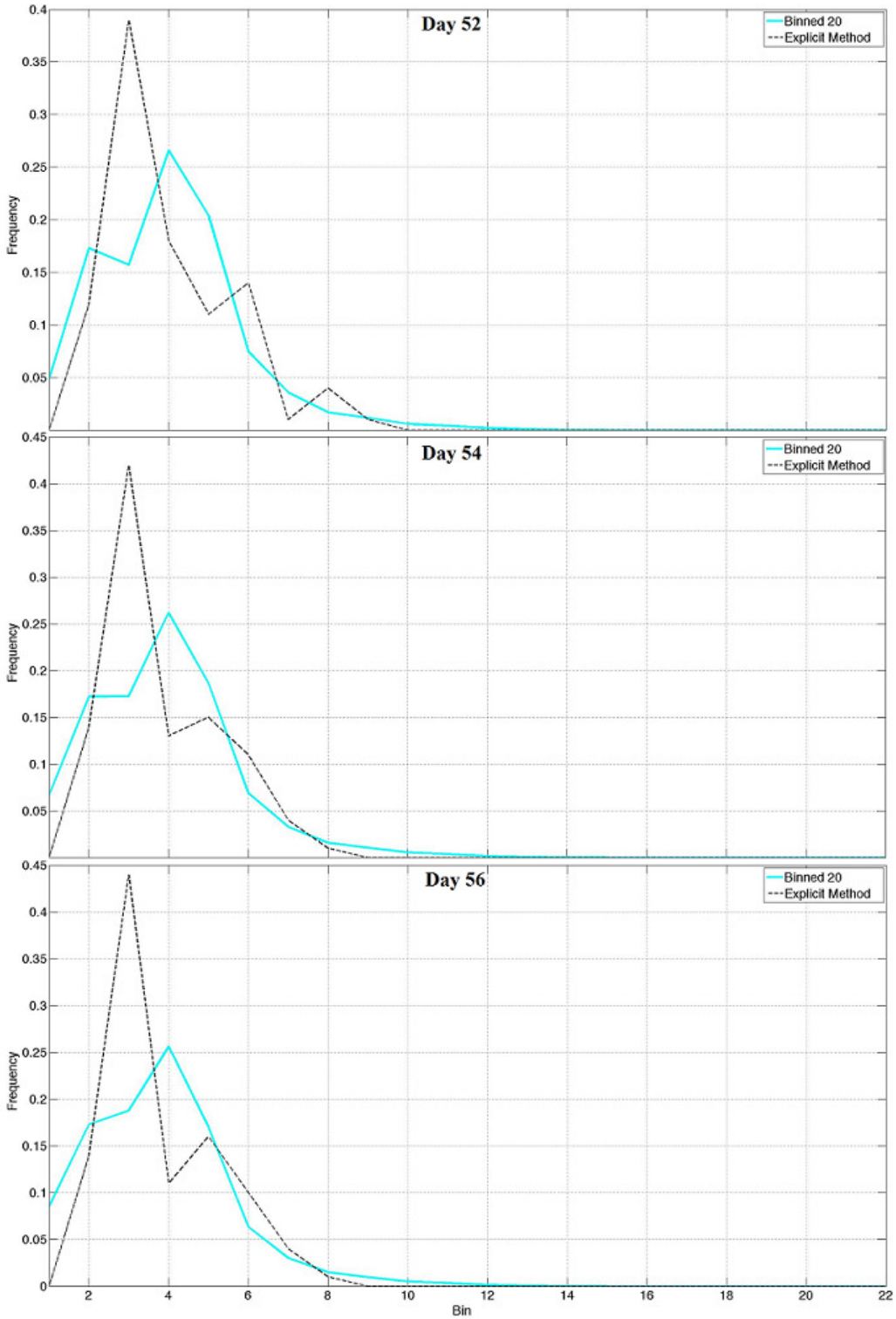

Figure 4.26h. Total plant available water distribution plots for the explicit and binned (20 bins) method, where precipitation events occur each day somewhere over the grid area as a result of the highly spatially varying precipitation distribution (bin wetness increases to the right).

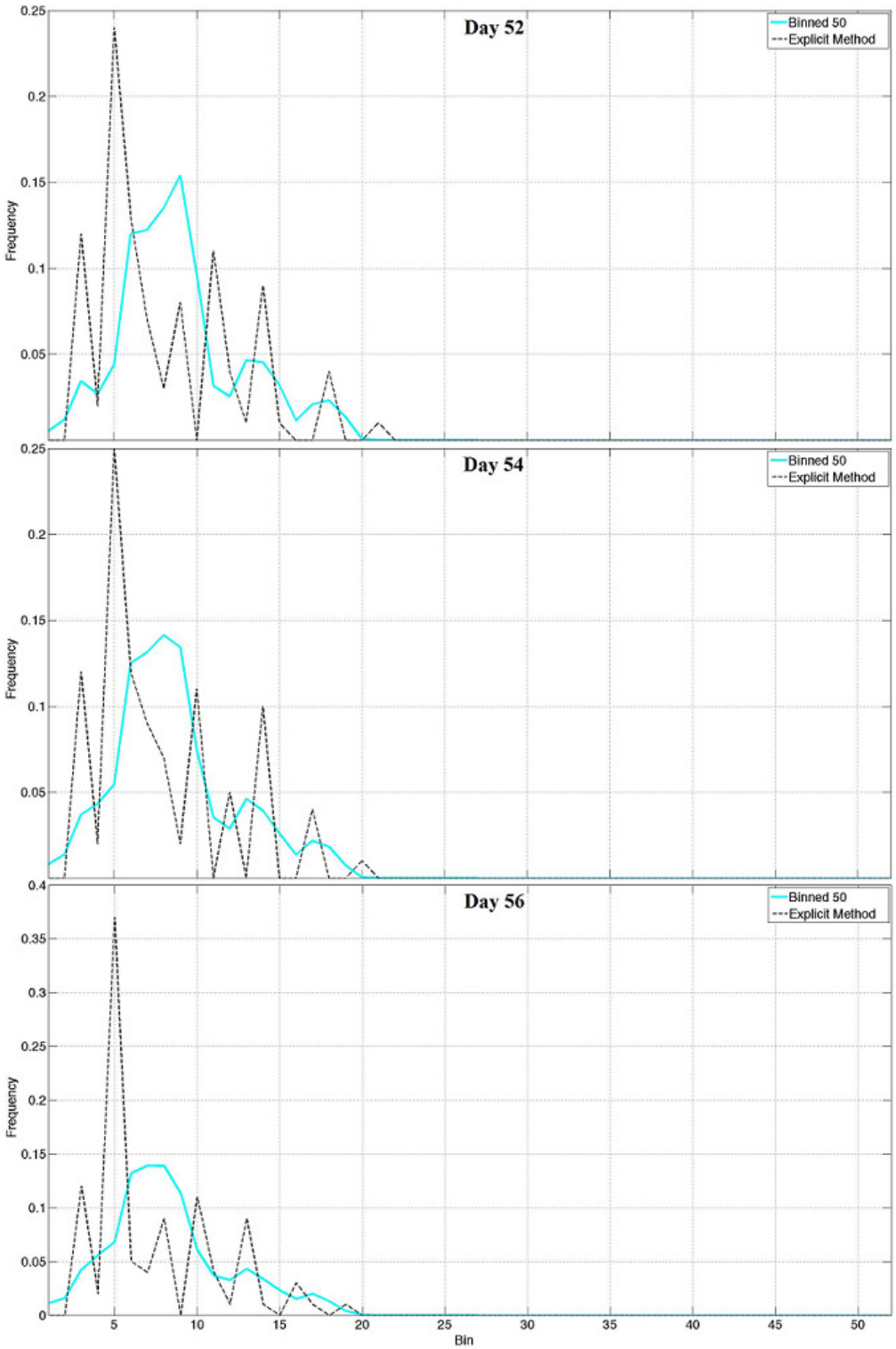

Figure 4.26i. Total plant available water distribution plots for the explicit and binned (50 bins) method, where precipitation events occur each day somewhere over the grid area as a result of the highly spatially varying precipitation distribution (bin wetness increases to the right).

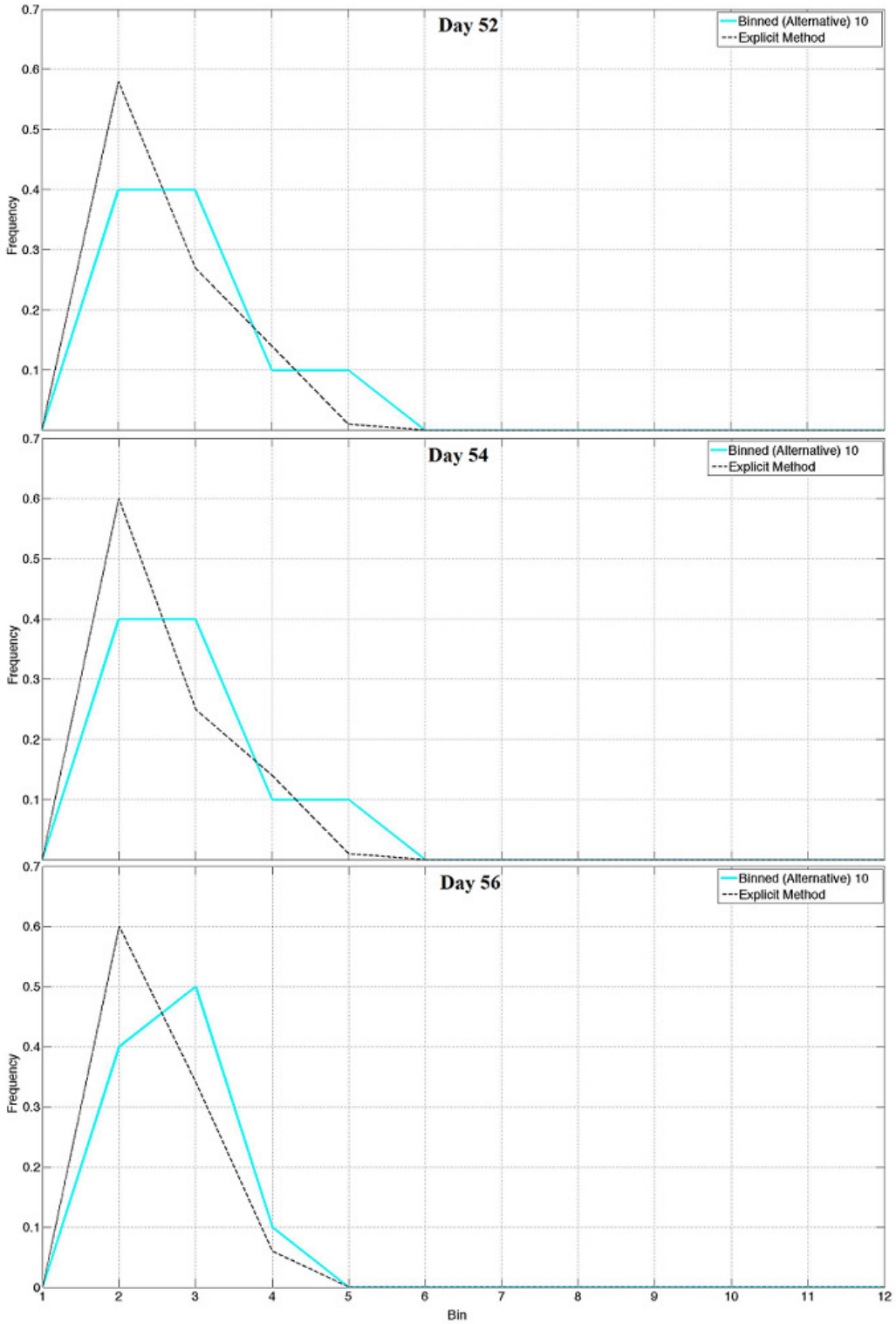

Figure 4.26j. Total plant available water distribution plots for the explicit and alternative binned (10 bins) method, where precipitation events occur each day somewhere over the grid area as a result of the highly spatially varying precipitation distribution (bin wetness increases to the right).

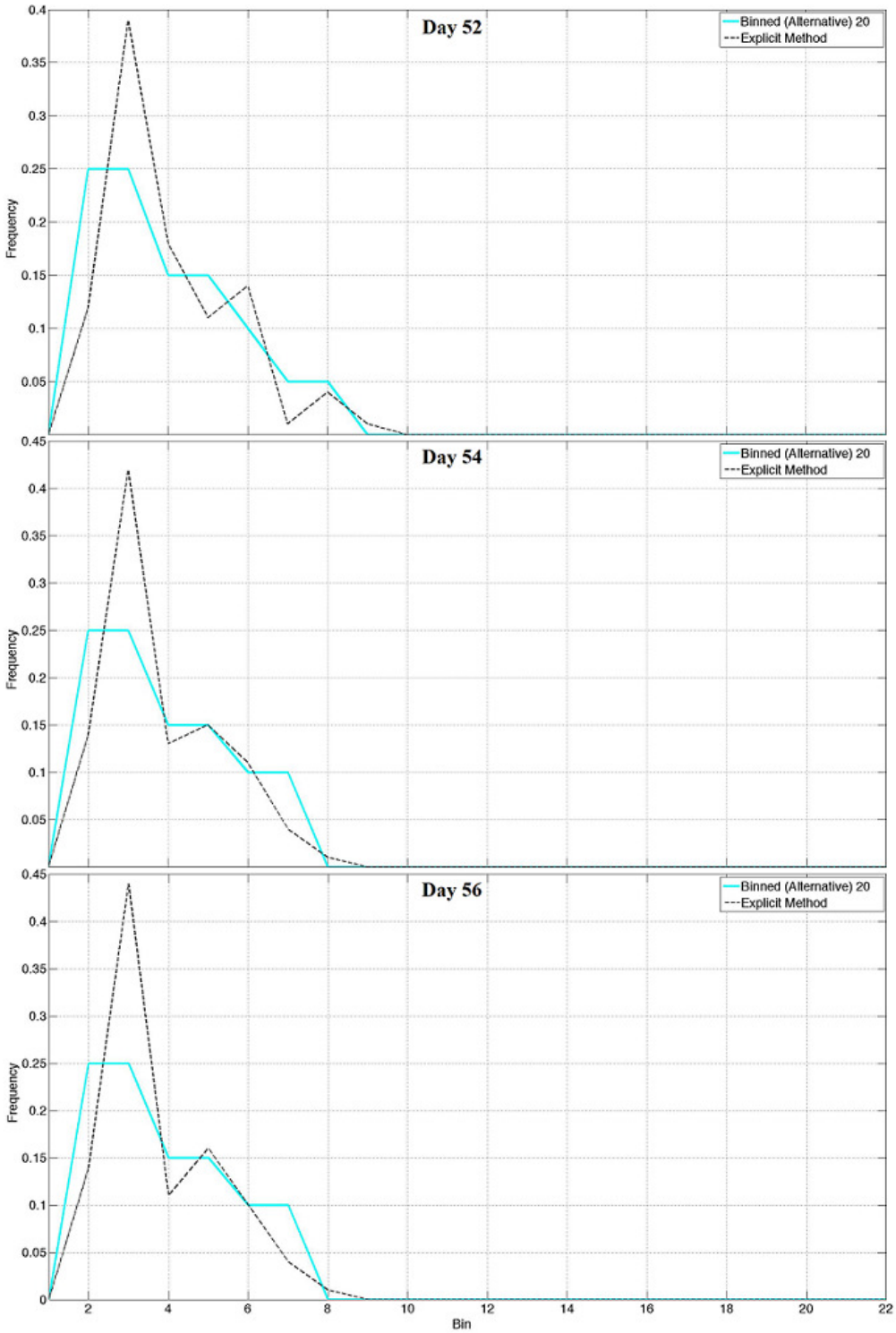

Figure 4.26k. Total plant available water distribution plots for the explicit and alternative binned (20 bins) method, where precipitation events occur each day somewhere over the grid area as a result of the highly spatially varying precipitation distribution (bin wetness increases to the right).

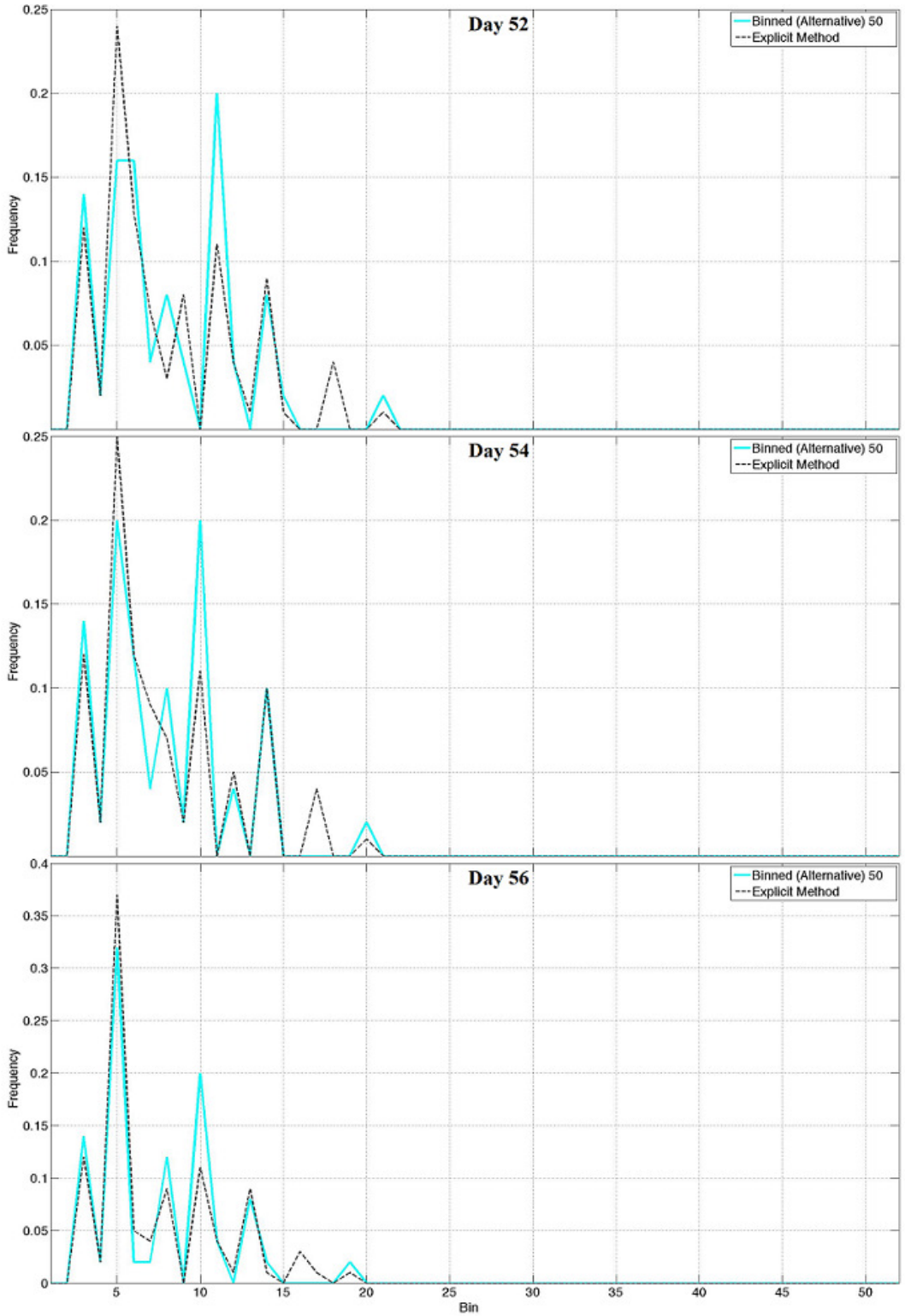

Figure 4.26l. Total plant available water distribution plots for the explicit and alternative binned (50 bins) method, where precipitation events occur each day somewhere over the grid area as a result of the highly spatially varying precipitation distribution (bin wetness increases to the right).

CHAPTER 5

Concluding Remarks and Future Work

5.1 Concluding Remarks

To improve the representation of soil moisture heterogeneity and spatially varying precipitation, the methods of Sellers et al. (2007), which include the explicit, bulk, binned, and alternative binned method, were applied to the land surface model SiB version 3.0. By applying the methods to the PawTot, a SiB variable representative of the soil column saturation and used to diagnose the water stress for the vegetation canopy, the representation of the spatially varying soil column saturation as well as surface fluxes for the bulk, binned, and alternative binned method were compared to the explicit method for two precipitation experiments. Precipitation was randomly distributed over the grid area for the explicit, binned, and alternative binned method, and the exponential distribution used in SiB to distribute convective precipitation was eliminated and precipitation events were evenly distributed on the randomly selected SiB models.

Results from this study were different from the results of Sellers et al. (2007), because of the model and precipitation distribution. In the study by Sellers et al. (2007), the highly simplified toy model did not have multiple soil layers or vegetation, and evapotranspiration was only a function of a constant potential evapotranspiration and a highly non linear stress function that only depended on soil wetness. Furthermore, precipitation was randomly distributed in the explicit method, but in the two binned methods, precipitation fell on the same fraction of each bin. For this study the random precipitation distribution in the two binned methods was chosen

to increase the physical realism of precipitation events, which are not limited to specific parts of the grid. Additionally, we wanted to avoid spatial variability within the spatial variability. When compared to the explicit method, Sellers et al. (2007) found that the binned method with 10 or more bins captured the spatial heterogeneity in soil wetness and grid area LH fluxes, and the alternative binned method was problematic.

In chapter 4, we found that the bulk method when compared to the explicit method was dominated by canopy interception due to lighter rainfall rates and had a much higher LH flux. The greatest contributions to the LH flux came from the canopy interception as well as the ground. Even though the time series for the column integrated soil water and PawTot were drier than in the explicit method, the water that did reach the soil surface during precipitation events allowed for a higher ground LH flux since the flux came from the entire grid area rather than a fraction of the grid as in the explicit method. Additionally, as a result of the high LH flux, the CAS temperature was lower and the CAS relative humidity was higher than in the explicit method.

The binned method was problematic when compared to the explicit method because of the initialization issue, where the average of the bin midpoint values that represented the initial PawTot distribution was either above or below the average of the actual distribution, and the precipitation distribution, where the total area occupied by the randomly selected bins was either smaller or larger than the area occupied by the wet bins in the explicit method, which resulted in either very heavy rainfall rates and excessive runoff or very light rainfall rates and results that were similar to the bulk method. Depending on the total fractional area occupied by the wet bins (this varied for the duration of the study), the grid area was either dominated by runoff or canopy interception relative to the explicit method. When the grid area was dominated by runoff, the

grid area was much drier, the LH flux was much lower, the CAS temperature was warmer and the CAS relative humidity was lower than in the explicit method, and when canopy interception dominated, the grid area was slightly wetter (the grid area gets drier as the total fractional area of the wet bins approaches the total fractional area of the bulk method), the LH flux was higher, the CAS temperature was lower, and the CAS relative humidity was higher than in the explicit method.

When compared to the explicit method, the alternative binned method performed the best. The precipitation distribution was not problematic with this method because of constant fractional areas. For the duration of the study, the total fractional area occupied by the wet bins was very close to the area occupied in the explicit method. This resulted in similar rainfall rates, total runoff, canopy interception, and surface fluxes. We also learned from the PawTot distribution plots in chapter 4, that the alternative binned method better captured the spatial heterogeneity in the distribution of PawTot produced by the explicit method.

Clearly, the alternative binned method performs the best and produces results that are very close to those produced by the explicit method. Choosing the alternative binned method over the bulk method, the grid area transitions from being dominated by canopy interception, and having a cool and humid CAS to a grid area dominated by a warmer and less humid CAS. Of course, using a large bin size will produce results that are in closer agreement with the explicit method, but using a bin size of 10 is a vast improvement from the bulk method and better captures the sub-grid scale heterogeneity.

5.2 Future Work

We plan on applying the methods from this research to other biomes to evaluate the performances there, and use a number of different distributions of PawTot for initialization. Other experiments have been suggested and involve saturating certain soil layers and perhaps mixing biomes within the grid area. We also plan on performing on-line runs with these methods and evaluating the results there.

REFERENCES

Avissar, R., and M. M. Verstraete (1990), The representation of continental surface processes in atmospheric models, *Rev. Geophys.*, 28(1), 35–52, doi:10.1029/RG028i001p00035.

Clapp, R. B., and G. M. Hornberger (1978), Empirical equations for some soil hydraulic properties, *Water Resour. Res.*, 14(4), 601–604, doi:10.1029/WR014i004p00601.

Colello, G. D., C. Grivet, P. J. Sellers, J. A. Berry, 1998: Modeling of Energy, Water, and CO2 Flux in a Temperate Grassland Ecosystem with SiB2: May–October 1987. *J. Atmos. Sci.*, **55**, 1141–1169.

Dai, Y., and Coauthors, cited 2001: Common Land Model: Technical Documentation and user's guide. [Available online at http://climate.eas.gatech.edu/dai/clmdoc.pdf.]

Dai, Y., et al. (2003), The Common Land Model, Bull. Am. Meteorol. Soc., 84(8), 1013-1023.

Eltahir, EAB, Bras RL. 1993: A Description of Rainfall Interception over Large Areas. *J. Climate*, **6**, 1002-1008.

Essery, R L H, Best, M J, Betts, R A, Cox, P M & Taylor, C M, 2003: Explicit representation of subgrid heterogeneity in a GCM land-surface scheme. *J. Hydrometeorology* **4**, 530-543.

Gedney, N., P. M. Cox, 2003: The Sensitivity of Global Climate Model Simulations to the Representation of Soil Moisture Heterogeneity. *J. Hydrometeor*, **4**, 1265–1275.

Giorgi, F., and R. Avissar (1997), Representation of heterogeneity effects in Earth system modeling: Experience from land surface modeling, *Rev. Geophys*., 35(4), 413 437.

Koster, Randal D., Max J. Suarez, Mark Heiser, 2000: Variance and Predictability of Precipitation at Seasonal-to-Interannual Timescales. *J. Hydrometeor*, **1**, 26–46.

Koster, R.D., P. A. Dirmeyer, Z. Guo, G. Bonan, E. Chan, P. Cox, C. T. Gordon, S. Kanae, E. Kowalczyk, D. Lawrence, P. Liu, C. –H. Lu, S. Malyshev, B. McAvaney, K. Mitchell, D. Mocko, T. Oki, K. Oleson, A. Pitman, Y. C. Sud, C. M. Taylor, D. Verseghy, R. Vasic, Y. Xue, and T. Yamada, 2004: Regions of strong coupling between soil moisture and precipitation. *Science*, 305, 1138-1140.

Lin, S., J., and R.B. Rood. Multidimensional flux-form semi-Lagrangian transport schemes. *Monthly Weather Review*, 124:2046-2070, September 1996.

Miguez-Macho, G., Y. Fan, C. P. Weaver, R. Walko, and A. Robock (2007),

Incorporating water table dynamics in climate modeling: 2. Formulation, validation, and soil moisture simulation, *J. Geophys. Res.,* 112, D13108, doi:10.1029/2006JD008112.

Oleson, K. W., et al. (2008), Improvements to the Community Land Model and their impact on the hydrological cycle, *J. Geophys. Res.*, 113, G01021, doi:10.1029/2007JG000563.

Peters-Lidard, C., D., E. Blackburn, X. Liang and E.F. Wood , The effect of soil thermal conductivity parameterization on surface energy fluxes and temperatures. *J. Atmos. Sci.* **55** 7 (1998), pp. 1209–1224.

Pitman, A., A. Henderson-Sellers, and Z. L. Yang, Sensitivity of regional climates to localized precipitation in global models, *Nature, 346*, 734-737, 1992.

Randall, D.A., et al., 1996: A revised land surface parameterization (SiB2) for GCMs. Part III: The greening of the Colorado State University General Circulation Model. *J. Climate*, **9**, 738-763.

Richardson, C. W.: 1981, 'Stochastic Simulation of Daily Precipitation, Temperature and Solar Radiation', *Water Resources Research* **17**, 182–190.

Richardson, C. W. and D. A. Wright, 1984: WGEN: A Model for Generating Daily Weather Variables (ARS-8). US Department of Agriculture.

Ronda, R. J., B. J J. M. van den Hurk, A. A M. Holtslag, 2002: Spatial Heterogeneity of the Soil Moisture Content and Its Impact on Surface Flux Densities and Near Surface Meteorology. *J. Hydrometeor*, **3**, 556–570.

Ryu, D., and J.S. Famiglietti. 2006. Multi-scale spatial correlation and scaling behavior of surface soil moisture. *Geophys. Res. Lett.* **33**:L08404, doi:10.1029/2006GL025831.

Sato, N., P. J. Sellers, D. A. Randall, E. K. Schneider, J. Shukla, J. L. Kinter III, Y.-T. Hou, and E. Albertazzi, 1989b: Implementing the Simple Biosphere Model (SiB) in a General Circulation Model: Methodologies and Results. NASA Contractor Report, NASA HQ, 70 pp. [Available from Independence Avenue, Washington D.C. 20545].

Sellers, P. J., Y. Mintz, Y. C. Sud, and A. Dalcher, 1986: A Simple Biosphere Model (SiB) for Use within General Circulation Models. *J. Atmos. Sci.*, **43**, pp. 505-531, 1986.

Sellers, P. J., Berry, J. A., Collatz, G. J., Field, C. B., and Hall, F. G., (1992) Canopy reflectance, photosynthesis, and transpiration. III. A reanalysis using improved leaf models and a new canopy integration scheme. *Remote Sensing of Environment* **42**, 187-216.

Sellers, P. J., M. D. Heiser, F. G. Hall, S. J. Goetz, D. E. Stebel, S. B. Verma, R. L. Desjardins, P. M. Schuepp, and J. I. MacPherson, Effects of spatial variability in topography, vegetation cover, and soil moisture on area-averaged surface fluxes: A case study using the FIFE 1989 data, *J. Geophys. Res., 100*, 25,607-25,630, 1995.

Sellers, P. J., D. A. Randall, G. J. Collatz, J. A. Berry, C. B, Field, D. A. Dazlich, C. Zhang, G. D. Collelo, and L. Bounoua, 1996a: A Revised Land Surface Parameterization (SiB2) for Atmospheric GCMs. Part I: Model Formulation. *J. Climate,* **9**, 676-705.

Sellers, P. J., S. O. Los, C. J. Tucker, C. O. Justice, D. A. Dazlich, G. J. Collatz, and D. A. Randall, 1996b: A Revised Land Surface Parameterization (SiB2) for Atmospheric GCMS. Part II: The Generation of Global Fields of Terrestrial Biophysical Parameters from Satellite Data. *J. Climate*, **9**, 706-737.

Sellers, P. J., Dickinson, R. E., Randall, D. A., Betts, A. K., Hall, F. G., Berry, J. A., Collatz, G. J., Denning, A. S., Mooney, H. A., Nobre, C. A., Sato, N., Field, C. B., & Henderson-Sellers, A. (1997). Modeling the exchanges of energy, water, and carbon between continents and the atmosphere. *Science, 275*(5299), 502 – 509.

Sellers, P. J., M. J. Fennessy, and R. E. Dickinson (2007), A numerical approach to calculating soil wetness and evapotranspiration over large grid areas, *J. Geophys. Res., 112*, D18106, doi:10.1029/2007JD008781.\

Stieglitz, Marc, David Rind, James Famiglietti, Cynthia Rosenzweig, 1997: An Efficient Approach to Modeling the Topographic Control of Surface Hydrology for Regional and Global Climate Modeling. *J. Climate*, **10**, 118–137.

Stöckli, Reto, Pier Luigi Vidale, Aaron Boone, Christoph Schär, 2007: Impact of Scale and Aggregation on the Terrestrial Water Exchange: Integrating Land Surface Models and Rhône Catchment Observations. *J. Hydrometeor*, **8**, 1002–1015.

Vidale, P. L., and R. Sto¨ ckli (2005), Prognostic canopy air space solutions for land surface exchanges, *Theor. Appl. Climatol., 80*, 245 – 257.

Wetzel, P., and J. T. Chang, Concerning the relationship between evapotranspiration and soil moisture, *J. Clim, Appl. Meteorol., 26*, 18-27, 1987.

Wetzel, P. J., J.-T. Chang (1987), Evapotranspiration from Nonuniform Surfaces: A First Approach for Short-Term Numerical Weather Prediction, *Mon. Wea. Rev*., **116**, 600-621.

Wilks DS, Wilby RL. 1999. The weather generation game: a review of stochastic weather models. *Progress in Physical Geography* **23**: 329 – 357.